

Spring 5-2016

Phosphonium/Phosphate Ionic Liquids as Lubricant Additives: The Synthesis and Testing of Six Novel ILs

Matthew Scott Welmers
Rose-Hulman Institute of Technology

Follow this and additional works at: http://scholar.rose-hulman.edu/chem_biochem_grad_theses



Part of the [Materials Chemistry Commons](#)

Recommended Citation

Welmers, Matthew Scott, "Phosphonium/Phosphate Ionic Liquids as Lubricant Additives: The Synthesis and Testing of Six Novel ILs" (2016). *Graduate Theses – Chemistry and Biochemistry*. Paper 2.

This Thesis is brought to you for free and open access by the Graduate Theses at Rose-Hulman Scholar. It has been accepted for inclusion in Graduate Theses – Chemistry and Biochemistry by an authorized administrator of Rose-Hulman Scholar. For more information, please contact weirl@rose-hulman.edu.

**Phosphonium/Phosphate Ionic Liquids as Lubricant Additives:
The Synthesis and Testing of Six Novel ILs**

A Thesis

Submitted to the Faculty

of

Rose-Hulman Institute of Technology

by

Matthew Scott Welmers

In Partial Fulfillment of the Requirements of the Degree

of

Master of Science in Chemistry

May 2016

©2016 Matthew Scott Welmers



ROSE-HULMAN INSTITUTE OF TECHNOLOGY

Final Examination Report

Matthew Welmers Chemistry
Name Graduate Major

Thesis Title Phosphonium/Phosphate Ionic Liquids as Lubricant Additives: The Synthesis and Testing
of Six Novel ILs

DATE OF EXAM:

EXAMINATION COMMITTEE:

Thesis Advisory Committee	Department
Thesis Advisor: Michael Mueller	CHEM
Rebecca DeVasher	CHEM
Allen White	ME

PASSED X

FAILED

ABSTRACT

Welmers, Matthew Scott

M.S. Chem

Rose-Hulman Institute of Technology

May 2016

Phosphonium/Phosphate Ionic Liquids as Lubricant Additives: The Synthesis and Testing of Six Novel ILs

Thesis Advisor: Dr. Michael Mueller

In this study, ionic liquids (ILs) are defined as ionic materials with a melting temperature $>100^{\circ}\text{C}$. ILs are characterized by their organic moieties which prevent crystallization, forcing the liquid phase. ILs are desirable as lubricant additives because of their ability to be fine-tuned by varying the identity of the cation/anion as well as the various organic functional moieties therein. Several novel phosphonium/phosphate ILs have been successfully synthesized via a simple, straightforward process. In this work a series of symmetric and asymmetric anionic phosphodiester are developed and coordinated with two asymmetric alkyl phosphonium cations. These ILs are tested in SAE 10W30 engine oil for their tribological performance in wear reduction. At a 5 wt.% loading, phosphonium/phosphate ILs can reduce wear by up to 65% of the base oil wear. The correlation between a variety of organic functional moieties and their relative lubricities in SAE 10W30 oil is demonstrated in this work.

Keywords: chemistry, ionic liquids, tribology

DEDICATION

This work is dedicated to those who have stood by me, helped me when I struggled, and never stopped believing in me. Specifically, this work is dedicated to Lou Johnson, my father Martin, and the members of my committee whom all were ready to patiently listen to my gripes, offer suggestions and help me celebrate my success. Thank you from the bottom of my heart.

ACKNOWLEDGEMENTS

I would like to thank the following people for whom without this would not exist: my family and friends for supporting me by listening to my complaints and troubles; Dr. Corey Trobaugh and Cummins, Inc. for funding the original project that inspired the current work, and Dr. Weatherman who mentored me through said project; my advisory committee which consists of Dr. Michael Mueller, Dr. Rebecca DeVasher and Dr. Allen White for their guidance and advice; Cyndi Erwin and Lou Johnson who have always been there for all kinds of support and encouragement; Dr. Azad Siahmakoun and the staff of the Department of Graduate Studies at Rose-Hulman; Patti Staggs and Shelly Conder; the professors in the Chemistry and Biochemistry Department; Michael Fulk from the machine shop; the Rose-Hulman Mechanical Engineering department for loaning me their tribometer; Alexander Lacrampe for providing much needed assistance with the glossary; and you, the reader, for taking time to read this thesis. Thanks.

TABLE OF CONTENTS

Contents

LIST OF FIGURES	iii
LIST OF TABLES	viii
LIST OF ABBREVIATIONS	ix
LIST OF SYMBOLS	x
GLOSSARY.....	xii
1. INTRODUCTION.....	1
2. BACKGROUND	5
3. DESCRIPTION OF THE MODEL.....	12
4. METHODS.....	15
4.1. General Synthesis of Asymmetric Phosphodiester	15
4.2. General Synthesis of Asymmetric Tetraalkylphosphonium Bromide	16
4.3. Ionic Liquid Synthesis	17
4.4. Tribological Sample Preparation	17
4.5. Modified Tribological Sample Preparation	18
4.6. Standard Tribological Test Method	18
4.7. General Synthesis of Symmetric Phosphodiester	19
4.8. Procedure for Viscosity Measurements	20
5. RESULTS	21
6. DISCUSSION	27
7. LIMITATIONS.....	33
8. CONCLUSIONS	35
9. FUTURE WORKS.....	37
LIST OF REFERENCES.....	40
APPENDICES	43
APPENDIX A: Cation and Anion Structures	44
APPENDIX B: Raw Tribological Data	47
APPENDIX C: Precursor Structures.....	52
APPENDIX D: Reprint Permissions	54
APPENDIX E: Radial Hardness Testing Data	55
APPENDIX F: NMR Spectra	57

LIST OF FIGURES

Figure	Page
<u>Figure 2.1: A schematic for the Spire Corporation’s SPI-Tribotester™ Model 500 reproduced from the technical manual.....</u>	6
<u>Figure 2.2: Zinc-dialkyl-dithiophosphate, ZDDP, a common anti-wear lubricant additive.....</u>	7
<u>Figure 2.3: SEM images of the worn cast iron surfaces lubricated by (a) PAO oil and (b) PAO+IL blend.....</u>	8
<u>Figure 2.4: (a, b) TEM imaging and (c) EDS element mapping on the cross-section of the near surface zone of a cast iron worn surface lubricated by PAO+IL(5%). b and c correspond to the red dash line box and blue dot line box marked on a, respectively.....</u>	9
<u>Figure 4.1: General Reaction Mechanism for Asymmetric Phosphodiester Synthesis.....</u>	16
<u>Figure 4.2: Synthesis of Trioctyl Tetraoctyl Phosphonium Bromide.....</u>	16
<u>Figure 4.3: General Ionic Liquid Synthesis.....</u>	17
<u>Figure 4.4: General Reaction Mechanism for Symmetric Phosphodiester Synthesis.....</u>	20
<u>Figure 4.5: A Cannon-Fenske Routine Viscometer for transparent liquids.....</u>	20
<u>Figure 5.1: Mass loss after 2 hours of wear with 2,000 g of weight.....</u>	23
<u>Figure 5.2: Mass loss of heated samples after 2 hours of wear with 2,000 g of weight.....</u>	23
<u>Figure 5.3: The difference in the average wear and standard deviation between the modified and original sample preparation.....</u>	24
<u>Figure 6.1: FT-IR spectrum of the heated and unheated 10W-30 base oil from the same bottle.....</u>	30
<u>Figure 9.1: Bis(dodecyl) phosphate, a symmetric phosphodiester attempted to be synthesized for this study.....</u>	37
<u>Figure 9.2: Bis(ethyl) phosphate, a symmetric phosphodiester attempted to be synthesized for this study.....</u>	37
<u>Figure 9.3: Bis(2-ethylphenyl) phosphate, a symmetric phosphodiester attempted to be synthesized for this study.....</u>	38
<u>Figure A.2: Trioctyl octadecyl phosphonium bromide, one of the cations synthesized in this study.....</u>	44
<u>Figure A.1: Trihexyl tetradecyl phosphonium bromide, one of the cations purchased for this study.....</u>	44
<u>Figure A.3: Bis(2-ethylhexyl)phosphate, one of the anions purchased for this study.....</u>	45
<u>Figure A.4: 2-ethylhexyl 2-phenylethyl phosphate, one of the anions synthesized for this study.....</u>	45
<u>Figure A.5: 2-ethylhexyl dodecyl phosphate, one of the anions synthesized for this study.....</u>	45

Figure	Page
<u>Figure A.6: 2-ethylhexyl ethyl phosphate, one of the anions synthesized for this study</u>	46
<u>Figure C.1: 1-bromooctadecane, a precursor to trioctyl octadecyl phosphonium bromide</u>	52
<u>Figure C.2: Trioctyl phosphine, a precursor to trioctyl octadecyl phosphonium bromide</u>	52
<u>Figure C.3: 2-phenylethanol, a precursor to 2-ethylhexyl 2-phenylethyl phosphate</u>	53
<u>Figure C.4: Dodecanol, a precursor to 2-ethylhexyl dodecyl phosphate</u>	53
<u>Figure C.5: Ethanol, a precursor to 2-ethylhexyl ethyl phosphate</u>	53
<u>Figure C.6: 2-ethylhexanol, a precursor to all phosphodiester synthesized in this study</u>	53
<u>Figure C.7: Phosphoryl chloride, a precursor to all phosphodiester synthesized in this study</u>	53
<u>Figure E.1: Disk tested for radial hardness of steel rod machined into remaining test disks.</u> .	55
<u>Figure F.1: ^1H NMR of 1-bromooctadecane in CDCl_3</u>	61
<u>Figure F.2: ^{13}C NMR of 1-bromooctadecane in CDCl_3</u>	62
<u>Figure F.3: ^1H NMR of trihexyl tetradecyl phosphonium bromide in CDCl_3</u>	63
<u>Figure F.4: ^{13}C NMR of trihexyl tetradecyl phosphonium bromide in CDCl_3</u>	64
<u>Figure F.5: ^{31}P NMR of trihexyl tetradecyl phosphonium bromide in CDCl_3</u>	65
<u>Figure F.6: ^1H NMR of Bis(2-ethylhexyl) phosphate in CDCl_3</u>	66
<u>Figure F.7: ^{13}C NMR of Bis(2-ethylhexyl) phosphate in CDCl_3</u>	67
<u>Figure F.8: ^{31}P NMR of Bis(2-ethylhexyl) phosphate in CDCl_3</u>	68
<u>Figure F.9: ^1H NMR of trioctyl phosphine in CDCl_3</u>	69
<u>Figure F.10: ^{13}C NMR of trioctyl phosphine in CDCl_3</u>	70
<u>Figure F.11: ^{31}P NMR of trioctyl phosphine in CDCl_3</u>	71
<u>Figure F.12: ^1H NMR of 2-ethylhexanol in CDCl_3</u>	72
<u>Figure F.13: ^{13}C NMR of 2-ethylhexanol in CDCl_3</u>	73
<u>Figure F.14: ^{31}P NMR of phosphoryl chloride in CDCl_3</u>	74
<u>Figure F.15: ^1H NMR of 2-phenyl ethanol in CDCl_3</u>	75
<u>Figure F.16: ^1H NMR of ethanol in CDCl_3</u>	76
<u>Figure F.17: ^{13}C NMR of ethanol in CDCl_3</u>	77
<u>Figure F.18: ^1H NMR of 1-dodecanol in CDCl_3</u>	78
<u>Figure F.19: ^{13}C NMR of 1-dodecanol in CDCl_3</u>	79
<u>Figure F.20: ^1H NMR of trioctyl octadecyl phosphonium bromide in CDCl_3</u>	80
<u>Figure F.21: ^{13}C NMR of trioctyl octadecyl phosphonium bromide in CDCl_3</u>	81

Figure	Page
<u>Figure F.22: ^{31}P NMR of trioctyl octadecyl phosphonium bromide in CDCl_3.....</u>	82
<u>Figure F.23: ^1H NMR of 2-phenylethyl 2-ethylhexyl phosphate in CDCl_3.....</u>	83
<u>Figure F.24: ^{13}C NMR of 2-phenylethyl 2-ethylhexyl phosphate in CDCl_3.....</u>	84
<u>Figure F.25: ^{31}P NMR of 2-phenylethyl 2-ethylhexyl phosphate in CDCl_3.....</u>	85
<u>Figure F.26: ^1H NMR of ethyl 2-ethylhexyl phosphate in CDCl_3.....</u>	86
<u>Figure F.27: ^1H NMR of ethyl 2-ethylhexyl phosphate in CDCl_3 between 0 and 2.5 ppm.....</u>	87
<u>Figure F.28: ^{13}C NMR of ethyl 2-ethylhexyl phosphate in CDCl_3.....</u>	88
<u>Figure F.29: ^{31}P NMR of ethyl 2-ethylhexyl phosphate in CDCl_3.....</u>	89
<u>Figure F.30: ^1H NMR of trihexyl tetradecyl phosphonium bis(2-ethylhexyl) phosphate in CDCl_3.....</u>	90
<u>Figure F.31: ^{13}C NMR of trihexyl tetradecyl phosphonium bis(2-ethylhexyl) phosphate in CDCl_3.....</u>	91
<u>Figure F.32: ^{31}P NMR of trihexyl tetradecyl phosphonium bis(2-ethylhexyl) phosphate in CDCl_3.....</u>	92
<u>Figure F.33: ^1H NMR of trihexyl tetradecyl phosphonium ethyl 2-ethylhexyl phosphate in CDCl_3.....</u>	93
<u>Figure F.34: ^{13}C NMR of trihexyl tetradecyl phosphonium ethyl 2-ethylhexyl phosphate in CDCl_3.....</u>	94
<u>Figure F.35: ^{31}P NMR of trihexyl tetradecyl phosphonium ethyl 2-ethylhexyl phosphate in CDCl_3.....</u>	95
<u>Figure F.36: ^1H NMR of trihexyl tetradecyl phosphonium 2-phenylethyl 2-ethylhexyl phosphate in CDCl_3.....</u>	96
<u>Figure F.37: ^{31}P NMR of trihexyl tetradecyl phosphonium 2-phenylethyl 2-ethylhexyl phosphate in CDCl_3.....</u>	97
<u>Figure F.38: ^1H NMR of trihexyl tetradecyl phosphonium dodecyl 2-ethylhexyl phosphate in CDCl_3.....</u>	98
<u>Figure F.39: ^{31}P NMR of trihexyl tetradecyl phosphonium dodecyl 2-ethylhexyl phosphate in CDCl_3.....</u>	99
<u>Figure F.40: ^1H NMR of trioctyl octadecyl phosphonium bis(2-ethylhexyl) phosphate in CDCl_3.....</u>	100
<u>Figure F.41: ^{13}C NMR of trioctyl octadecyl phosphonium bis(2-ethylhexyl) phosphate in CDCl_3.....</u>	101
<u>Figure F.42: ^{31}P NMR of trioctyl octadecyl phosphonium bis(2-ethylhexyl) phosphate in CDCl_3.....</u>	102

Figure	Page
<u>Figure F.43: ^1H NMR of trioctyl octadecyl phosphonium 2-phenylethyl 2-ethylhexyl phosphate in CDCl_3.....</u>	103
<u>Figure F.44: ^{31}P NMR of trioctyl octadecyl phosphonium 2-phenylethyl 2-ethylhexyl phosphate in CDCl_3.....</u>	104
<u>Figure F.45: ^1H NMR of trioctyl octadecyl phosphonium ethyl 2-ethylhexyl phosphate in CDCl_3.....</u>	105
<u>Figure F.46: ^{31}P NMR of trioctyl octadecyl phosphonium ethyl 2-ethylhexyl phosphate in CDCl_3.....</u>	106
<u>Figure F.47: ^1H NMR of trioctyl octadecyl phosphonium dodecyl 2-ethylhexyl phosphate in CDCl_3.....</u>	107
<u>Figure F.48: ^{31}P NMR of trioctyl octadecyl phosphonium dodecyl 2-ethylhexyl phosphate in CDCl_3.....</u>	108
<u>Figure F.49: ^1H NMR of ethyl 2-ethylhexyl phosphate in CDCl_3.....</u>	109
<u>Figure F.50: ^1H NMR of dodecyl 2-ethylhexyl phosphate in CDCl_3.....</u>	110
<u>Figure F.51: ^1H NMR of 2-phenylethyl 2-ethylhexyl phosphate in CDCl_3.....</u>	111
<u>Figure F.52: ^1H NMR of trioctyl octadecyl phosphonium bromide in CDCl_3.....</u>	112
<u>Figure F.53: ^1H NMR of trihexyl tetradecyl phosphonium bis(2-ethylhexyl) phosphate in CDCl_3.....</u>	113
<u>Figure F.54: ^1H NMR of trihexyl tetradecyl phosphonium dodecyl 2-ethylhexyl phosphate in CDCl_3.....</u>	114
<u>Figure F.55: ^1H NMR of trihexyl tetradecyl phosphonium ethyl 2-ethylhexyl phosphate in CDCl_3.....</u>	115
<u>Figure F.56: ^1H NMR of trihexyl tetradecyl phosphonium 2-phenylethyl 2-ethylhexyl phosphate in CDCl_3.....</u>	116
<u>Figure F.57: ^1H NMR of trioctyl octadecyl phosphonium bis(2-ethylhexyl) phosphate in CDCl_3.....</u>	117
<u>Figure F.58: ^1H NMR of trioctyl octadecyl phosphonium 2-phenylethyl 2-ethylhexyl phosphate in CDCl_3.....</u>	118
<u>Figure F.59: ^1H NMR of heated trihexyl tetradecyl phosphonium bis(2-ethylhexyl) phosphate in CDCl_3.....</u>	119
<u>Figure F.60: ^1H NMR of heated trioctyl octadecyl phosphonium bis(2-ethylhexyl) phosphate in CDCl_3.....</u>	120
<u>Figure F.61: ^1H NMR of heated trihexyl tetradecyl phosphonium 2-phenylethyl 2-ethylhexyl phosphate in CDCl_3.....</u>	121
<u>Figure F.62: ^1H NMR of heated trioctyl octadecyl phosphonium 2-phenylethyl 2-ethylhexyl phosphate in CDCl_3.....</u>	122

Figure	Page
<u>Figure F.63: ¹H NMR of heated trihexyl tetradecyl phosphonium ethyl 2-ethylhexyl phosphate in CDCl₃</u>	123
<u>Figure F.64: ¹H NMR of heated trioctyl octadecyl phosphonium ethyl 2-ethylhexyl phosphate in CDCl₃</u>	124
<u>Figure F.65: ¹H NMR of heated trihexyl tetradecyl phosphonium dodecyl 2-ethylhexyl phosphate in CDCl₃</u>	125
<u>Figure F.66: ¹H NMR of heated trioctyl octadecyl phosphonium dodecyl 2-ethylhexyl phosphate in CDCl₃</u>	126

LIST OF TABLES

Table	Page
<u>Table 5.1: Substituent alcohols, structures, and percent yields of novel phosphodiester synthesized for this study</u>	21
<u>Table 5.2: Name, formula and percent yield of ionic liquids synthesized for this study</u>	22
<u>Table 5.3: Number of trials performed for each sample tested by method of sample preparation</u>	25
<u>Table 5.4: Attempted Symmetric Phosphodiester of interest for this study</u>	25
<u>Table 5.5: Viscosity flow times of heated and unheated 10W-30 base oil from the same bottle</u>	26
<u>Table A.1: Molecular weights of all ionic liquids synthesized for this study</u>	47
<u>Table B.1: Raw tribological data from the base oil with average mass loss and standard deviation</u>	48
<u>Table B.2: Raw tribological data for 6~Bis/oil solution including average mass loss and standard deviation</u>	49
<u>Table B.3: Raw tribological data for 8~Bis/oil solution including average mass loss and standard deviation</u>	49
<u>Table B.4: Raw tribological data for 6~PhEt/oil solution including average mass loss and standard deviation</u>	50
<u>Table B.5: Raw tribological data for 8~PhEt /oil solution including average mass loss and standard deviation</u>	50
<u>Table B.6: Raw tribological data for 6~Dod/oil solution including average mass loss and standard deviation</u>	51
<u>Table B.7: Raw tribological data for 8~Dod/oil solution including average mass loss and standard deviation</u>	51
<u>Table B.8: Raw tribological data for 6~Et/oil solution including average mass loss and standard deviation</u>	52
<u>Table B.9: Raw tribological data for 8~Et/oil solution including average mass loss and standard deviation</u>	52
<u>Table E.1: HRC Hardness values at various distances from the center of the test disk</u>	56
<u>Table E.2: HRC Hardness tested at roughly equidistant points from the center hole in the approximate location of the wear scar</u>	57
<u>Table E.3: ASTM Hardness Value and Average Hardness Value of Disk Material measured between 0.3810" and 0.5476" from Disk Center</u>	57

LIST OF ABBREVIATIONS

ASTM	American Society of Testing and Materials
DI	DeIonized
EDS	Energy Dispersive x-ray Spectroscopy
EPA	Environmental Protection Agency
FT-IR	Fourier Transform InfraRed spectroscopy
IL	Ionic Liquid
NMR	Nuclear Magnetic Resonance spectroscopy
PAO	Poly Alpha (α) Olefin
RTIL	Room Temperature Ionic Liquid
SAE	Society of Automotive Engineers
SEM	Scanning Electron Microscope
TEM	Transmission Electron Microscopy
TLC	Thin Layer Chromatography
ZDDP	Zinc Dialkyl-DithioPhosphate

LIST OF SYMBOLS**Chemical Formulas**

H ₂ SO ₄	sulfuric acid
H ₃ PO ₄	phosphoric acid
KOH	potassium hydroxide
MgSO ₄	magnesium sulfate
NaOH	sodium hydroxide
Na ₂ SO ₄	sodium sulfate
POCl ₃	phosphoryl chloride

Chemical Symbols

C	carbon
Cl	chlorine
H	hydrogen
K	potassium
Mg	magnesium
Na	sodium
O	oxygen
P	phosphorous

Ionic Liquids

Bis ⁻	Bis(2-ethylhexyl) Phosphate
Dod ⁻	2-ethylhexyl Dodecyl Phosphate
Et ⁻	2-ethylhexyl Ethyl Phosphate

PhEt ⁻	2-ethylhexyl 2-phenylethyl Phosphate
6~	Trihexyl Tetradecyl Phosphonium
8~	Trioctyl Octadecyl Phosphonium
PF ₆ ⁻	Hexafluorophosphate
BF ₄ ⁻	Tetrafluoroborate
C ₄ min	Butylmethylimidazolium

Units

cSt	centiStokes
-----	-------------

GLOSSARY

- Alkyl/Alkylated** – Containing only carbon-carbon, and carbon-hydrogen single bonds
- Anion** – A negatively charged ion; the species attracted to the anode
- Aromaticity** – A cyclic, planar group of carbon atoms that exhibits unusual stability compared to similar groupings of atoms
- Asymmetric** – The presence of different groups beyond the central atom or group
- Cation** – A positively charged ion; the species attracted to the cathode
- Chain Length** – Number of carbon atoms involved in a linear chain
- Desiccator** – An air-tight flask filled with moisture absorbent materials for the purpose of creating a moisture free environment to dry samples
- Energy dispersive X-ray spectroscopy** – An analytical technique used to determine the elemental composition or chemical make-up of a sample via high energy x-rays
- Heteroatom** – Any atom in organic chemistry that is not carbon or hydrogen
- Heterogeneous** – The state of having multiple, distinct phases
- Homogeneous** – The state of having one continuous phase
- Ionic Liquid** – Any ionic compound that does not decompose or vaporize when heated beyond its melting temperature
- Ligand** – An atom, ion or functional group that donates one or more of its electrons to form a covalent bond with a central atom
- Melting Temperature** – The temperature at which the phase transition from the solid state to the liquid state takes place
- Miscibility** – The property of mixing in all possible proportions to create homogeneous mixtures
- NMR Spectroscopy** – A spectroscopic technique that is used to confirm structure through the rotation of isotopes
- Oil-miscible non corrosive anti-wear additive** – Any additive that is miscible with oil, does not corrode specific metal surfaces, and prevents surface wear
- Optical profilometer** – A noncontact instrument used to measure a surfaces profile, usually used to quantitatively determine surface roughness
- Organic Moiety** – A group that behaves similarly under similar conditions; a functional group

Phosphodiester – A molecule that has a phosphorous atom with one double bonded oxygen and three single bonded oxygen atom two of which are connected to a carbon atom

Phosphonium – A molecule that has a cationic phosphorous atom bonded to four carbon atoms

Room Temperature Ionic Liquids – Any ionic substance that has a melting temperature less than 100°C due to large, flexible organic groups on charged heteroatoms

Rotary evaporation – A technique used to remove solvent; an apparatus that rotates a sample at an elevated temperature under vacuum to remove undesirable solvent

Sonication – The use of high frequency sound waves to agitate a sample for the purpose of increased mixing

Symmetric – The presence of the same group beyond the central atom or group

Tachometer – An instrument designed to measure the rotational speed of a shaft powered by an engine

Transmission electron microscopy – An electron microscope technique that uses high energy electrons to produce high resolution images

Tribo-Layer – A measurable surface layer that prevents wear by lowering the friction; usually arises due to anti-wear additives in lubricants

Tribology – The study of sliding surfaces; a subset of mechanical engineering, chemical engineering, chemistry and material science

Tribometer – An instrument used to study tribology; an instrument that provides information about wear, friction and lubrication

Vacuum distillation – A process by which materials with lower boiling points are removed from the bulk with the aid of heat and vacuum

1. INTRODUCTION

In an effort to combat global climate change, the US government and the Environmental Protection Agency (EPA) adopted new regulations for the control of greenhouse gas emissions from fossil fuel burning engines [1]. Carbon dioxide (CO₂) is a greenhouse gas of major concern due to human emissions [2]. The new regulations impose stricter limits on the emission of CO₂ by creating higher benchmarks for fuel economy, or miles per gallon, of the engine. One method to increase efficiency of the engine is to change to a lubricant of lower viscosity, which allows the engine to run with less constraint. Low viscosity engine oils however, provide less wear protection and are of both interest and concern to engine manufacturers. This led to increased research into new anti-wear additives that can provide better protection than conventional additives currently on the market. One such family of anti-wear additives is ionic liquids (ILs). In recent years, research into ionic liquids as lubricant additives has dramatically increased as funding and popularity have also risen. In this chapter, the definition of ionic liquids, and their rationale for use as anti-wear additives will be presented while their suspected mechanism of action, the science of tribology, and how lubricants are tested for wear properties will be discussed in Chapter 2.

The simplest definition of an ionic liquid is a salt in the liquid state. A slightly more technical definition is any salt that melts without decomposing or vaporizing yields an ionic liquid. As this definition allows for salts like sodium chloride (NaCl) to be ionic liquids above their extremely high melting temperature like 801°C, scientists have redefined an arbitrary upper limit for melting temperature, frequently 100°C [3], [4]. For clarification, this class of salts and ionic liquids are often referred to as room temperature ionic liquids or RTILs. These RTILs have

low melting temperature due to their structure; a delocalized charge coupled with flexible organic moieties prevents regular crystallization at room temperature, forcing the liquid state.

While the origin and “discoverer” of the first IL is disputed, these earliest examples relied on a tetraalkyl substituted nitrogen as the cation with a nitrogen oxyanion [5], [6]. During the 1970s and 1980s, ILs were developed around this alkylated nitrogen moiety by using imidazolium and pyridinium cations with halide or tetrahalogenoaluminate as anions for battery applications [7], [8]. In 1992, Wilkes and Zaworotko synthesized ILs using anions like hexafluorophosphate (PF_6^-) and tetrafluoroborate (BF_4^-), which are weakly coordinating and considered ‘neutral’ [9]. One major advantage discovered about ionic liquids is that physical properties like viscosity, solubility, and melting point can be adjusted by changing the identity of the cation or anion. For example, butylmethylimidazolium hexafluorophosphate [C_4min][PF_6] is immiscible with water while butylmethylimidazolium tetrafluoroborate [C_4min][BF_4] is water soluble [10]. This tunability has resulted in a variety of uses for ionic liquids including electrochemical uses [7], [8].

While a significant amount of research has been performed for nitrogen based ionic liquids, a number of phosphonium cation-based ILs exist and are commercially available, but unfortunately, they are not being researched as heavily. Some of the earliest research regarding phosphonium cation-based ILs was published in the 1970s by Parshall [11]. In the 1980s, research was also published by Knifton et al. concerning the use of tetrabutylphosphonium bromide as an ionic solvent [12], [13], [14]. The struggle behind researching phosphonium cation-based ILs is the synthesis of their precursor phosphine. It was not until 1990 that tributylphosphine became commercially available on a large scale [15]. Since then, the increase in the number of commercially available precursor phosphines has allowed for an explosion of

phosphonium cation-based ILs to come to market. Published in 2008 by Fraser and MacFarlane, a review of phosphonium cation-based ILs listed over 44 commercially available ILs [16]. The availability of precursors resulted in a phosphonium cation-based IL being chosen for this study.

This study investigates if there is a link between the structures of phosphonium/phosphate ILs and their wear protection profiles. This is accomplished through careful synthesis of a series of cations and anions designed to investigate the structural moieties of length, bulkiness, and aromaticity. These cations and anions are then coordinated to form a total of 8 ILs, 6 of which are novel to the current literature base. These ILs are tested for compatibility in aftermarket SAE 10W-30 engine oil and after determining compatibility, tribology was used to determine their wear profiles. Based on the specifics of their wear profile, conclusions can be drawn about the relationship between the structure and functionality of phosphorous-based ILs as friction reduction additives.

Chapter 2 covers a review of the literature on phosphorus-based ILs pertinent to the study. This chapter also discusses the proposed tribological mechanism of action in the friction reducing qualities of phosphonium/phosphate ILs. This requires an understanding of tribology, which will also be presented in this chapter. Chapter 3 provides a justification of the choices in experimentation, instrumentation, and the design of experiments. While this chapter does not provide specifics on the experiments, it does provide an overview of the decisions made in regard to the synthesis of ionic liquids, the choice of side chains for the various phosphodiester synthesized, and an explanation of the instrument used in this study to gather the wear data.

Chapter 4 details the experiments and syntheses performed during this study. This includes the reaction conditions, the chemicals purchased and their usages, the exact details of

the tribological experiments performed, including sample preparation, standard test method, and a modified sample preparation procedure.

Chapter 5 is used to present the results of the aforementioned experiments in Chapter 4; the bulk of the raw data used to obtain these results is presented in Appendix B. This chapter will highlight any inconsistencies in presented values and provide a concise explanation for these inconsistencies. Chapter 5 will also provide a simple explanation of both the graphs and tables and the any data manipulation used therein. Chapter 6 discusses the significance of these results as they pertain to the relationship between structure and function. This chapter will be used to highlight the rationale behind modifying the standard tribological testing procedure as well as explain the results of this procedural modification, and their significance.

Chapter 7 offers insight into limitations of the system. The main purpose of this chapter is to provide validation of the data obtained and explain the limitations of the instrumentation. This chapter will also cover the results of some failed experiments and how these failures changed the results of this study. Chapter 8 ultimately offers some conclusions that can be drawn from the data obtained from this study.

Chapter 9 outlines potential future routes to continue studying these phosphorous-based ILs as fuel additives. Specifically, Chapter 9 will cover the possibility of studying symmetric phosphodiester to better understand the potential importance of asymmetric phosphodiester in wear prevention, among additionally discussed future routes for research.

2. BACKGROUND

Tribology is defined as the study of sliding surfaces. Due to the wide variety of complex interactions that occur at sliding surfaces or interfaces, tribology is an inherently multidisciplinary field that combines mechanical engineering, materials science and engineering, chemical engineering and chemistry, among other fields. Tribology is broken down into three main topics: friction, wear, and lubrication. Friction is defined as the resistance to movement, wear is defined as the loss of mass due to friction and lubrication is the use of materials to prevent both friction and, ultimately, wear [17]. One of the goals of tribology is to use lubricants to minimize friction and reduce wear. As friction occurs at every interface, objects with intricate moving parts, such as mechanical components, are most susceptible to wear. Simple mechanical components like hinges require simple lubrication such as grease, which usually contains long chain hydrocarbon oils mixed with soaps or other emulsifiers to create a semisolid lubricant. Rolling mechanical components like bicycle tires use ball bearings to reduce friction, as the coefficient of friction for rolling surfaces is much lower than for sliding surfaces. Extremely complex mechanical components, combustion engines for example, use a liquid lubricant that has the ability to flow around the moving components in order to lubricate the entire system.

In tribology, lubricants are tested using a tribometer. Tribometers work by creating wear between two surfaces. Tribometers can measure a variety of tribological quantities: coefficient of friction, friction force, and wear volume. Wear volume can be calculated either through imaging of the surface to determine volume lost or by determining the mass lost by measuring the difference between pre-trial and post-trial masses. Frequently, coefficient of friction and friction force are calculated based off readings provided from the tribometer. While tribometers

come in a wide variety of configurations, there are several key elements to all tribometer set-ups. The first feature common to all tribometer set-ups is the use of a pin, typically a ball bearing, and a flat testing surface placed in tangential contact that are allowed to move independently. This feature is essential as tribology is defined as the interactions between surfaces in motion. The configuration of each instrument is unique and this results in a diversity of instrument types; however, four main tribometers are commonly used. These are a four ball, pin on disk, block on ring, and bouncing ball tribometer. As the tribology in this study was performed using a pin on disk tribometer, this instrument set-up will be focused on herein.

Figure 2.1 shows the schematic for the pin on disk tribometer used in this study. This instrument is unique in that while most pin on disk tribometers feature a rotating disk, this instrument allows for the pin to rotate and holds the disk stationary. The load is attached to the

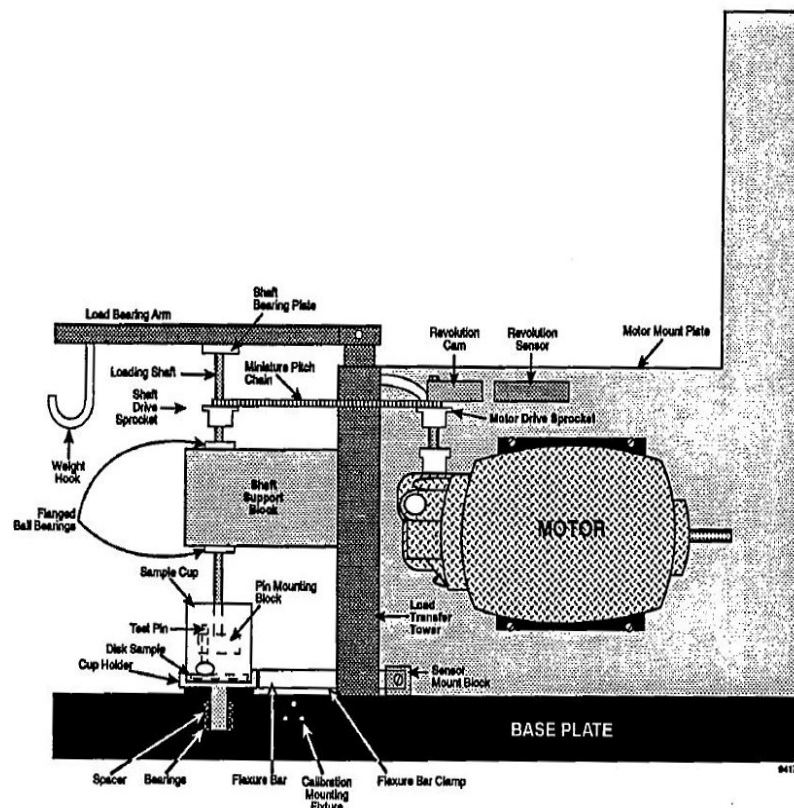


Figure 2.1: A schematic for the Spire Corporation's SPI-Tribotester™ Model 500 reproduced from the technical manual. Reprinted with permission. [50]

weight hook, which applies force to the load bearing arm and in turn transfers this load to the pin. The motor turns and ultimately allows the pin to move against the surface of the testing disk which has been submerged in the lubricant of interest. The tribometer displays a variety of information, including a tachometer and friction factor display. These can be used to calculate the coefficient of friction, in theory. Unfortunately, the instrument used in this study had damaged sensors and accurate data to calculate the coefficient of friction was unable to be collected.

As stated above in the introduction, ionic liquids have a variety of uses and one of these uses is as neat lubricants or lubricant additives [18], [19], [20]. The mechanism by which most anti-wear additives function is through the formation of nanometer thick surface depositions called tribo-layers. One of the current industry standard anti-wear additives is a zinc-based compound called zinc-dialkyl-dithiophosphate (ZDDP whose general structure can be found in Figure 2.2. The anti-wear mechanism of ZDDP is well documented [21]. ZDDP works to prevent wear by forming a layer on the metals surface that can be between tens to hundreds of nanometers thick [22]. A similar anti-wear mechanism has been demonstrated for ionic liquid additives recently. Work by Qu et al. has demonstrated the presence of IL tribo-layers on both ferrous and aluminum surfaces whose thickness, nanostructures and composition are dependent on material identity [23].

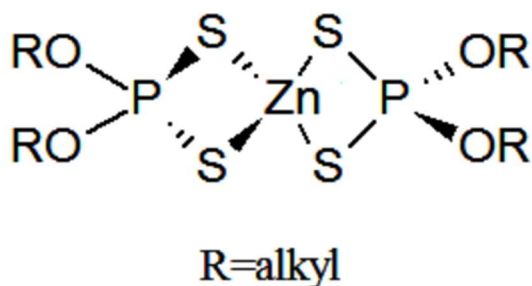


Figure 2.2: Zinc-dialkyl-dithiophosphate, ZDDP, a common anti-wear lubricant additive

Further evidence for the existence of tribo-layers as the anti-wear mechanism of phosphorous-based ILs was published by J. Qu, D.G. Bansal, and B. Yu et al. in 2012 [18]. In their work, after synthesizing 6~Bis, they tested its effectiveness as both an aftermarket anti-wear additive in 5W-30 oil, and as a standalone anti-wear additive in poly α -olefin (PAO) oil, each at a 5 wt% loading. The performance of the oil/IL solutions was compared to the base oil. The data showed that the initial wear rate for the pure PAO oil was stable; however, it quickly increased and proceeded to fluctuate for the remainder of the test. This behavior is indicative of a lubricant failure and ultimately surface scuffing damage. This damage is identifiable in a SEM image of the testing surface in Figure 2.3a as the flakey regions. In contrast, the blend of 6~Bis and the PAO oil demonstrates no such damage and the friction data supports the visual in Figure 2.3b. Most impressive is the fact that despite only having one ingredient, the friction data shows that the PAO-IL solution is just as effective as the baseline data from the SAE 5W-30 oil.

Through the use of transmission electron microscopy (TEM) and energy dispersive spectroscopy (EDS), the authors demonstrate that the presence of phosphorous in the wear scar is

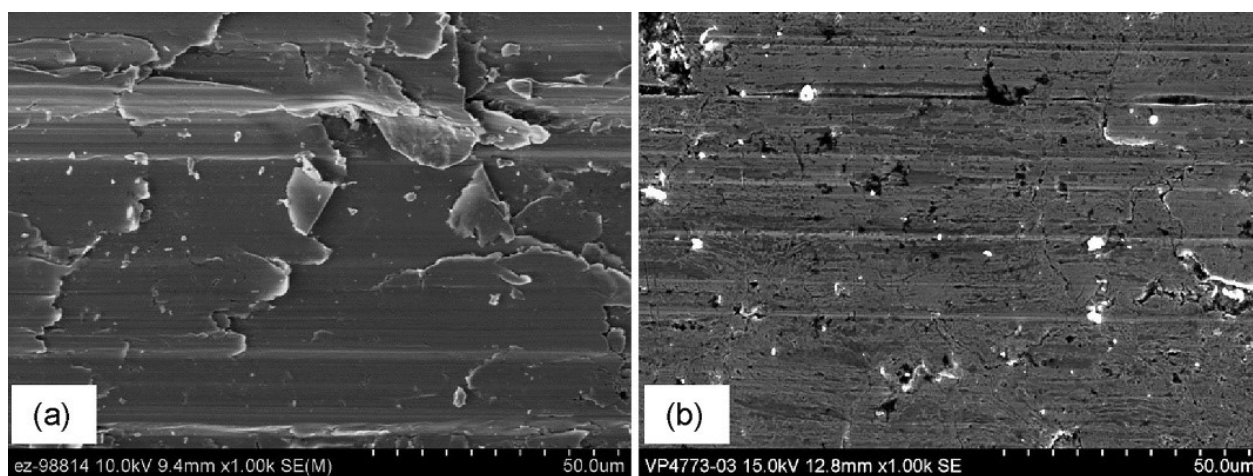


Figure 2.3: SEM images of the worn cast iron surfaces lubricated by (a) PAO oil and (b) PAO+IL blend. Reprinted with permission from “Antiwear Performance and Mechanism of an Oil-Miscible Ionic Liquid as a Lubricant Additive” Jun Qu et al. ACS Applied Materials & Interfaces 2012 4(2) 997-1002. Copyright 2012 American Chemical Society.

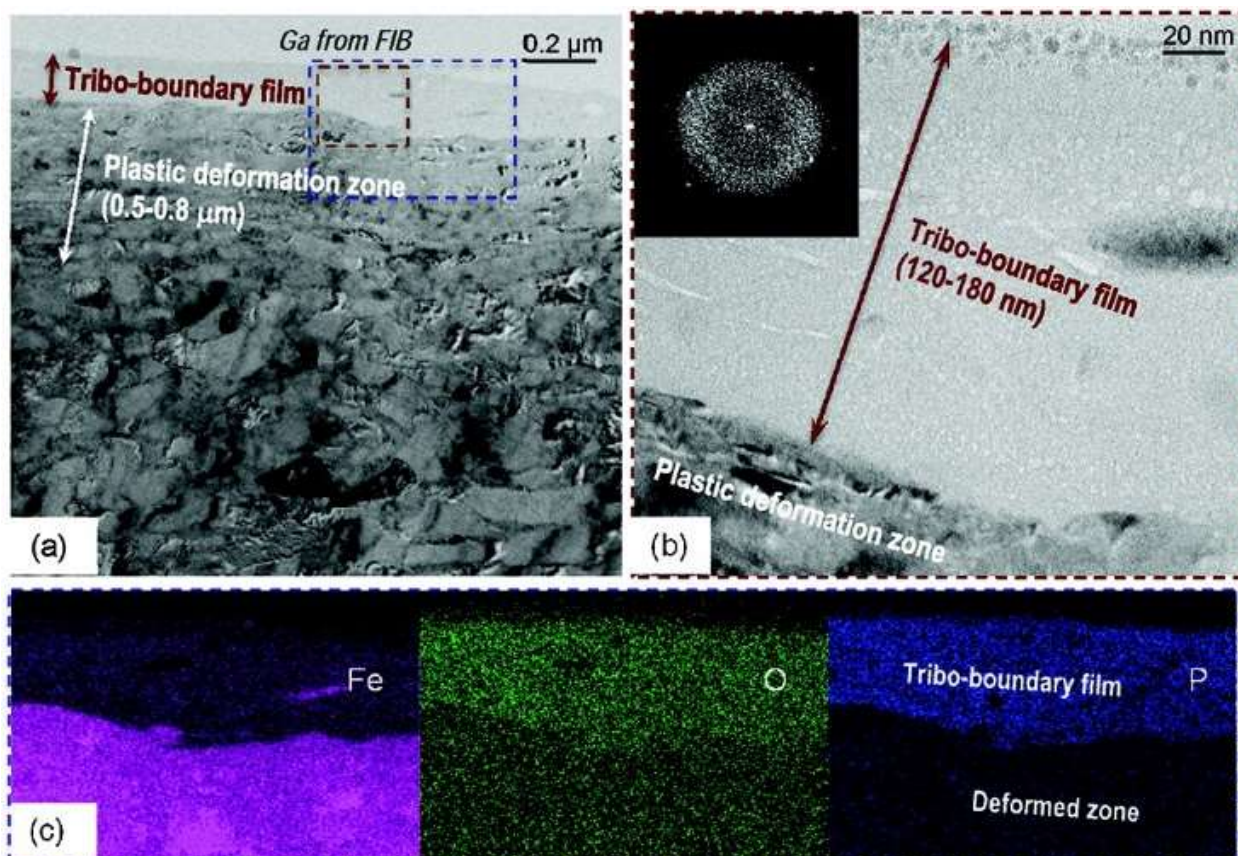


Figure 2.4: (a, b) TEM imaging and (c) EDS element mapping on the cross-section of the near surface zone of a cast iron worn surface lubricated by PAO+IL(5%). b and c correspond to the red dash line box and blue dot line box marked on a, respectively. Reprinted with permission from “Antiwear Performance and Mechanism of an Oil-Miscible Ionic Liquid as a Lubricant Additive” Jun Qu et al. ACS Applied Materials & Interfaces 2012 4(2) 997-1002. Copyright 2012 American Chemical Society.

due to the formation of a tribo-layer. The lack of phosphorous on the general surface is due to the need for thermochemical excitations to create a tribo-layer, a frequently observed phenomena [21], [22], [24]. Figure 2.4 shows the cross-sectional TEM and EDS elemental mapping for a cast iron sample lubricated with the PAO/IL blend. Similar images were captured for both the pure SAE 5W-30 as well as the SAE 5W-30/IL blend and ultimately the study was able to conclude that although the images have similarly structured layers, the layer thickness was dependent on the anti-wear additive present. They concluded that the tribo-boundary layer

increased in thickness in the following order, from thinnest to thickest: ZDDP, 6~Bis, both ZDDP and 6~Bis. The current hypothesis to explain the tribo-boundary layer trend is that the effectiveness of the IL is due to its ionic nature. While ZDDP requires either high contact pressures or increased temperatures to ionize, 6~Bis is already ionic and can more easily form the tribo-layer [21], [22], [24]. This is supported by the fact that the thickness of the layer formed from both ZDDP and 6~Bis is thicker than the sum of the layers formed by ZDDP and 6~Bis; however, it is important to know that this conclusion is drawn from cross-sectional graphs and might not represent the true average.

While the mechanism of lubrication of phosphorous-based ILs is well understood, the biggest challenge to their adaptation as anti-wear additives is their solubility in conventional non-polar lubricants. This insolubility has led some researchers to investigate phosphorous-based ILs in polar oils which frequently contain ester functionalities or are derived from vegetables. Somers et al. is working with a variety of polar oils including polyol esters, mineral oils, PAO oils, vegetable oils, and trimethylolpropanes [25]. Otero et al. have also been working with phosphorous-based ILs in ester based oils [26]. The importance of this research to this study is that the ionic liquids of this study are soluble in 10W-30 engine oil which is a non-polar oil.

An additional area of research for phosphorous-based ILs are as lubricants in extreme environments. Zhang et al. are studying the use of phosphonium cation-based ionic liquids as both neat lubricants and as additives for multialkylated cyclopentanes, which are used as lubricants for systems under vacuum [27]. A good potential use of these ILs is as lubricants for systems in space which experience both extremely low pressures and extremely low temperatures. The research of Weng et al. is exploring the other temperature extreme; they have

found phosphorous-based ILs can outperform current high temperature lubricants and have the ability to increase the performance of these high temperature lubricants [28]. These researchers are helping to show the versatility of phosphorous-based ILs and their importance in lubrication science.

3. DESCRIPTION OF THE MODEL

In an effort to better understand the relationship between the structure of the phosphonium/phosphate ionic liquid and its tribological performance, a unique set of structures were chosen. The first IL chosen was 6~Bis; the synthesis of which was published by Forsyth et al. as a potential corrosion mitigation agent for magnesium alloys [29]. In a study performed by Yu et al. 6~Bis was shown to have promise as an oil-miscible non-corrosive anti-wear additive [30]. This study chose to duplicate these results and use the bis(2-ethylhexyl) phosphate as a basis for the structure of the asymmetric phosphodiester synthesized in this study.

To gain a better understanding of the relationship between anion structure and tribological performance, three different alcohols were chosen based on their structure: ethanol, 2-phenylethanol and dodecanol. Ethanol provides a considerably shorter chain compared with 2-ethylhexanol; at the opposing end, dodecanol, containing 12 carbons, provides a significantly longer carbon chain. 2-phenylethanol introduces an aromatic ring while containing the same number of carbons as 2-ethylhexanol. The introduction of an aromatic ring is hypothesized to potentially help act as a ligand for the metal ions which are removed during the wear process. For these reasons, 2-phenylethanol was chosen as the source for an asymmetric phosphodiester.

With the anions chosen, a second cation was chosen for study, trioctyl octadecyl phosphonium. This cation is considerably larger in both molecular weight and carbon chain length. Kagimoto et al. not only published the synthesis of this cation but also observed a lower density, a lower viscosity and a lower water content with this particular cation [31]. This extra length should increase solubility in the oil, which has the potential to increase effectiveness due to the increased mobility of the ion in the oil. This increased mobility should allow the tribolayer

to form more easily demonstrating less wear. These properties resulted in trioctyl octadecyl phosphonium being chosen as the second cation of study.

While the cation and anion for the synthesis of 6~Bis are both commercially available for purchase, the remainder of the ionic liquids studied needed to be synthesized; the synthesis of both the cation, trioctyl octadecyl phosphonium bromide, and the remaining asymmetric phosphodiester is covered in Chapter 4. The final structures of the ionic liquids synthesized in this study can be found in Appendix A.

The choice of material for the tribological testing was the result of initial experimentation. The tribometer originally came with a set of aluminum disks which were used in an attempt to get the base oil wear. Unfortunately, the aluminum disks required a test time of 48 hours and provided no consistency in mass lost. After a consultation with Dr. Corey Trobaugh, a materials chemist working at Cummins, Inc., a decision was made to switch materials to a steel that had a hardness much less than that of the new set of steel ball bearings to be used as the pin. Dr. Trobaugh was contacted because the work that originally inspired this study was performed under his guidance.

Easy-to-machine 303 stainless steel was purchased from McMaster-Carr Supply Company and machined in the Rose-Hulman Mechanical Engineering machine shop. The older ball bearings previously used by the tribometer had started to degrade and were a source of concern, and so a new set of ball bearings, 10 mm in diameter, were purchased from McMaster-Carr Supply Company to act as pins. It is important to note that the variation of the hardness in the test region is comparable to the variation published in the ASTM G99-05(2010) standard under the characteristics of the interlaboratory wear test specimens [32]. This comparison is important as it allows for the variation of the data obtained from the instrument in this study to

be due to the randomness of the instrument and not the variation of the hardness of the test material. The ASTM standard also provides a standard method to perform tribological testing as well as standard methods to report data.

In order to ensure that the data gathered in this study is comparable, the surface hardness was measured. The data from the radial hardness testing of the disk material as well as the percent variations can be found in Appendix E. As shown in Table E.3 in Appendix E, the hardness variation as a percent of the whole measured value is similar to within 1%. This comparison of variations is made due to the difference in hardness scale used by the ASTM standard and this study. In conclusion, this similarity allows for the data presented in this study to be compared to data from other studies.

4. METHODS

In this section, the various methods and means through which the research was performed are presented. The general synthesis of an asymmetric phosphodiester, an asymmetric phosphonium bromide, coordination of an ionic liquid, tribological test sample preparation, and standard tribological test procedures are covered. Specific structures and results will be presented in the Results section; however, general reaction schemes will be presented here. All structures were confirmed with ^1H , ^{13}C , and ^{31}P NMR, where applicable. These spectra are reproduced in Appendix F. Chemicals were primarily purchased from Sigma-Aldrich; if a chemical was purchased from an alternate source the source will be named.

4.1 General Synthesis of Asymmetric Phosphodiesters

The following procedure was adopted from a patent by Ihara et al. [33]. In an appropriately sized round bottom flask, 1 molar equivalent of sodium acetate is dissolved in 50 mL of hexanes and cooled to 10°C . To this, 1 molar equivalent of POCl_3 was added with stirring. Afterwards, 1 molar equivalent of the first alcohol dissolved in 20 mL of hexanes is added using a dropping funnel. This solution is added over an hour while the reaction is kept at 10°C . After an hour, 1 molar equivalent of the second alcohol dissolved in 25 mL of hexanes is added with the dropping funnel and the reaction is stirred at 60°C for three hours. Upon completion, 1 molar equivalent of sodium hydroxide in 40 mL of DI water is added at 40°C ; 1 molar equivalent of $18\text{M H}_2\text{SO}_4$ in 10 mL of DI water is added and the reaction is stirred for 1 hour at 40°C . Once the pH has reached a value near 3, the reaction is transferred to a separatory funnel; the aqueous layer is removed and the organic layer is washed thrice with 40 mL of DI water each wash. The organic layer is then dried with sodium sulfate and the hexanes are removed with rotary evaporation. Yield and purity are determined. Figure 4.1 shows the general

reaction mechanism. In this figure, R-OH represents the first alcohol and R²-OH represents the second alcohol. The OH⁻ and H⁺ come from the NaOH and H₂SO₄ respectively.

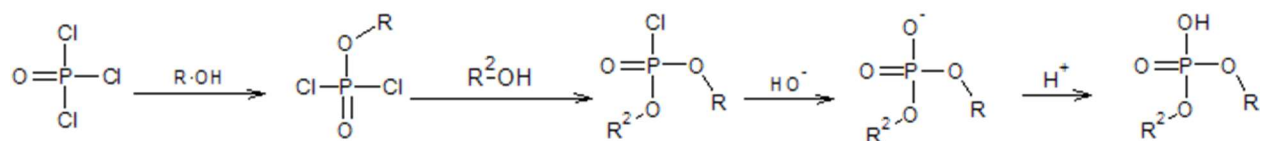


Figure 4.1: General Reaction Mechanism for Asymmetric Phosphodiester Synthesis

4.2 General Synthesis of Asymmetric Tetraalkylphosphonium Bromide

The following protocol was adopted from a paper by Ohno et al. [31]. To a 250 mL round bottom flask under a nitrogen atmosphere, 1 molar equivalent of 1-bromooctadecane was dissolved in 20 mL of toluene. To this, 1 molar equivalent of trioctyl phosphine was added via syringe, as phosphines are air sensitive. The reaction was allowed to stir at 100°C for 72 hours. This time was determined to be optimal by thin layer chromatography (TLC) stained with *p*-anisaldehyde. After 72 hours, the reaction solvent was removed by rotary evaporation at 50°C and rinsed with ~20 mL of hexanes to co-evaporate the toluene. After removing the hexanes, via rotary evaporation, the liquid product was recrystallized in 300 mL of hexanes. This was accomplished in a freezer to ensure the resulting phosphonium bromide is solid. After

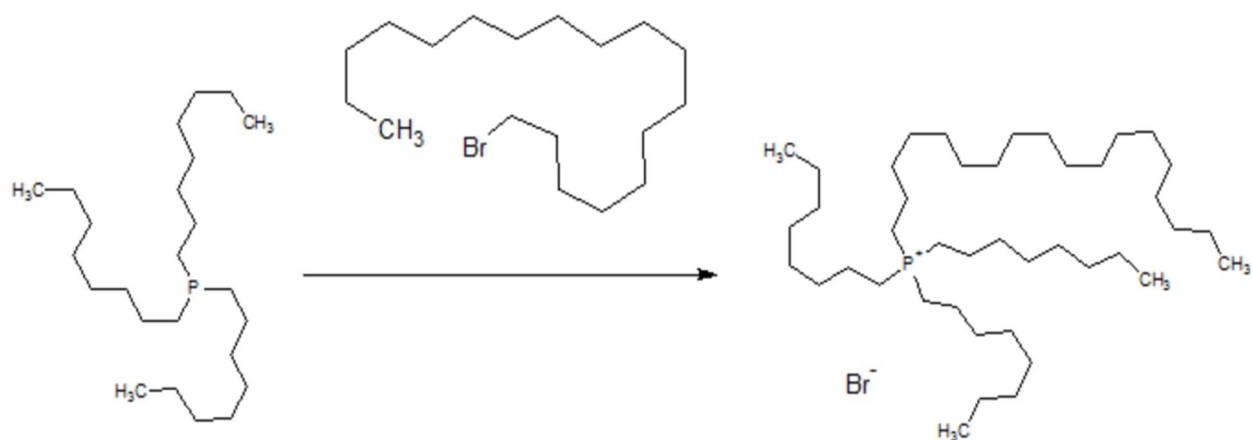


Figure 4.2: Synthesis of Trioctyl Tetraoctyl Phosphonium Bromide

completely recrystallizing, a white solid is obtained through vacuum filtration and rotary evaporation of any excess solvent. Yield is calculated and purity is determined. Figure 4.2 shows the reaction for the synthesis of the phosphonium bromide.

4.3 Ionic Liquid Synthesis

The following protocol was adapted from a paper by Forsyth et al. [29]. Equimolar amounts of desired cation and anion are dissolved by hexanes in a 250 mL round bottom flask. To this flask, an equimolar amount of KOH in 6 g of DI water is added dropwise via burette and stirred overnight to ensure complete mixing and coordination. The next day, the mixture is transferred to a separatory funnel and the organic layer is washed thrice with 40 mL of DI water each wash. The organic layer is dried with MgSO₄ and the hexanes are removed via rotary evaporation. Yield and purity are determined. If the NMR spectra indicate the presence of any hexanes or impurities they were removed via vacuum distillation using an ethanol/dry ice solvent trap. Figure 4.3 shows the general synthesis of an ionic liquid. The '+' indicates a separation of products or reactants while a space indicates coordination between two ionic species.

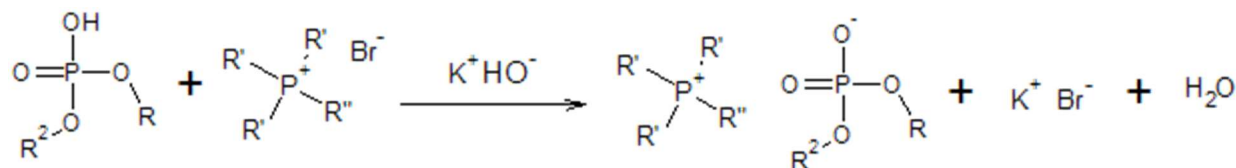


Figure 4.3: General Ionic Liquid Synthesis

4.4 Tribological Sample Preparation

Based on the work of Yu et al., 50 g of a 5% by weight solution of each ionic liquid in API Service SN ILSAC GF-5 SAE 10W30 engine oil provided by SuperTech™ were prepared [30]. 2.5 g of the ionic liquid of investigation was massed out in a glass container and 10W30 oil was added until a total mass of 50 g was obtained. The bottle was capped with a Teflon coated

lid and inverted several times to ensure mixing. The bottle was then sonicated for five minutes and set on a magnetic stir plate to stir overnight and while samples were being drawn for tribological testing.. A sample of pure 10W30 engine oil was prepared in this manner to act as a control

4.5 Modified Tribological Sample Preparation

A modified sample preparation method was developed after an initial round of experimentation. Similar to the sample preparation outlined in §4.4 Tribological Sample Preparation the samples were prepared in glass containers with Teflon coated lids. After 5 minutes of sonication, the sample was then heated with stirring for an hour at 100°C and left to stir overnight at room temperature. Likewise, a sample of pure oil was prepared in this manner and tested to provide a control. This procedure should be used in future sample preparation; the justification for this decision will be covered in Chapter 6.

4.6 Standard Tribological Test Method

A Spire Corporation SPI-Tribotester™ 500-S ball on disk tribometer was used for tribological measurements. The test disk material is Easy-to-Machine 303 stainless steel (Rockwell Hardness C of 15.7±4.3) purchased from McMaster Carr Supply Company and machined to specification by the Rose-Hulman Mechanical Engineering machine shop. The hardness of the disk material was measured radially on a sample of the bulk material; this raw data and data manipulation can be found in Appendix E. The ball bearings are E52100 alloy steel hardened 10 mm ball bearings (Rockwell Hardness C of 62), also purchased from McMaster-Carr Supply Company. The test disk was cleaned with hexanes using a paper towel and sonicated for 5 minutes in a water bath. After sonication, the test disk was dried with a clean

paper towel and placed in a desiccator for at least 5 minutes. When not in use, disks were stored in the desiccator to prevent oxidation from overexposure to moisture.

Prior to testing, the disk was removed from the desiccator and its mass was measured five times on a balance accurate to ± 0.0003 g. The disk was then loaded into the sample cup and placed into the cup holder. The appropriate ball bearing was placed into the pin holder and the entire disk was submerged in approximately 6 g of the lubricant of interest. The instrument was then set on an electrical timer to ensure the accuracy of each trial run time. The motor speed for each trial was set to 50 AU. Upon completion of each trial, the used lubricant was removed via disposable transfer pipette and disposed of according to local, state, and federal regulations. The test disk was again cleaned using hexanes, sonicated, placed in the desiccator, and re-weighed to determine a final mass. Mass loss was calculated based on the difference between the average of the pre- and post-trial masses.

4.7 General Synthesis of Symmetric Phosphodiester

The following procedure was adopted from a patent by Ihara et al. [33]. In an appropriately sized round bottom flask, 2.1 molar equivalents of sodium acetate is dissolved in 50 mL of hexanes and cooled to 10°C. To this solution, 2 molar equivalents of the desired alcohol are added. After reaching 10°C, 1 molar equivalent of POCl₃ is added and left to stir at 10°C for one hour and then at room temperature for 10 hours. Upon completion, 1 molar equivalent of 48% aqueous sodium hydroxide is added at 40°C, and the reaction is stirred for 30 minutes at 40°C. Afterwards, 1 molar equivalent of 18M H₂SO₄ in 10 mL of DI water is added, and the reaction is stirred for 2 hours at 90°C. Once the pH has reached a value near 3, the reaction is transferred to a separatory funnel; the aqueous layer is removed and the organic layer is washed thrice with 40 mL of DI water each wash. The organic layer is then dried with sodium

sulfate and the hexanes are removed with rotary evaporation. Yield and purity are determined.

Figure 4.4 shows the general mechanism for the symmetric phosphodiester synthesis.

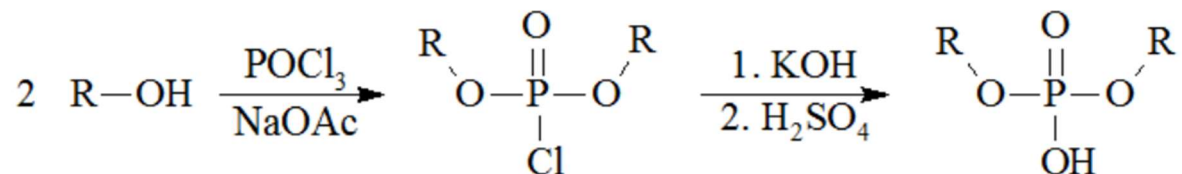


Figure 4.4: General Reaction Mechanism for Symmetric Phosphodiester Synthesis

4.8 Procedure for Viscosity Measurements

The viscosity measurements made in this study were taken using a Canon-Fenske glass capillary viscometer, a diagram of which is shown in Figure 4.5. Liquid is drawn up tube ‘N’ to

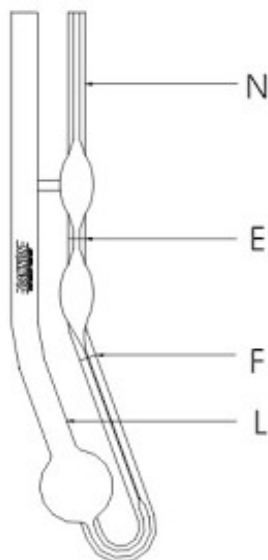


Figure 4.5: A Cannon-Fenske Routine Viscometer for transparent liquids [51]

mark ‘F’. The viscometer is then inverted and the liquid settles in the bulb at the bottom of tube ‘L’. During the test, the liquid of interest is drawn up past mark ‘E’ and the time required for the liquid to flow between mark ‘E’ and ‘F’ is recorded. The test was repeated five times to get an

average flow time which can be converted to viscosity by multiplying by a constant provided with the viscometer. The results of the viscometer testing are presented in Chapter 5

5. RESULTS

This chapter will focus solely on the results of the synthesis as well as the tribological testing; however, this chapter will not focus on the analysis of this data which be covered in Chapter 6. Table 5.1 lists the structures and percent yields of the three novel phosphodiester synthesized for this study. The synthesis, outlined in Figure 4.1, requires both an R-OH and R²-OH in the synthesis; however, in this study R-OH was always 2-ethylhexanol, whose structure can be found in Appendix C, regardless of the identity of R²-OH.

Table 5.1: Substituent alcohols, structures, and percent yields of novel phosphodiester synthesized for this study

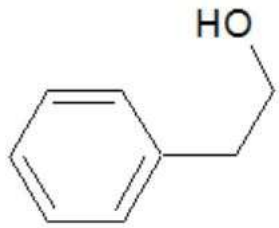
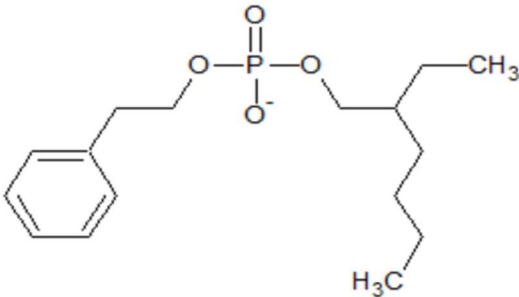

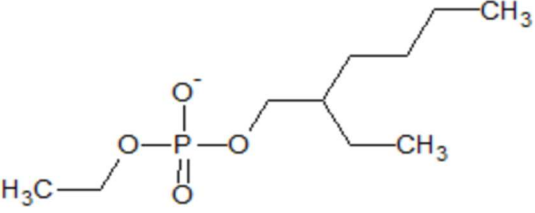
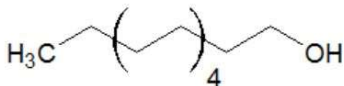
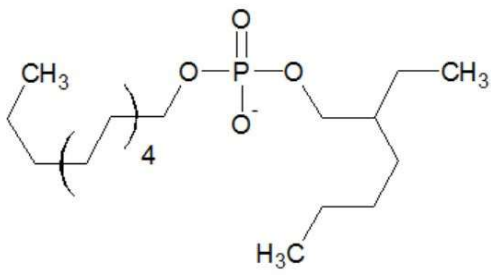
R ² -OH	Phosphodiester	Percent Yield
		88.91%
		71.12%
		89.41%

Table 5.2: Name, formula and percent yield of ionic liquids synthesized for this study

Name	Cation	Anion	Percent Yield
6~Bis	$P_{6,6,6,14}^+$	$Bis-PO_4^-$	93.51%
8~Bis	$P_{8,8,8,18}^+$	$Bis-PO_4^-$	83.54%
6~PhEt	$P_{6,6,6,14}^+$	$PhEt-PO_4^-$	87.22%
8~PhEt	$P_{8,8,8,18}^+$	$PhEt-PO_4^-$	70.85%
6~Dod	$P_{6,6,6,14}^+$	$Dod-PO_4^-$	82.36%
8~Dod	$P_{8,8,8,18}^+$	$Dod-PO_4^-$	49.47%
6~Et	$P_{6,6,6,14}^+$	$Et-PO_4^-$	69.65%
8~Et	$P_{8,8,8,18}^+$	$Et-PO_4^-$	84.55%

Table 5.2 lists the ionic liquids successfully synthesized for this study. The structures for these ionic liquids can be found in Appendix A. The yields for all the IL syntheses are quite high however, it is worth noting that the yield for the 8~Dod IL is rather low due to issues during isolation. The product appeared to crystallize in the hexanes and as a result got caught in the filter paper making isolation difficult. The yield calculated was a result of the amount of product isolated, but this does not reflect the true yield of the reaction which is likely to be near 75-85%.

Figure 5.1 shows the tribological data based on the sample preparation listed in §4.4. These data points represent the average of five to eight individual trials and their standard deviations; the data and a set of sample calculations can be found in Appendix B. After observing potential solubility issues and in an attempt to reduce the high standard deviation of some samples, the samples were then prepared using the method found in §4.5 and retested. Figure 5.6 shows the wear data for these samples. In an effort to better understand these results, the mathematical difference between the values in Figure 5.1 and Figure 5.6 is shown in Figure 5.2. The bars represent the differences in the mass loss calculated by subtracting the average of the heated samples from the samples prepared without heating while the points represent the difference in standard deviation calculated by the same method.

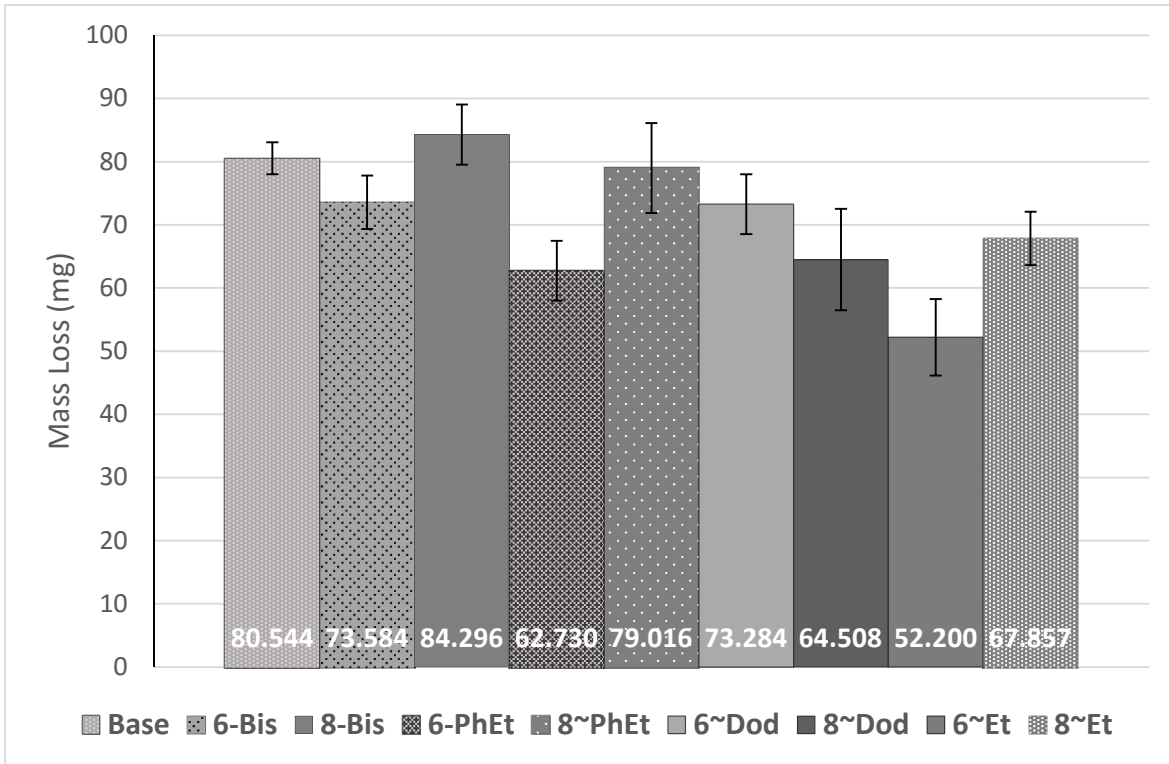


Figure 5.1: Mass loss after 2 hours of wear with 2,000 g of weight

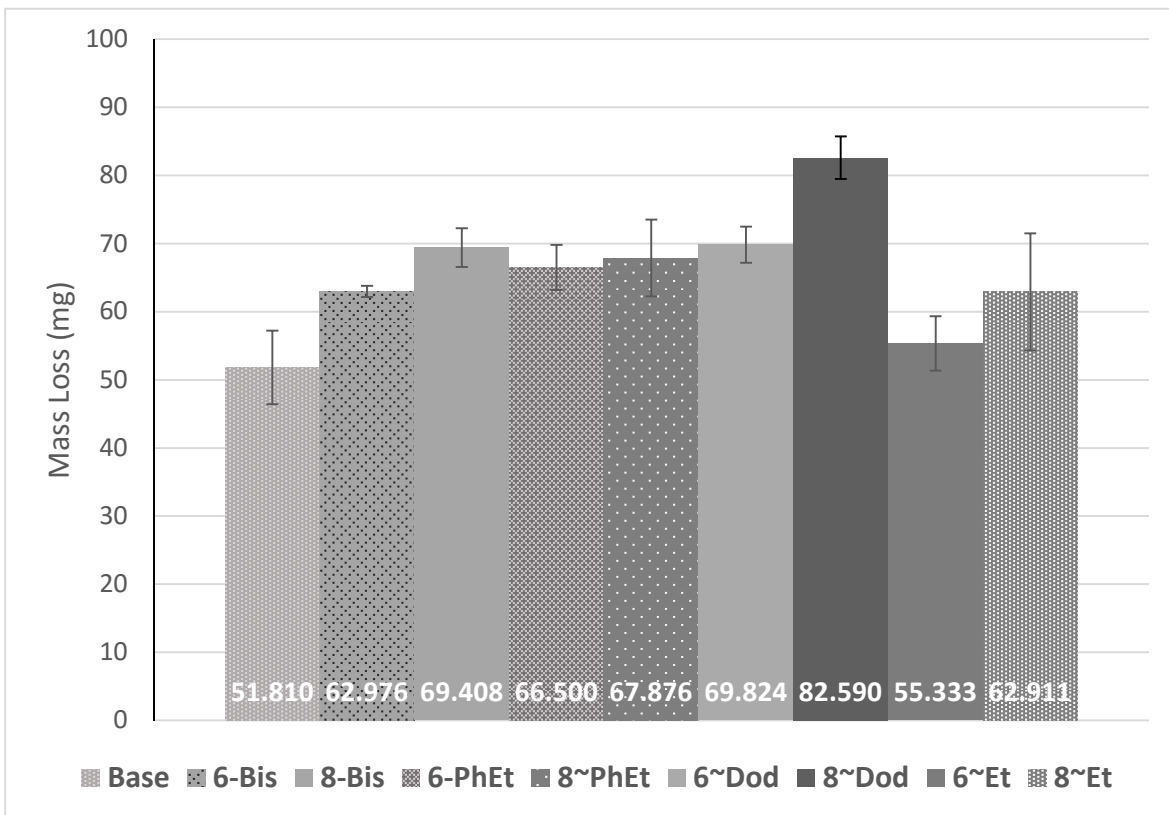


Figure 5.6: Mass loss of heated samples after 2 hours of wear with 2,000 g of weight

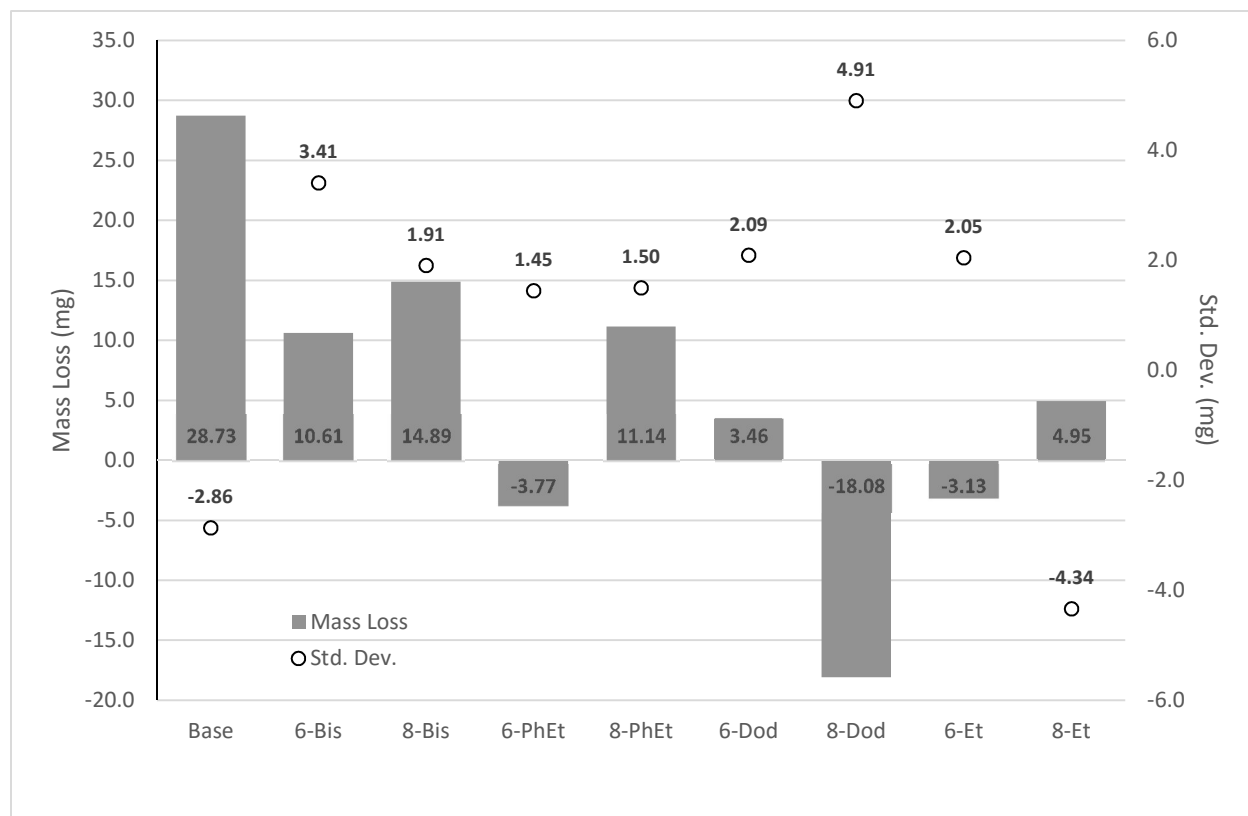


Figure 5.2: The difference in the average wear and standard deviation between the modified and original sample preparation

In Figure 5.2 a positive value represents the heating of the samples pretesting having a lower value than the corresponding unheated value. For the majority of the samples, this is the case; the notable exceptions are the average mass loss of the 6-PhEt, 6-Et, and 8-Dod samples and the standard deviation in the base oil and the 8-Et sample. Table 5.3 lists the number of trials performed for the various lubricant solutions investigated in this study. The raw data used to obtain this can be found in Appendix B tabulated by lubricant.

Table 5.4 lists the two symmetric phosphodiesteres whose synthesis was attempted for this study. Unfortunately, no identifiable product was isolated despite multiple attempts. This avenue of research was abandoned for this study and is explored in Chapter 9.

Table 5.5 lists the data from the viscosity measurements of the heated and unheated 10W-30 base oil. The time format is MM:SS.S±S.SS for the data included. The significance of this data is presented in Chapter 6.

Table 5.3: Number of trials performed for each sample tested by method of sample preparation

Sample	Number of Trials	
	Not heated	Heated
Base Oil	7	5
6~Bis	8	7
8~Bis	7	6
6~PhEt	8	7
8~PhEt	5	7
6~Dod	8	7
8~Dod	5	6
6~Et	5	6
8~Et	6	7
Average	6.56	6.44

Table 5.4: Attempted Symmetric Phosphodiester of interest for this study

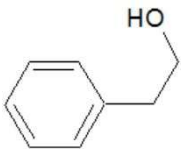
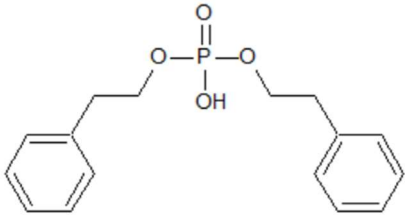
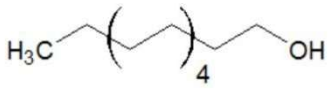
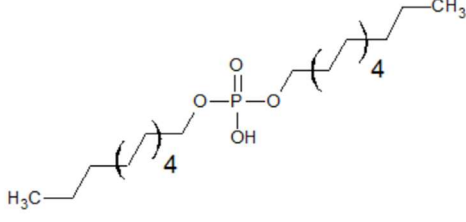
R-OH	Phosphodiester	Percent Yield
		0%
		0%

Table 5.5: Viscosity flow times of heated and unheated 10W-30 base oil from the same bottle

	Heated 10W-30	Unheated 10W-30
Trial 1	24:57.5	24:25.0
Trial 2	25:28.1	24:25.8
Trial 3	26:31.0	24:36.9
Trial 4	25:25.4	24:26.5
Trial 5	25:24.6	24:33.8
Average	25:33.3	24:29.6
Standard Deviation	3.996E-04	6.23925E-05

6. DISCUSSION

As demonstrated in Chapter 5, the yields of the asymmetric phosphodiester syntheses were quite high, each phosphodiester had a yield of 70% or greater. The ionic liquid synthesis also was high yield, with an average yield of about 80%. Previously mentioned was the exceptionally low yield of the 8~Dod, which is likely due to the solubility of the ionic liquid in the hexanes post ion coordination. This particular ionic liquid appeared to be solidifying in the hexanes after the separation of the organic and aqueous layer, prior to the final removal of the hexanes. Ultimately, the ionic liquid was able to be separated at the cost of much of the product being retained in the filter paper and not isolated. The actual yield of this synthesis is estimated to be closer to 75-85% rather than the 49% reported. After having successfully synthesized all eight ionic liquids, tribological testing was performed.

While the graphical representation of the tribological data can be found in Figure 5.1, Figure 5.6, and Figure 5.2 the actual data is located in Appendix B. It is important to notice that in both cases, the base oil and each oil/ionic liquid solution were tested according to the same methods. This was to ensure any effect observed was solely due to the ionic liquid being tested. During the first few trials, it became apparent that a tweak to the procedure was needed. Prior to the testing of the 8~PhEt solution, a single ball bearing had been used. As a result, the amount of variation among trials of the same IL grew quickly out of control. A potential explanation for this observation is that, as covered in the Chapter 2, ILs are effective as lubricants or lubricant additives due to the formation of a tribo-layer on the oxidized surfaces of the metals in contact. These surfaces would include both the testing disk as well as the ball bearing being used as a pin. As a result, the pin is likely to acquire a tribo-layer based on each IL being tested. In order to negate any effects of this beneficial layer, a new ball bearing was used for each new IL tested.

An interesting result of the first set of data is the shorter cation, trihexyl tetradecyl phosphonium, appeared to prevent more wear than the longer cation, trioctyl octadecyl phosphonium, in most cases. The notable exceptions to this observation is the pair of ILs with the dodecyl phosphate. In this case, the longer trioctyl octadecyl phosphonium demonstrated less wear than most of the other ILs tested. This result is inconsistent, as the other three trioctyl octadecyl phosphates showed more wear than their trihexyl tetradecyl counterparts. A potential explanation for this discrepancy is a potential concentration gradient arising from a nonhomogeneous solution.

In an effort to address this issue, a second sample preparation method was developed. After five minutes of sonication the solution is then heated with stirring for one hour at 100°C, and then left to stir at room temperature overnight. Research by Yu et al. has demonstrated that 6~Bis has a thermal stability up to 349°C based on thermal degradation data acquired from a thermogravimetric analysis of 6~Bis [30]. While the remaining ILs vary in structure compared to 6~Bis it is safe to assume that there is no thermal degradation after heating at 100°C for one hour. To verify this, samples of the various ionic liquids were heated for one hour at 100°C and ¹H NMR spectra were obtained. Using this new procedure, the ionic liquids were retested. The modified sample preparation resulted in the data presented in Figure 5.6. In this data set, the longer trioctyl octadecyl phosphonium showed more wear than its trihexyl tetradecyl phosphonium counterparts.

Using this data set, conclusions about the effect of the structure of the anion can also be drawn. Based on the fact that the ionic liquid which demonstrated the least wear is 6~Et, it can be concluded that the shorter the chain length, the less wear observed. This fact is further supported by the 6~Dod and 8~Dod having the highest wear among the set. The inclusion of an

aromatic ring does not appear to have a significant effect on the wear observed as both the 6~PhEt and 8~PhEt performed similarly to their Bis counterparts. This observation supports the hypothesis that the effectiveness of an asymmetric phosphodiester compared to the symmetric phosphodiester is related to the difference in the length of the carbon side chains.

In addition to providing information on the structure function relationship of ILs as lubricant additives, an analysis of the differences between the heated and unheated values highlights advantages that aren't immediately obvious in a visual comparison. The first of these advantages to heating the solution is the general decrease in the standard deviation of each data point. Of the eight ionic liquids tested, all but one showed a positive difference between their unheated values and their heated values; this positive value indicates that the heated samples had standard deviations that are less than their unheated counterparts. This conclusion is further supported by the fact that the average number of trials required for the heated method is less than the number of trials required for the unheated method. Table 5.3 lists the number of trials performed for each lubricant by sample preparation method.

An additional advantage displayed in Figure 5.6 is the average mass loss of five of the ILs studied also improves. This observation is likely due to the heated stirring creating a more homogeneous solution which results in the concentration being constant throughout the entire volume of the solution. This homogeneity results in the concentration of the samples from the first trial and the last trial being roughly equal. The reason that this is an issue is the viscosity of both the ionic liquid and the engine oil. The viscosity of the engine oil and the viscosity of the ionic liquids are both quite high at room temperature which leads to difficulty obtaining a homogeneous solution without the use of heat. While heated, the viscosity is lower which allows

for better mixing, creating a more homogenous solution. Ultimately this homogeneity leads to better data both in terms of the average mass loss value as well as the standard deviation.

One interesting unintended consequence of heating was the stark increase of the base oil performance. Initially, this was concerning as the heated trials were supplied from a new bottle of oil different than the previous unheated trials. As the remainder of the ionic liquid solutions performed comparably to their unheated counterparts this great increase in performance was confusing. One possible explanation is that the oil underwent a chemical degradation as a result of the extended exposure to heat. In an attempt to verify this, FT-IR spectroscopy was performed on the heated oil and a sample of oil from the same container that had not been heated. Figure 6.1 shows the resulting FT-IR spectrum. The lack of any additional peaks in the heated sample indicates that any potential chemical degradation is ultimately undetectable by FT-IR; this means that there must be another explanation for the increased performance.

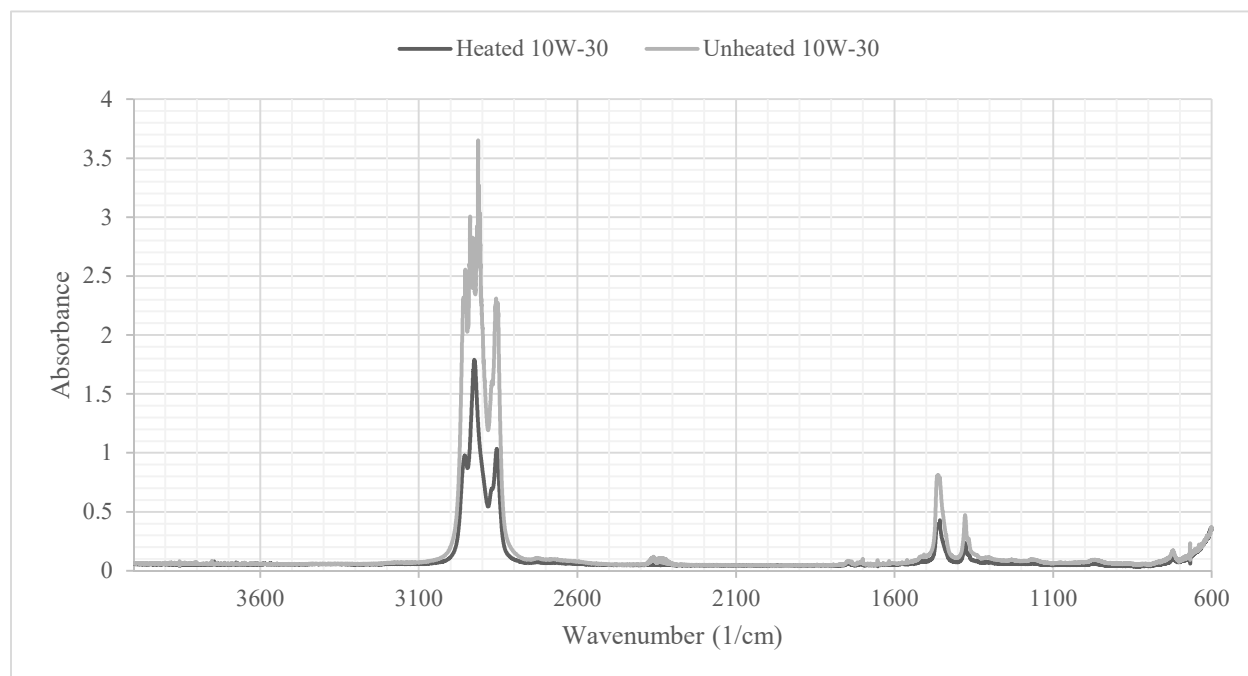


Figure 6.1: FT-IR spectrum of the heated and unheated 10W-30 base oil from the same bottle

As stated in Chapter 1, the effectiveness of a lubricant is related to the viscosity of the lubricant; the base oil for this study is a multi-grade oil meaning that it has a different viscosity at high temperatures than it does at lower temperatures. The advantage of multi-grade oils is, at startup, engines will have an oil that has the appropriate viscosity to reduce the amount of wear on the engine. As the engine heats up the oil's viscosity changes to accommodate the higher temperatures. This is valuable as the startup is where the majority of the wear on an engine occurs. For example, a 10W-30 engine oil performs at the viscosity of a 10W oil at startup and lower temperatures and performs at a viscosity of a 30W oil after startup.

It is important to mention that the viscosity testing for oil grading is done at 100°C, a temperature similar to that of the engine the oil will lubricate. The tribological testing performed in this study was performed at room temperature without much heat being generated; the ramifications of this will be covered in more detail in Chapter 7. Ultimately, the increased performance was due to a measurable change in viscosity at room temperature. Table 5.5 shows that the measured flow time varied by almost a minute and according to the viscometer manufacturer, this correlates to a 6.4 cSt difference in viscosity. This minor change in viscosity is likely negligible in the presence of an IL/oil solution viscosity which would explain the similarity in results between the heated IL/oil solutions and the unheated IL solutions. The causes of this difference in viscosity was not discovered however, a possible explanation is that the exposure to heat may have provided enough energy to allow ZDDP to begin to ionize. This ionization would have allowed it to form a tribo-layer and provide more protection than unionized ZDDP. This hypothesis is plausible as the MSDS of the oil used in this study lists ZDDP as an additive [34]. As this hypothesis was not tested, it can act as a potential future avenue of research. The remaining potential future directions will be discussed in Chapter 9.

7. LIMITATIONS

For this study, an instrument was provided from the Mechanical Engineering department at Rose-Hulman Institute of Technology. This instrument was designed by the Spire Corporation who unfortunately no longer makes tribometers. As the instrument used in this study is not current with industry standards, slight modifications to general procedures were required. One of these modifications was the average length of each test; while the industry standard is much shorter, the length of each test was approximately two hours which allowed for measurable wear to occur. An additional modification was the use of a high precision balance as opposed to the industry standard of using an optical profilometer to image the wear scar and determine the amount of material lost by volume. The lack of instrumentation current with industry standards resulted in the mass loss being the only obtainable piece of tribological data.

An additional consequence of the instrument used in this study being out of date was the need for an excess of multiple trials to acquire reasonable data. As the data in Appendix B can show, each ionic liquid mixture required at least five trials to provide a reasonable average with a standard deviation that is representative of the instrument. The maximum number of trials possible was calculated to be about 8 due to the volume of solution being made. This volume was based on the amount of each IL synthesized and if the percent yields or the synthetic scale of the ILs could be increased this number would also increase. The amount of IL available was also a major factor in the number of trials; the majority of solutions were made based off of a 50 g total weight however, the 8~Et solution that was heated had a total of 40 g due to limited supply of 8~Et.

As mentioned in the previous chapter, a major limitation is the temperature of the test. The average run temperature of most engines is much warmer than room temperature which is

the operating temperature of the tribometer. This means that while the tribological data can be used to make generalizations about the effectiveness of a lubricant additive, the tribometer used in this study cannot provide information on how a lubricant additive will perform at the run temperature of an average gasoline combustion engine. One potential method to understand how the additive will perform under heat is to obtain a thermogravimetric analysis (TGA) of the additive. In this test, a small sample of a material is placed on a delicate balance and is slowly heated to several hundred degrees. As it heats, it decomposes and loses mass; this mass difference is measured and reported as a percentage of the original mass. A TGA yields a graph with temperature on the x-axis and percent mass on the y-axis. Unfortunately, thermogravimetric analyses were not run on the ionic liquids in this study. This will be further discussed in Chapter 9.

8. CONCLUSIONS

As discussed in Chapter 1, the purpose of this study is to investigate the use of tetraalkylated phosphonium as cations and phosphodiester phosphates as anions in the formation of phosphorous-based ILs. To accomplish this, these ions were synthesized based on methods published in literature, their structures confirmed with spectroscopic techniques such as ^1H , ^{13}C and ^{31}P NMR, coordinated by ion exchange, isolated, weighed and dissolved into 10W-30 engine oil. These solutions were then tested for their wear prevention capabilities on a pin on disk tribometer provided by Spire.

The synthesis of the ionic liquids used in this study had yields between 49 and 93%. The synthesis of the precursor anions have a yield greater than 70% and the synthesis of the tetraalkylated phosphonium is almost 90%. These reactions are high yielding and can be optimized to be one-pot syntheses. They are soluble in commercial engine oil which allows their use as anti-wear additives. The literature has demonstrated the anti-corrosive capabilities of phosphorous-based ILs

After determining their wear prevention capabilities, some conclusions are able to be drawn. The first is the shorter trihexyl tetradecyl phosphonium cation consistently demonstrated less wear than the longer trioctyl octadecyl phosphonium. The identity of the cation appears to affect the anti-wear capabilities of the ionic liquid and this should be optimized for potential industrial use.

In addition to the cation identity, the anion identity is also important. This study found that the asymmetric 2-ethylhexyl ethyl phosphate anion performed better than the symmetric bis(2-ethylhexyl) phosphate, and the inclusion of the aromatic ring in the asymmetric 2-ethylhexyl 2-phenylethyl phosphate demonstrated no advantage over the symmetric bis(2-

ethylhexyl)phosphate. The first observation indicates that the asymmetric anion has an advantage over the symmetric anion while the second observation indicates that the size of the side chains, and not their identity, is what is important in the anti-wear capability of the IL. Additionally, the second observation indicates that coordination to the aromatic phenyl ring by the metal ion does not significantly contribute to the ILs performance.

Lastly, this study found that heating the ionic liquid/oil solutions provided the minimum standard deviation in wear data. This is important to the process of incorporating these ionic liquids in to the engine oil and any future preparations should be made according to that method. The importance of these conclusions will hopefully help guide research in using phosphorous-based ILs in the future. Understanding the relationship between structure and function will ultimately lead to more predictive work and a better understanding of the relationship between ionic liquids and their anti-wear properties.

The potential future avenues of this research are quite limitless as the field is relatively young. The majority of the future work of this study is in the area of optimization. The first of these would be to confirm the findings of this study on an instrument current with industry standards; this will help cement the findings of this study and pave the way for the future directions highlighted in Chapter 9.

9. FUTURE WORKS

After confirming the findings of this study the next area to research would be in the differences between the symmetric and asymmetric anions synthesized. This could allow a better understanding of the purpose of asymmetry and if asymmetric anions are more effective than symmetric anions. This would also allow any high performing anion to be used as a potential for the start of an asymmetric study based on one ester being that high performing group. The structures that this study attempted to synthesize are presented below in Figure 9.1, Figure 9.2, and Figure 9.3.

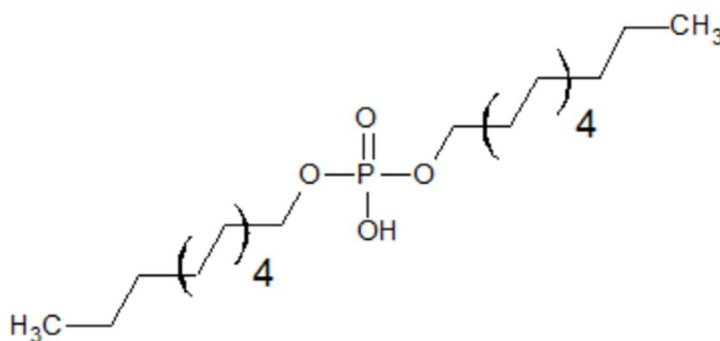


Figure 9.1: Bis(dodecyl) phosphate, a symmetric phosphodiester attempted to be synthesized for this study

The synthesis for these anions is presented in §4.7 however, as the results in Chapter 5 indicate, this synthesis was unsuccessful. The yields and identity of the products were not confirmed and the reaction conditions listed in §4.7 did not yield useable product. The future

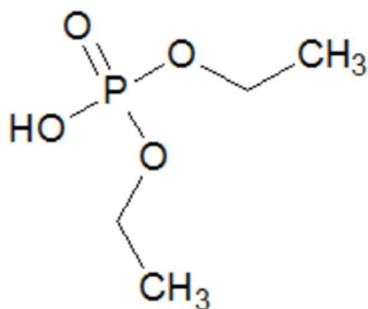


Figure 9.2: Bis(ethyl) phosphate, a symmetric phosphodiester attempted to be synthesized for this study

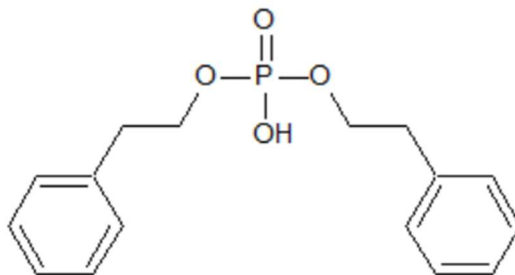


Figure 9.3: Bis(2-ethylphenyl) phosphate, a symmetric phosphodiester attempted to be synthesized for this study

work of this study would be to determine the exact reaction conditions for this synthesis and optimize them for maximum yield. Then, these structures could be synthesized and their effectiveness tested.

An additional route for future research would be to test the individual cations and anions as additives because they are technically ionic liquids. The tetraalkylated phosphonium bromides and the potassium phosphates are ionic liquids. Testing the cationic and anionic species separately allows for better understanding to their role in both the formation of the tribo-layer as well as the general importance of the phosphonium or the phosphate in the wear reduction mechanism. Beyond the information attainable about their roles in the wear reduction mechanism, these studies could also provide a platform to probe the possibilities of structure without performing coordination of each phosphorous-based ionic species into an IL. This would greatly speed the process of IL discovery and hopefully generate marketable additives that greatly improve the performance of engine oil and combustion engines.

Beyond the synthesis of new additives, the tribological data about the ILs synthesized in this study is functionally nonexistent. The viscosity, thermogravimetric analysis, coefficient of friction, melting point and decomposition point are all unknown. This data should be collected and published and is a probable future direction for this research. In addition to the 8 ILs

synthesized in this study, the phosphates and the tetraalkylated phosphonium bromide could also have this data gathered and published. This would help expand the potential feasibility of these ILs as additives in engine oil.

While this study focused on the usage of these ILs as additives in SAE 10W30 engine oil, they could also be used as neat lubricants. A possible future direction for this research could be studying these ILs as neat lubricants and determining if they have any potential to be valuable beyond being an additive. This potential could also be applied to their use as additives in lubricants beyond SAE 10W30 engine oil. As an example, diesel engines require a different type of oil and while these ILs have been tested in gasoline engine oil they could also be tested in diesel engine oil.

While the future routes outlined in this chapter represent some of the possible outcomes of furthering this research, there are others that were not mentioned. The best part about ILs is their versatility associated with changing the organic moieties and the identities of the cations and anions. This tunability is the greatest advantage to using ILs and while a most optimal set may exist, the only limiting factor in the exploration of ILs is the ability to synthesize them. This study has explored a convenient method to synthesize asymmetric phosphodiester for use as anions in ILs. While this method is not novel, this study demonstrates its effectiveness and will hopefully inspire additional research into phosphonium/phosphate ionic liquids as lubricant additives.

LIST OF REFERENCES

- [1] *2017 and Later Model Year Light-Duty Vehicle Greenhouse Gas Emissions and Corporate Average Fuel Economy Standards; Final Rule*; Federal Register; Environmental Protection Agency, Department of Transportation, National Highway Traffic Safety Administration: Washington, D.C., 2012.
- [2] Etheridge, D. M.; Steele, L. P.; Langenfelds, R. L.; Francey, R. J.; Barnola, J. -M.; Morgan, V. I. Natural and anthropogenic changes in atmospheric CO₂ over the last 1000 years from air in Antarctic ice and firn. *J. Geophys. Res., [Atmos.]* **1996**, *101* (D2), 4115-4128.
- [3] Freemantle, M. *An Introduction to Ionic Liquids*, 1st ed.; Royal Society of Chemistry Publishing: Cambridge, UK, 2010.
- [4] Welton, T. Room-Temperature Ionic Liquids. Solvents for Synthesis and Catalysis. *Chem. Rev.* **1999**, *99* (8), 2071-2083.
- [5] Walden, P. *Bull. Ada. Imper. Sci. (St. Petersburg)* **1914**, *1800*, 405-422.
- [6] Sugden, S.; Wilkins, H. CLXVII.—The parachor and chemical constitution. Part XII. Fused metals and salts. *J. Chem. Soc.* **1929**, No. 0, 1291-1298.
- [7] Chum, H. L.; Koch, V. R.; Miller, L. L.; Osteryoung, R. A. Electrochemical scrutiny of organometallic iron complexes and hexamethylbenzene in a room temperature molten salt. *J. Amer. Chem. Soc.* **1975**, *97* (11), 3264-3265.
- [8] Wilkes, J. S.; Levisky, J. A.; Wilson, R. A.; Hussey, C. L. Dialkylimidazolium chloroaluminate melts: a new class of room-temperature ionic liquids for electrochemistry, spectroscopy and synthesis. *Inorg. Chem.* **1982**, *21* (3), 1263-1264.
- [9] Wilkes, J. S.; Zaworotko, M. J. Air and water stable 1-ethyl-3-methylimidazolium based ionic liquids. *J. Chem. Soc.* **1992**, *Chem. Commun.* (13), 965-967.
- [10] Davis, Jr., J. H.; Fox, P. A. From curiosities to commodities: ionic liquids begin the transition. *Chem. Commun.* **2003**, 1209-1212.
- [11] Parshall, G. W. Catalysis in molten salt media. *J. Am. Chem. Soc.* **1972**, *94* (25), 8716-8719.
- [12] Knifton, J. F. Ethylene-glycol from synthetic gas via ruthenium melt catalysis. *J. Am. Chem. Soc.* **1981**, *103* (13), 3959-3961.
- [13] Knifton, J. K. Syngas reactions. 11. The ruthenium melt catalyzed oxonation of internal olefins. *J. Mol. Catal.* **1987**, *43* (1), 65-78.
- [14] Knifton, J. F. Syngas reactions. 13. The ruthenium melt-catalyzed oxonation of terminal olefins. *J. Mol. Catal.* **1988**, *47* (1), 99-116.
- [15] Bradaric, C. J.; Kennedy, C.; Robertson, A. J.; Zhou, Y.; Downard, A. Industrial preparation of phosphonium ionic liquids. *Green Chem.* **2003**, *5* (2), 143-152.
- [16] Fraser, K. J.; MacFarlane, D. R. Phosphonium-Based Ionic Liquids: An Overview. *Aust. J. Chem.* **2009**, *62*, 309-321.
- [17] Martini, A. Fundamental Tribology. <http://faculty2.ucmerced.edu/amartini/tribology.shtml> (accessed February 9, 2016).

- [18] Qu, J.; Bansal, D. G.; Yu, B.; Howe, J. Y.; Luo, H. M.; Dai, S.; Li, H. Q.; Blau, P. J.; Bunting, B. G.; Mordukhovich, G.; Smolenski, D. J. Antiwear Performance and Mechanism of an Oil-Miscible Ionic Liquid as a Lubricant Additive. *ACS Appl. Mater. & Interfaces* **2012**, *4* (2), 997-1002.
- [19] Bermudez, M.-D.; Jimenez, A.-E.; Sanes, J.; Carion, F.-J. Ioinic Liquids as Advanced Lubricant Fluids. *Molecules* **2009**, *14*, 2888-2908.
- [20] Kondo, Y.; Koyama, T.; Tsuboi, R.; Nakano, M.; Miyake, K.; Sasaki, S. Tribological Performance of Halogen-Free Ionic Liquids as Lubricants of Hard Coatings and Ceramics. *Tribol. Lett.* **2013**, *51* (2).
- [21] Nicholls, M. A.; Do, T.; Norton, P. R.; Kasrai, M.; Bancroft, G. M. Review of the lubrication of metallic surfaces by zinc dialkyl-dithiophosphates. *Tribol. Int.* **2005**, *38* (1), 15-39.
- [22] Qu, J.; Blau, P. J.; Howe, J. Y.; Meyer III, H. M. Oxygen diffusion enables anti-wear boundary film formation on titanium surfaces in zinc-dialkyl-dithiophosphate (ZDDP)-containing lubricants. *Scr. Mater.* **2009**, *60* (10), 886-889.
- [23] Qu, J.; Truhan, J. J.; Dai, S.; Luo, H. M.; Blau, P. J. Lubricants or Lubricant Additives Composed of Ionic Liquids Containing Ammonium Cations. 7,754,664, July 13, 2010.
- [24] Qu, J.; Chi, M.; Meyer III, H. M.; Blau, P. J.; Dai, S.; Luo, H. Nanostructure and Composition of Tribo-Boundary Films Formed in Ionic Liquid Lubrication. *Tribol. Lett.* **2011**, *43* (2), 205-211.
- [25] Somers, A. E.; Khemchandani, B.; Howlett, P. C.; Sun, J.; MacFarlane, D. R.; Forsyth, M. Ionic Liquids as Antiwear Additives in Base Oils: Influence of Structure on Miscibility and Antiwear Performance for Steel on Aluminum. *ACS Appl. Mater. & Interfaces* **2013**, *5*, 11544-11553.
- [26] Otero, I.; Lopez, E. R.; Reichelt, M.; Villanueva, M.; Salgado, J.; Fernandez, J. Ionic Liquids Based on Phosphonium Cations As Neat Lubricants or Lubricant Additives for a Steel/Steel Contact. *ACS Appl. Mater. & Interfaces* **2014**, *6*, 13115-13128.
- [27] Zhang, S. W.; Hu, L.; Qiao, D.; Feng, D.; Wang, H. Vacuum tribological performance of phosphonium-based ionic liquids as lubricants and lubricant additives of multialkylated cyclopentanes. *Tribol. Int.* **2013**, *66*, 289-295.
- [28] Weng, L.; Lui, X.; Liang, Y.; Xue, Q. Effect of tetraalkylphosphonium based ionic liquids as lubricants on the tribological performance of steel-on-steel system. *Tribol. Lett.* **2007**, *26* (1).
- [29] Sun, J.; Howlett, P. C.; MacFarlane, D. R.; Lin, J.; Forsyth, M. Synthesis and physical property characterisation of phosphonium ionic liquids based on P(O)2(OR)2 and P(O)2(R)2 anions with potential application for corrosion mitigation of magnesium alloys. *Electrochim. Acta* **2008**, *54*, 254-260.
- [30] Yu, B.; Bansal, D. G.; Qu, J.; Sun, X.; Luo, H.; Dai, S.; Blau, P. J.; Bunting, B. G.; Mordukhovich, G.; Smolenski, D. J. Oil-miscible and non-corrosive phosphonium-based ionic liquids as candidate lubricant additives. *Wear* **2012**, *289*, 58-64.
- [31] Kagimoto, J.; Taguchi, S.; Fukutomo, K.; Ohno, H. Hydrophobic and low-density amino acid ionic liquids. *J. Mol. Liq.* **2010**, *153*, 113-138.

- [32] ASTM Standard G99-05, 2. "Standard Test Method for Wear Testing with a Pin-on-Disk Apparatus"; ASTM International: West Conshohocken, PA, 2010.
- [33] Ihara, T.; Yano, S.; Kita, K. Process for Producing Phosphoric Esters. 5,565,601, Oct 15, 1996.
- [34] *SuperTech Motor Oil, SAE 10W-30*; Safety Data Sheet; CITGO Petroleum Corporation: Houston, TX, 2014.
- [35] Song, Z.; Liang, Y.; Fan, M.; Zhou, F.; Liu, W. Lithium-based ionic liquids as novel lubricant additives for multiply alkylated cyclopentanes (MACs). *Friction* **2013**, *1* (3).
- [36] Zhang, L.; Feng, D. P.; Xu, B.; Liu, X. Q.; Liu, W. M. The friction and wear characteristics and lubrication mechanism of imidazole phosphate ionic liquid. *Science in China Series E: Technological Sciences* **2009**, *52* (5).
- [37] Parshall, G. W.; Shive, L. W.; Cotton, F. A. Phosphine Complexes of Rhenium. In *Inorganic Synthesis*; MacDiamrid, A. G., Ed.; John Wiley & Sons, Inc.: Hoboken, 1977; Vol. 17.
- [38] Jimenez, A. E.; Bermudez, M. D.; Iglesias, P.; Carrion, F. J.; *Wear* **2006**, *260*, 766-782.
- [39] Jimenez, A. E.; Burmunde, M. D. *Wear* **2008**, *265*, 787-798.
- [40] Ye, C. F.; Liu, W. M.; Chen, Y. X.; Yu, L. G. Room Temperature ionic liquids: A kind of novel versatile lubricant. *Chem. Commun.* **2001**, No. 21, 2244-2245.
- [41] Rafiee, F.; Hajipour, A. R. Basic Ionic Liquids. A short review. *J. Iranian Chem. Soc.* **2009**, *6* (4).
- [42] Qu, J.; Truhan, J. J.; Dai, S.; Luo, H. M.; Blau, P. J. *Tribol. Lett.* **2006**, *22*, 207-214.
- [43] Pensado, A. S.; Comunas, M. J. P.; Fernandez, J. The Pressure-Viscosity Coefficient of Several Ionic Liquids. *Tribol. Lett.* **2008**, *31* (2).
- [44] Mu, Z.; Liu, W.; Zhang, S.; Zhou, F. Functional Room-temperature Ionic Liquids as Lubricants for an Aluminum-on-Steel System. *Chem. Lett.* **2004**, *33* (5), 524-525.
- [45] Minami, I.; Inada, T.; Sasaki, R.; Nanao, H. Tribo-Chemistry of Phosphonium-Derived Ionic Liquids. *Tribol. Lett.* **2010**, *40* (2), 225-235.
- [46] Lu, R. G.; Nanao, H.; Kobayashi, K.; Kubo, T.; Mori, S. Effect of Lubricant Additives on Tribochemical Decomposition of Hydrocarbon Oil on Nascent Steel Surfaces. *J. Jpn. Pet. Inst.* **2010**, *53* (1), 55-56.
- [47] Qu, J.; Blau, P. J.; Dai, S.; Luo, H. M.; Meyer III, H. M. Ionic Liquids as Novel Lubricants and Additives for Diesel Engine Applications. *Tribol. Lett.* **2009**, *35* (3), 181-189.
- [48] Totolin, V.; Minami, I.; Gabler, C.; Brenner, J.; Dorr, N. Lubrication Mechanism of Phosphonium Phosphate Ionic Liquid Additive in Alkylborane-Imidazole Complexes. *Tribol. Lett.* **2014**, *53* (2).
- [49] Somers, A. E.; Howlett, P. C.; Sun, J.; MacFarlane, D. R.; Forsyth, M. Transition in Wear Performance for Ionic Liquid Lubricants under Increasing Load. *Tribol. Lett.* **2010**, *40* (2).
- [50] *A Technical Manual for: SPI TRIBOTESTEER(TM) MODEL 500 WEAR/FRICTION TESTING APPARATUS*; Technical Manual; SPIRE Corporation: Bedford, MA.

[51] *Instructions for the use of The Cannon-Fenske Routine Viscometer*; Cannon Instrument Company: State College, PA, 2004.

APPENDICES

APPENDIX A: Cation and Anion Structures

Appendix A shows the various structures of the ions used to synthesize the ionic liquids investigated in this study. Figure A.1 and Figure A.2 are the two cations used in this study,

$P_{6,6,6,14}^+ Br^-$ and $P_{8,8,8,18}^+ Br^-$ respectively.

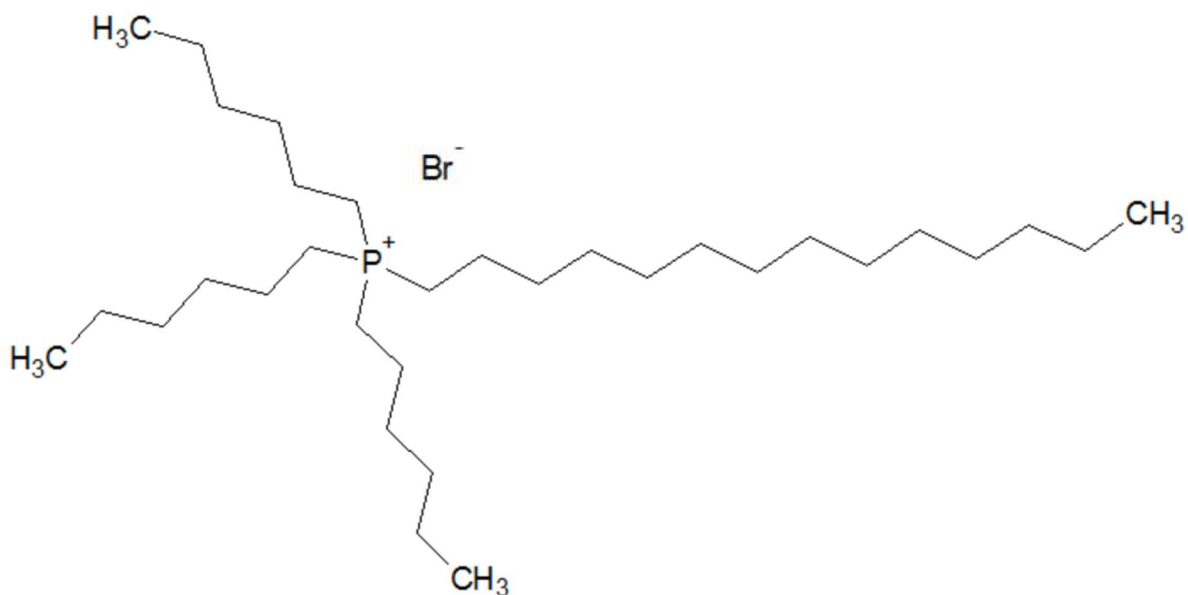


Figure A.1: Trihexyl tetradecyl phosphonium bromide, one of the cations purchased for this study

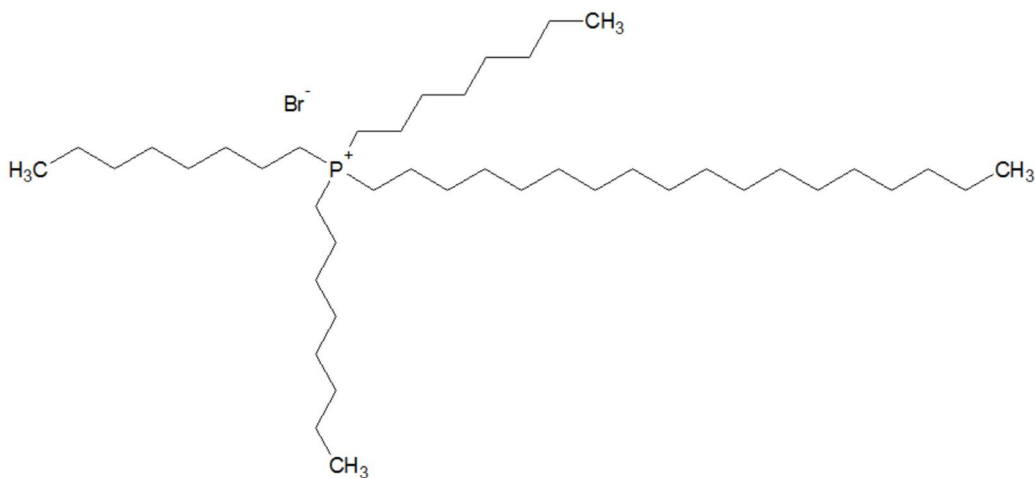


Figure A.2: Trioctyl octadecyl phosphonium bromide, one of the cations synthesized in this study

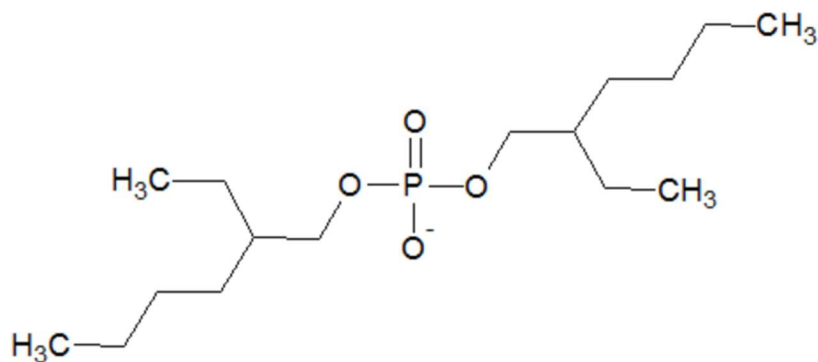


Figure A.3: Bis(2-ethylhexyl)phosphate, one of the anions purchased for this study

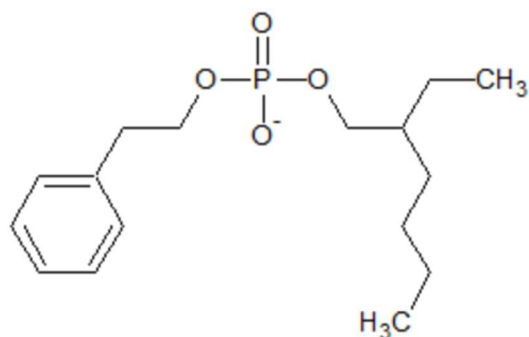


Figure A.4: 2-ethylhexyl 2-phenylethyl phosphate, one of the anions synthesized for this study

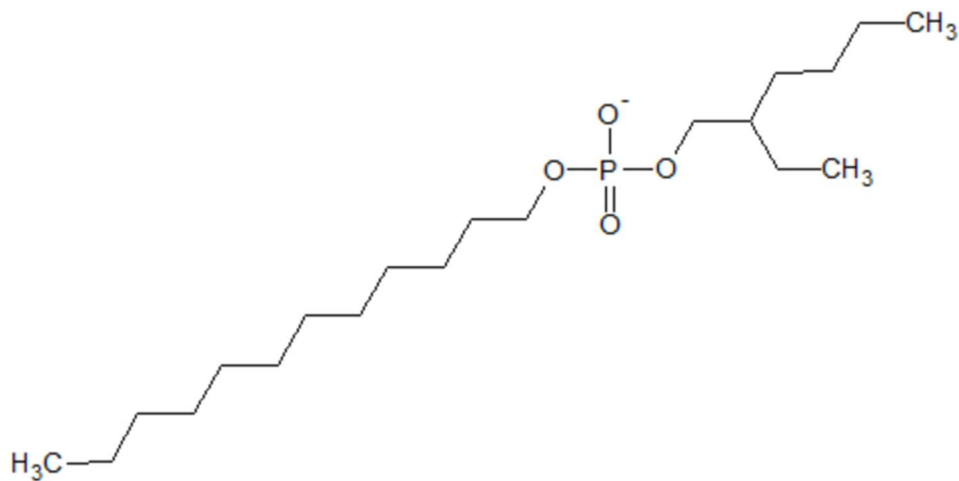


Figure A.5: 2-ethylhexyl dodecyl phosphate, one of the anions synthesized for this study

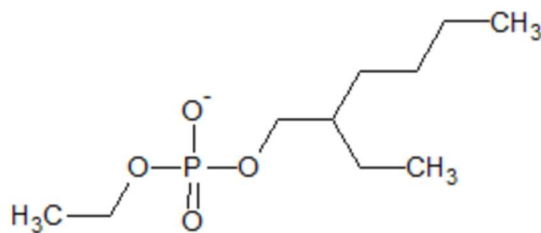


Figure A.6: 2-ethylhexyl ethyl phosphate, one of the anions synthesized for this study

Figure A.3, Figure A.4, Figure A.5, and Figure A.6 are the four anions that were successfully synthesized in this study Bis, PhEt, Dod and Et respectively. Table A.1 lists the molecular weights, names, and condensed formulas of all eight ionic liquids synthesized for this study.

Table A.1: Molecular weights of all ionic liquids synthesized for this study

Name	Cation	Anion	Molecular Weight (g/mol)
6~Bis	$P_{6,6,6,14}^+$	$Bis-PO_4^-$	805
8~Bis	$P_{8,8,8,18}^+$	$Bis-PO_4^-$	945
6~PhEt	$P_{6,6,6,14}^+$	$PhEt-PO_4^-$	797
8~PhEt	$P_{8,8,8,18}^+$	$PhEt-PO_4^-$	937
6~Dod	$P_{6,6,6,14}^+$	$Dod-PO_4^-$	861
8~Dod	$P_{8,8,8,18}^+$	$Dod-PO_4^-$	1001
6~Et	$P_{6,6,6,14}^+$	$Et-PO_4^-$	721
8~Et	$P_{8,8,8,18}^+$	$Et-PO_4^-$	861

APPENDIX B: Raw Tribological Data

Appendix B shows the mass loss data for the various tribological experiments performed for this study. This data is representative of the difference of the average of five different masses taken prior to and after a trial. The specific trials that were used to calculate the average mass loss for each lubricant are bolded. The formulas used to calculate the average and standard deviation are Equations (B.1) and (B.2). For the sake of uniformity, each data set assumed 8 trials however, in the event that eight trials were not completed, a marking of ‘--’ was used as a placeholder.

$$\bar{x} = \frac{\sum_{i=1}^n x_i}{n} \quad (\text{B.1})$$

$$\sigma = \sqrt{\frac{\sum_{i=1}^n (x_i - \bar{x})^2}{n - 1}} \quad (\text{B.2})$$

Table B.1: Raw tribological data from the base oil with average mass loss and standard deviation

Oil 10W-30 Control			Oil 10W-30 Control Heated		
	Mass Loss (mg)	Std. Dev. (mg)		Mass Loss (mg)	Std. Dev. (mg)
Trial 1	58.920	0.638	Trial 1	49.54	0.167332
Trial 2	78.860	0.158	Trial 2	52.74	0.2345208
Trial 3	35.720	0.202	Trial 3	45.36	0.1974842
Trial 4	81.280	0.161	Trial 4	59.60	0.1549193
Trial 5	83.940	0.200	Trial 5	54.98	0.212132
Trial 6	77.360	0.241	Trial 6	--	--
Trial 7	81.280	0.293	Trial 7	--	--
Trial 8	--	--	Trial 8	--	--
Average	80.544	2.529	Average	51.810	5.3931327

Table B.2: Raw tribological data for 6~Bis/oil solution including average mass loss and standard deviation

6~Bis			6~Bis Heated		
	Mass Loss (mg)	Std. Dev. (mg)		Mass Loss (mg)	Std. Dev. (mg)
Trial 1	64.960	0.221	Trial 1	62.160	0.197
Trial 2	73.120	0.192	Trial 2	69.160	0.122
Trial 3	77.200	0.126	Trial 3	74.780	4.363
Trial 4	67.220	0.141	Trial 4	62.480	0.105
Trial 5	86.480	0.300	Trial 5	62.700	0.161
Trial 6	77.680	0.268	Trial 6	64.220	0.148
Trial 7 ¹	41.460	0.100	Trial 7	63.320	0.110
Trial 8	72.700	0.105	Trial 8	--	--
Average	73.584	4.223	Average	62.976	0.815

Table B.3: Raw tribological data for 8~Bis/oil solution including average mass loss and standard deviation

8~Bis			8~Bis Heated		
	Mass Loss (mg)	Std. Dev. (mg)		Mass Loss (mg)	Std. Dev. (mg)
Trial 1	73.480	0.141	Trial 1	77.720	0.161
Trial 2	78.300	0.184	Trial 2	72.760	0.200
Trial 3	86.360	0.122	Trial 3	68.440	0.063
Trial 4	94.580	0.141	Trial 4	71.140	0.141
Trial 5	85.640	0.141	Trial 5	65.280	0.084
Trial 6	80.860	0.235	Trial 6	69.420	0.130
Trial 7	90.320	0.356	Trial 7	--	--
Trial 8	--	--	Trial 8	--	--
Average	84.296	4.746	Average	69.408	2.838

¹ During this trial the instrument froze and the actual wear time was less than the standard 2 hours explaining the lower-than-average discrepancy.

Table B.4: Raw tribological data for 6~PhEt/oil solution including average mass loss and standard deviation

6~PhEt			6~PhEt Heated		
	Mass Loss (mg)	Std. Dev. (mg)		Mass Loss (mg)	Std. Dev. (mg)
Trial 1	58.860	0.365	Trial 1	63.280	0.173
Trial 2	58.560	0.235	Trial 2	73.480	0.161
Trial 3	70.460	0.195	Trial 3	68.260	0.100
Trial 4	67.220	0.141	Trial 4	70.760	0.118
Trial 5	57.120	0.148	Trial 5	63.080	0.141
Trial 6	90.320	0.214	Trial 6	67.120	0.158
Trial 7	77.760	0.141	Trial 7	52.760	0.138
Trial 8	66.280	0.228	Trial 8	--	--
Average	62.730	4.751		66.500	3.305

Table B.5: Raw tribological data for 8~PhEt /oil solution including average mass loss and standard deviation

8~PhEt			8~PhEt Heated		
	Mass Loss (mg)	Std. Dev. (mg)		Mass Loss (mg)	Std. Dev. (mg)
Trial 1	76.220	0.179	Trial 1	57.160	0.122
Trial 2	78.160	0.219	Trial 2	82.920	0.077
Trial 3	79.920	0.224	Trial 3	71.760	0.100
Trial 4	70.660	0.187	Trial 4	61.040	0.141
Trial 5	90.120	0.126	Trial 5	74.660	0.100
Trial 6	--	--	Trial 6	63.620	0.190
Trial 7	--	--	Trial 7	68.300	0.214
Trial 8	--	--	Trial 8	--	--
Average	79.016	7.115	Average	67.876	5.615

Table B.6: Raw tribological data for 6~Dod/oil solution including average mass loss and standard deviation

6~Dod			6~Dod Heated		
	Mass Loss (mg)	Std. Dev. (mg)		Mass Loss (mg)	Std. Dev. (mg)
Trial 1	75.000	0.197	Trial 1	71.140	0.100
Trial 2	68.080	0.122	Trial 2	64.580	0.173
Trial 3	68.460	0.089	Trial 3	71.820	0.161
Trial 4	78.460	0.114	Trial 4	72.140	0.167
Trial 5	85.980	0.141	Trial 5	67.760	0.158
Trial 6	95.100	0.161	Trial 6	63.940	0.158
Trial 7	84.720	0.130	Trial 7	66.260	0.100
Trial 8	76.420	0.130	Trial 8	--	--
Average	73.284	4.741	Average	69.824	2.648

Table B.7: Raw tribological data for 8~Dod/oil solution including average mass loss and standard deviation

8~Dod			8~Dod Heated		
	Mass Loss (mg)	Std. Dev. (mg)		Mass Loss (mg)	Std. Dev. (mg)
Trial 1	63.780	0.158	Trial 1	63.500	0.161
Trial 2	59.600	0.176	Trial 2	83.320	0.145
Trial 3	74.480	0.110	Trial 3	85.700	0.176
Trial 4	70.240	0.118	Trial 4	78.240	0.138
Trial 5	54.440	0.114	Trial 5	83.100	0.095
Trial 6	--	--	Trial 6	70.640	0.170
Trial 7	--	--	Trial 7	--	--
Trial 8	--	--	Trial 8	--	--
Average	64.508	8.036	Average	82.590	3.130

Table B.8: Raw tribological data for 6~Et/oil solution including average mass loss and standard deviation

6~Et			6~Et Heated		
	Mass Loss (mg)	Std. Dev. (mg)		Mass Loss (mg)	Std. Dev. (mg)
Trial 1	46.220	0.164	Trial 1	51.680	0.130
Trial 2	49.220	0.130	Trial 2	56.300	0.118
Trial 3	50.960	0.152	Trial 3	51.500	0.138
Trial 4	52.420	0.122	Trial 4	60.020	0.110
Trial 5	62.180	0.224	Trial 5	59.920	0.158
Trial 6	--	--	Trial 6	52.580	0.122
Trial 7	--	--	Trial 7	--	--
Trial 8	--	--	Trial 8	--	--
Average	52.200	6.038	Average	55.333	3.989

Table B.9: Raw tribological data for 8~Et/oil solution including average mass loss and standard deviation

8~Et			8~Et Heated		
	Mass Loss (mg)	Std. Dev. (mg)		Mass Loss (mg)	Std. Dev. (mg)
Trial 1	64.000	0.155	Trial 1	74.720	0.071
Trial 2	63.360	0.118	Trial 2	59.960	0.114
Trial 3	73.900	0.155	Trial 3	61.460	0.134
Trial 4	71.640	0.212	Trial 4	72.120	0.161
Trial 5	68.400	0.141	Trial 5	51.860	0.212
Trial 6	65.840	0.195	Trial 6	66.040	0.063
Trial 7	--	--	Trial 7	54.220	0.122
Trial 8	--	--	Trial 8	--	--
Average	67.857	4.250	Average	62.911	8.588

APPENDIX C: Precursor Structures

Appendix C list the structures of the molecules used in the synthesis of every cation and anion synthesized for this study. Figure C.1 and Figure C.2 are the precursors to the cation $P_{8,8,8,18}^+ Br^-$ while Figure C.3, Figure C.4, and Figure C.5 are the various alcohol precursors to PhEt, Dod, and Et respectively. Figure C.6, and Figure C.7 are the structures of 2-ethylhexanol and phosphoryl chloride which were used in every anion synthesis.



Figure C.1: 1-bromooctadecane, a precursor to trioctyl octadecyl phosphonium bromide

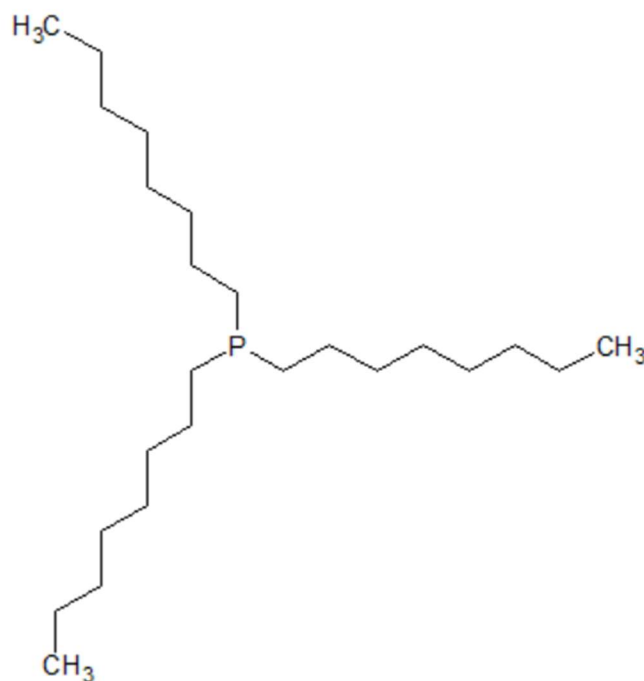


Figure C.2: Trioctyl phosphine, a precursor to trioctyl octadecyl phosphonium bromide

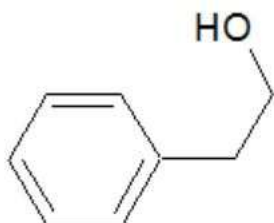


Figure C.3: 2-phenylethanol, a precursor to 2-ethylhexyl 2-phenylethyl phosphate



Figure C.4: Dodecanol, a precursor to 2-ethylhexyl dodecyl phosphate



Figure C.5: Ethanol, a precursor to 2-ethylhexyl ethyl phosphate

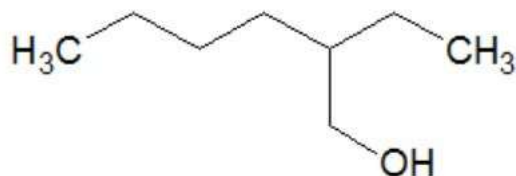


Figure C.6: 2-ethylhexanol, a precursor to all phosphodiester synthesized in this study

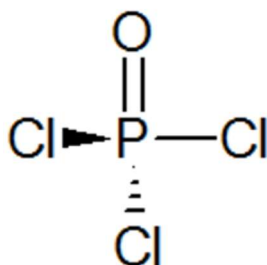


Figure C.7: Phosphoryl chloride, a precursor to all phosphodiester synthesized in this study

APPENDIX D: Reprint Permissions

This appendix contains the letter granting permissions to use Figure 2.3 and Figure 2.4.

Permissions were granted from the American Chemical Society



RightsLink®

Home

Create Account

Help



ACS Publications
Most Trusted. Most Cited. Most Read.

Title: Antiwear Performance and Mechanism of an Oil-Miscible Ionic Liquid as a Lubricant Additive

Author: Jun Qu, Dinesh G. Bansal, Bo Yu, et al

Publication: Applied Materials

Publisher: American Chemical Society

Date: Feb 1, 2012

Copyright © 2012, American Chemical Society

LOGIN

If you're a copyright.com user, you can login to RightsLink using your copyright.com credentials. Already a RightsLink user or want to learn more?

PERMISSION/LICENSE IS GRANTED FOR YOUR ORDER AT NO CHARGE

This type of permission/license, instead of the standard Terms & Conditions, is sent to you because no fee is being charged for your order. Please note the following:

- Permission is granted for your request in both print and electronic formats, and translations.
- If figures and/or tables were requested, they may be adapted or used in part.
- Please print this page for your records and send a copy of it to your publisher/graduate school.
- Appropriate credit for the requested material should be given as follows: "Reprinted (adapted) with permission from (COMPLETE REFERENCE CITATION). Copyright (YEAR) American Chemical Society." Insert appropriate information in place of the capitalized words.
- One-time permission is granted only for the use specified in your request. No additional uses are granted (such as derivative works or other editions). For any other uses, please submit a new request.

If credit is given to another source for the material you requested, permission must be obtained from that source.

BACK

CLOSE WINDOW

APPENDIX E: Radial Hardness Testing Data

Appendix E contains the radial hardness data from a disk of the steel rod used to create the steel test disks used in this study. The hardness was tested on a Wilson® Rockwell Hardness Tester Series 524 located in the Mechanical Engineering department at Rose-Hulman Institute of Technology. Figure E.1 is a diagram of the various test locations while Table E.1 and Table E.2 represent the distance and HR_c hardness value at those distances for each series 1, 2, and 3 as well as the roughly equidistant series starting at the arrow and moving counterclockwise among the points not included in series 1, 2 and 3. The total diameter of this disk is 2.0” while the distances listed in Table E.1 and Table E.2 are measured from the center hole.

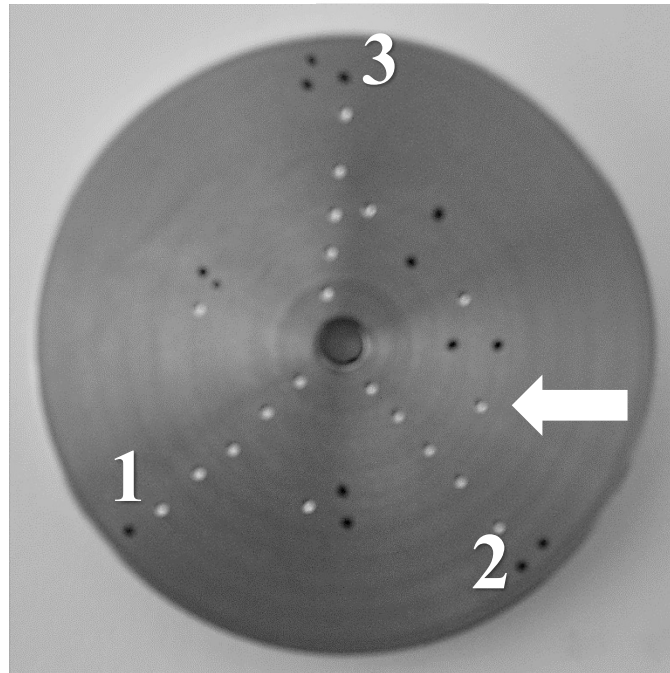


Figure E.1: Disk tested for radial hardness of steel rod machined into remaining test disks.

Table E.1: HRC Hardness values at various distances from the center of the test disk.

Series 1		Series 2		Series 3	
Distance (in.)	HR _c	Distance (in.)	HR _c	Distance (in.)	HR _c
0.1667	10.1	0.1429	9.7	0.1429	12.4
0.3095	13.3	0.2619	12.5	0.2619	13.0
0.4762	15.9	0.4048	13.3	0.3810	14.3
0.5952	18.2	0.5476	16.9	0.5238	17.3
0.7857	26.9	0.7619	23.4	0.7143	22.2

Table E.2: HRC Hardness tested at roughly equidistant points from the center hole in the approximate location of the wear scar.

Distance (in.)	HR _C Hardness
0.4762	14.2
0.4048	15.6
0.4048	14.3
0.5238	16.0
0.5476	15.1

The average hardness of the sample of disk material in the approximate wear region is 15.3 ± 1.3 on the HR_C scale. The average hardness value was calculated by averaging the hardness values for the measurements that were between 0.3810" and 0.5476" from the center of the disk as these fall within the test region. The error on this average was calculated using the standard deviation function presented in Equation (B.2). The values for the ASTM disk material were taken from Table 1: Characteristics of the Interlaboratory Wear Test Specimens published in the ASTM G99-05(2010) standards [32].

Table E.3: ASTM Hardness Value and Average Hardness Value of Disk Material measured between 0.3810" and 0.5476" from Disk Center

Material	Hardness Value (Scale)	Percent Variation (%)
ASTM disk material	1599±144 (HV 0.2)	9.01
Easy to Machine 303 Steel	15.3±1.3 (HR _C)	8.37

APPENDIX F: NMR Spectra

Appendix F contains the various NMR spectra that were obtained to confirm the identity and structure of the various compounds synthesized in this study. The first section contains the starting materials and purchased cations and anions. The second section contains the various intermediates synthesized for Cummins, Inc. that are used as a means to confirm future syntheses. The third section contains the ILs synthesized for Cummins, Inc. and used in this study as reference spectra for the various cations, anions and ILs synthesized. The fourth section contains the proton NMRs of the various cations, anions and ILs actually synthesized for this study. The fifth section contains the proton NMRs of the six ILs after heating at 100°C for one hour. A table of contents has been provided here as a quick reference.

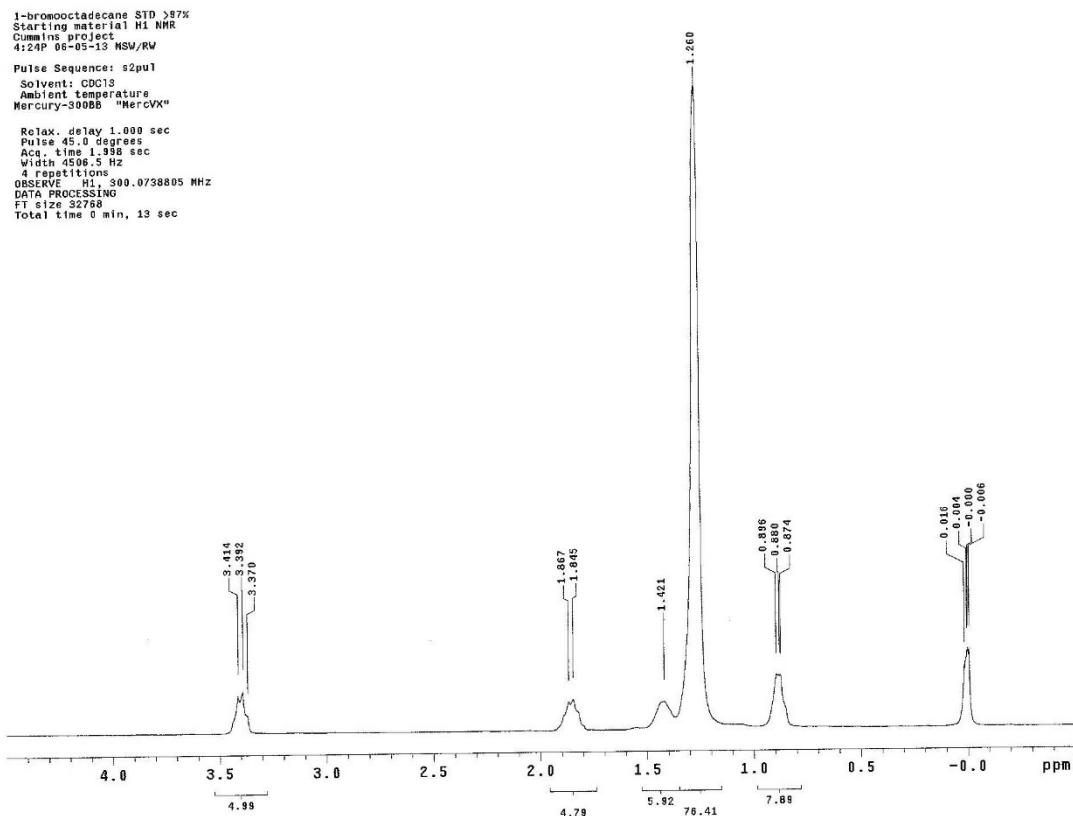
Spectra	Page
Figure F.1: ^1H NMR of 1-bromooctadecane in CDCl_3	62
Figure F.2: ^{13}C NMR of 1-bromooctadecane in CDCl_3	63
Figure F.3: ^1H NMR of trihexyl tetradecyl phosphonium bromide in CDCl_3	64
Figure F.4: ^{13}C NMR of trihexyl tetradecyl phosphonium bromide in CDCl_3	65
Figure F.5: ^{31}P NMR of trihexyl tetradecyl phosphonium bromide in CDCl_3	66
Figure F.6: ^1H NMR of Bis(2-ethylhexyl) phosphate in CDCl_3	67
Figure F.7: ^{13}C NMR of Bis(2-ethylhexyl) phosphate in CDCl_3	68
Figure F.8: ^{31}P NMR of Bis(2-ethylhexyl) phosphate in CDCl_3	69
Figure F.9: ^1H NMR of trioctyl phosphine in CDCl_3	70
Figure F.10: ^{13}C NMR of trioctyl phosphine in CDCl_3	71
Figure F.11: ^{31}P NMR of trioctyl phosphine in CDCl_3	72
Figure F.12: ^1H NMR of 2-ethylhexanol in CDCl_3	73
Figure F.13: ^{13}C NMR of 2-ethylhexanol in CDCl_3	74
Figure F.14: ^{31}P NMR of phosphoryl chloride in CDCl_3	75
Figure F.15: ^1H NMR of 2-phenyl ethanol in CDCl_3	76
Figure F.16: ^1H NMR of ethanol in CDCl_3	77
Figure F.17: ^{13}C NMR of ethanol in CDCl_3	78

Figure F.18: ^1H NMR of 1-dodecanol in CDCl_3	79
Figure F.19: ^{13}C NMR of 1-dodecanol in CDCl_3	80
Figure F.20: ^1H NMR of trioctyl octadecyl phosphonium bromide in CDCl_3	81
Figure F.21: ^{13}C NMR of trioctyl octadecyl phosphonium bromide in CDCl_3	82
Figure F.22: ^{31}P NMR of trioctyl octadecyl phosphonium bromide in CDCl_3	83
Figure F.23: ^1H NMR of 2-phenylethyl 2-ethylhexyl phosphate in CDCl_3	84
Figure F.24: ^{13}C NMR of 2-phenylethyl 2-ethylhexyl phosphate in CDCl_3	85
Figure F.25: ^{31}P NMR of 2-phenylethyl 2-ethylhexyl phosphate in CDCl_3	86
Figure F.26: ^1H NMR of ethyl 2-ethylhexyl phosphate in CDCl_3	87
Figure F.27: ^1H NMR of ethyl 2-ethylhexyl phosphate in CDCl_3 between 0 and 2.5 ppm.....	88
Figure F.28: ^{13}C NMR of ethyl 2-ethylhexyl phosphate in CDCl_3	89
Figure F.29: ^{31}P NMR of ethyl 2-ethylhexyl phosphate in CDCl_3	90
Figure F.30: ^1H NMR of trihexyl tetradecyl phosphonium bis(2-ethylhexyl) phosphate in CDCl_3	91
Figure F.31: ^{13}C NMR of trihexyl tetradecyl phosphonium bis(2-ethylhexyl) phosphate in CDCl_3	92
Figure F.32: ^{31}P NMR of trihexyl tetradecyl phosphonium bis(2-ethylhexyl) phosphate in CDCl_3	93
Figure F.33: ^1H NMR of trihexyl tetradecyl phosphonium ethyl 2-ethylhexyl phosphate in CDCl_3	94
Figure F.34: ^{13}C NMR of trihexyl tetradecyl phosphonium ethyl 2-ethylhexyl phosphate in CDCl_3	95
Figure F.35: ^{31}P NMR of trihexyl tetradecyl phosphonium ethyl 2-ethylhexyl phosphate in CDCl_3	96
Figure F.36: ^1H NMR of trihexyl tetradecyl phosphonium 2-phenylethyl 2-ethylhexyl phosphate in CDCl_3	97
Figure F.37: ^{31}P NMR of trihexyl tetradecyl phosphonium 2-phenylethyl 2-ethylhexyl phosphate in CDCl_3	98
Figure F.38: ^1H NMR of trihexyl tetradecyl phosphonium dodecyl 2-ethylhexyl phosphate in CDCl_3	99
Figure F.39: ^{31}P NMR of trihexyl tetradecyl phosphonium dodecyl 2-ethylhexyl phosphate in CDCl_3	100
Figure F.40: ^1H NMR of trioctyl octadecyl phosphonium bis(2-ethylhexyl) phosphate in CDCl_3	101
Figure F.41: ^{13}C NMR of trioctyl octadecyl phosphonium bis(2-ethylhexyl) phosphate in CDCl_3	102

Figure F.42: ^{31}P NMR of trioctyl octadecyl phosphonium bis(2-ethylhexyl) phosphate in CDCl_3	103
Figure F.43: ^1H NMR of trioctyl octadecyl phosphonium 2-phenylethyl 2-ethylhexyl phosphate in CDCl_3	104
Figure F.44: ^{31}P NMR of trioctyl octadecyl phosphonium 2-phenylethyl 2-ethylhexyl phosphate in CDCl_3	105
Figure F.45: ^1H NMR of trioctyl octadecyl phosphonium ethyl 2-ethylhexyl phosphate in CDCl_3	106
Figure F.46: ^{31}P NMR of trioctyl octadecyl phosphonium ethyl 2-ethylhexyl phosphate in CDCl_3	107
Figure F.47: ^1H NMR of trioctyl octadecyl phosphonium dodecyl 2-ethylhexyl phosphate in CDCl_3	108
Figure F.48: ^{31}P NMR of trioctyl octadecyl phosphonium dodecyl 2-ethylhexyl phosphate in CDCl_3	109
Figure F.49: ^1H NMR of ethyl 2-ethylhexyl phosphate in CDCl_3	110
Figure F.50: ^1H NMR of dodecyl 2-ethylhexyl phosphate in CDCl_3	111
Figure F.51: ^1H NMR of 2-phenylethyl 2-ethylhexyl phosphate in CDCl_3	112
Figure F.52: ^1H NMR of trioctyl octadecyl phosphonium bromide in CDCl_3	113
Figure F.53: ^1H NMR of trihexyl tetradecyl phosphonium bis(2-ethylhexyl) phosphate in CDCl_3	114
Figure F.54: ^1H NMR of trihexyl tetradecyl phosphonium dodecyl 2-ethylhexyl phosphate in CDCl_3	115
Figure F.55: ^1H NMR of trihexyl tetradecyl phosphonium ethyl 2-ethylhexyl phosphate in CDCl_3	116
Figure F.56: ^1H NMR of trihexyl tetradecyl phosphonium 2-phenylethyl 2-ethylhexyl phosphate in CDCl_3	117
Figure F.57: ^1H NMR of trioctyl octadecyl phosphonium bis(2-ethylhexyl) phosphate in CDCl_3	118
Figure F.58: ^1H NMR of trioctyl octadecyl phosphonium 2-phenylethyl 2-ethylhexyl phosphate in CDCl_3	119
Figure F.59: ^1H NMR of heated trihexyl tetradecyl phosphonium bis(2-ethylhexyl) phosphate in CDCl_3	120
Figure F.60: ^1H NMR of heated trioctyl octadecyl phosphonium bis(2-ethylhexyl) phosphate in CDCl_3	121
Figure F.61: ^1H NMR of heated trihexyl tetradecyl phosphonium 2-phenylethyl 2-ethylhexyl phosphate in CDCl_3	122
Figure F.62: ^1H NMR of heated trioctyl octadecyl phosphonium 2-phenylethyl 2-ethylhexyl phosphate in CDCl_3	123

Figure F.63: ^1H NMR of heated trihexyl tetradecyl phosphonium ethyl 2-ethylhexyl phosphate in CDCl_3	124
Figure F.64: ^1H NMR of heated trioctyl octadecyl phosphonium ethyl 2-ethylhexyl phosphate in CDCl_3	125
Figure F.65: ^1H NMR of heated trihexyl tetradecyl phosphonium dodecyl 2-ethylhexyl phosphate in CDCl_3	126
Figure F.66: ^1H NMR of heated trioctyl octadecyl phosphonium dodecyl 2-ethylhexyl phosphate in CDCl_3	127

Starting Materials/Purchased Products

Figure F.1: ^1H NMR of 1-bromooctadecane in CDCl_3

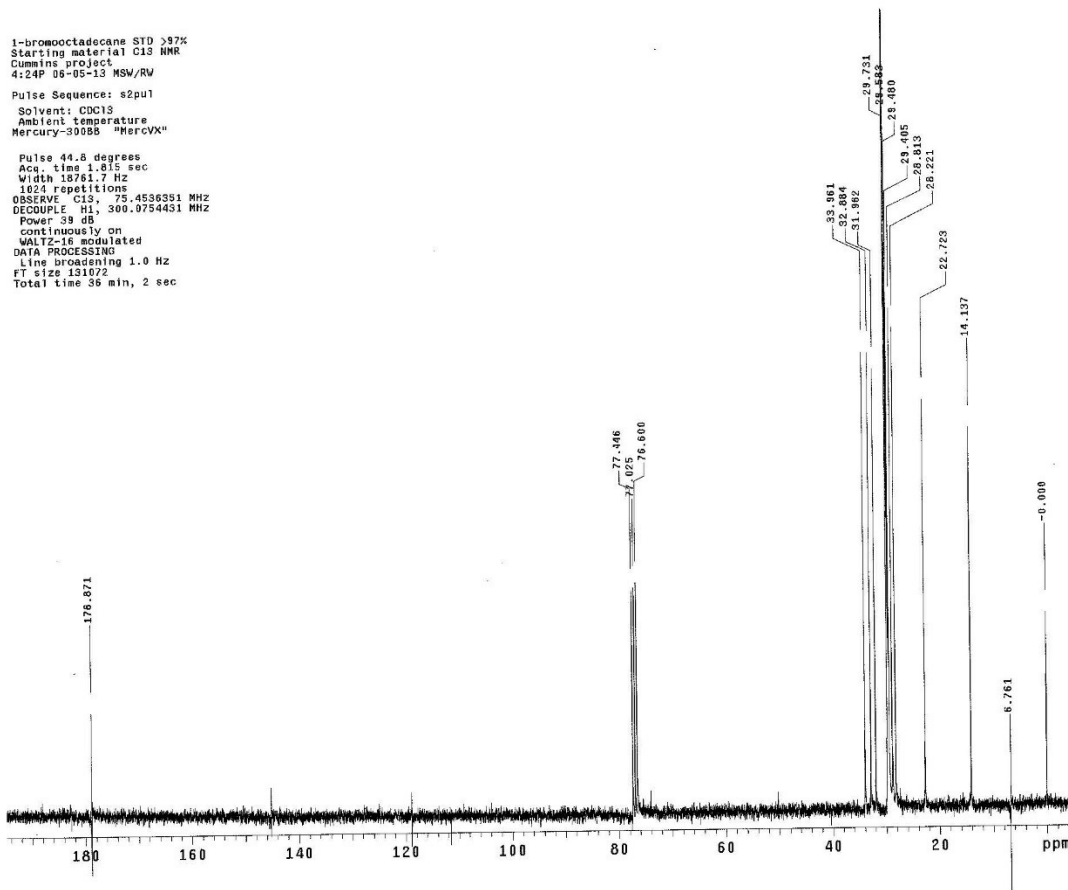


Figure F.2: ^{13}C NMR of 1-bromooctadecane in CDCl_3

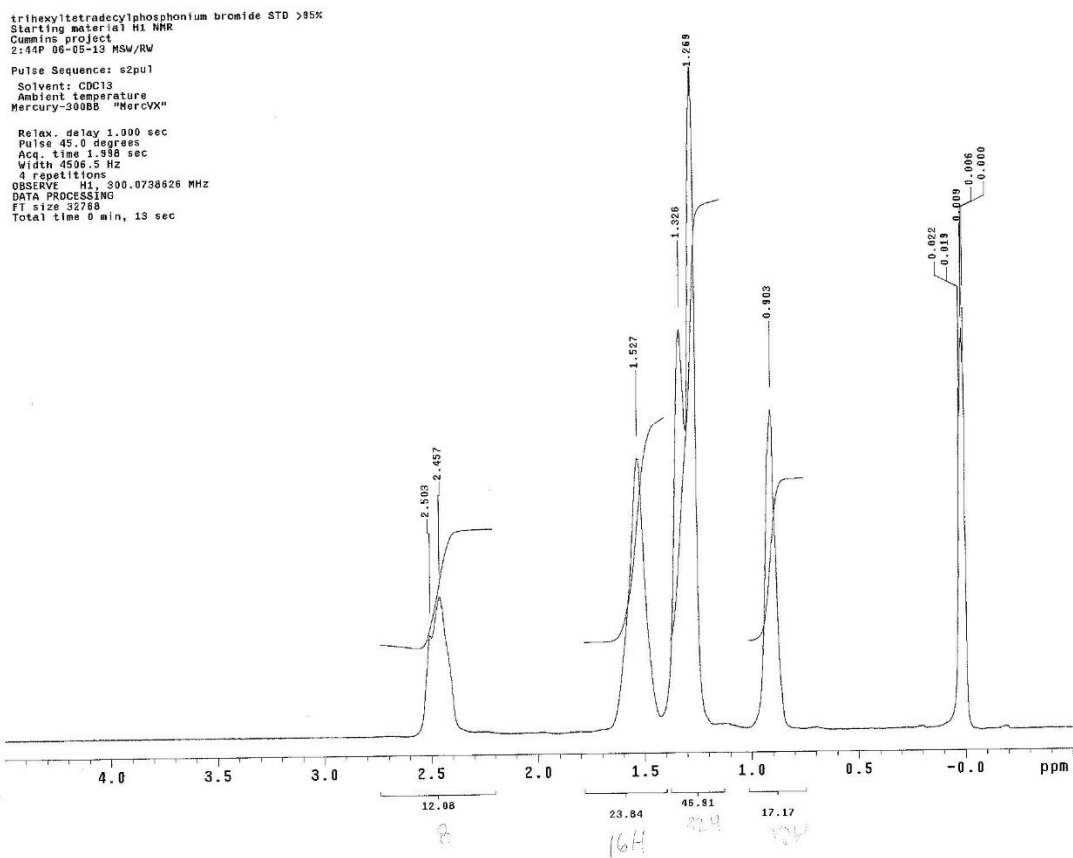


Figure F.3: ^1H NMR of trihexyl tetradecyl phosphonium bromide in CDCl_3

trihexyltetradecylphosphonium bromide STD >95%
Starting material C13 NMR
Cummins project
3:17P 06-05-13 MSW/RW
Pulse Sequence: s2pu1
Solvent: CDCl3
Ambient temperature
Mercury-30085 "MerCVX"
Pulse 44.8 degrees
Acq. time 1.815 sec
Width 10761.7 Hz
1024 repetitions
OBSERVE C13, 75.4536185 MHz
DECOUPLE H1, 300.0754431 MHz
Power 39 dB
continuously on
WALTZ-16 modulated
DATA PROCESSING
Line broadening 1.0 Hz
FT size 131072
Total time 36 min, 2 sec

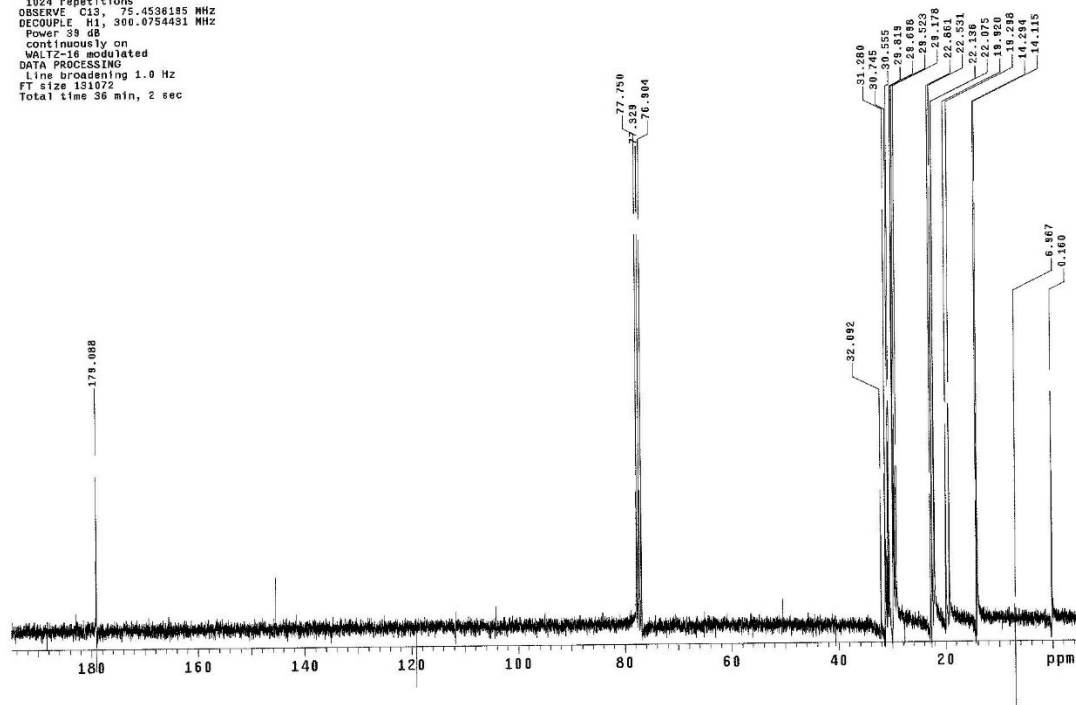


Figure F.4: ^{13}C NMR of trihexyl tetradecyl phosphonium bromide in CDCl_3

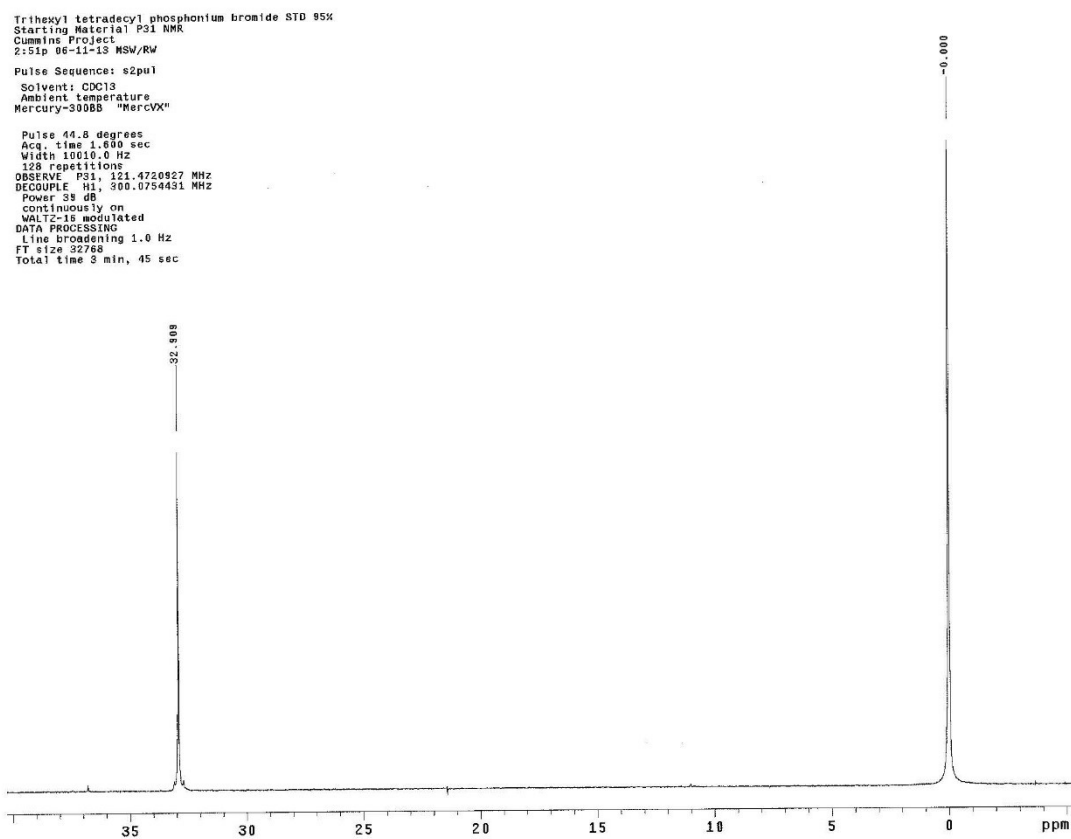


Figure F.5: ^{31}P NMR of trihexyl tetradecyl phosphonium bromide in CDCl_3

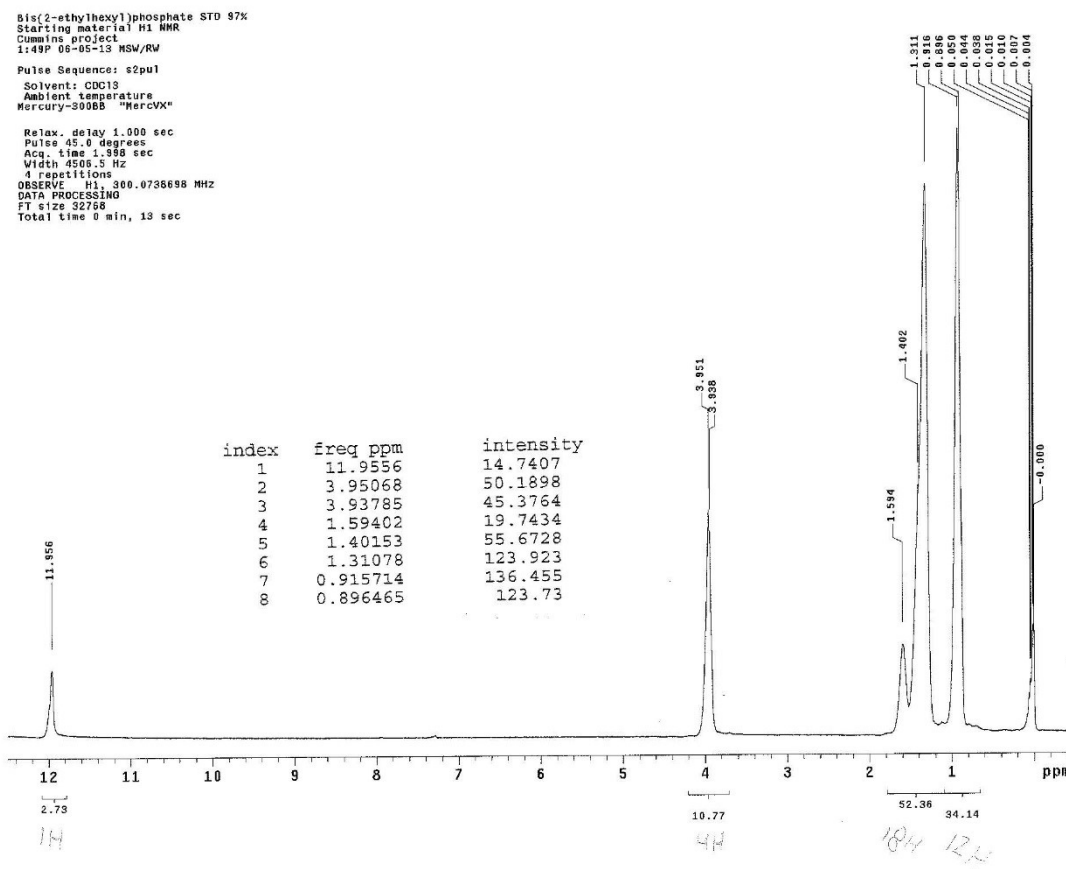


Figure F.6: ^1H NMR of Bis(2-ethylhexyl) phosphate in CDCl_3

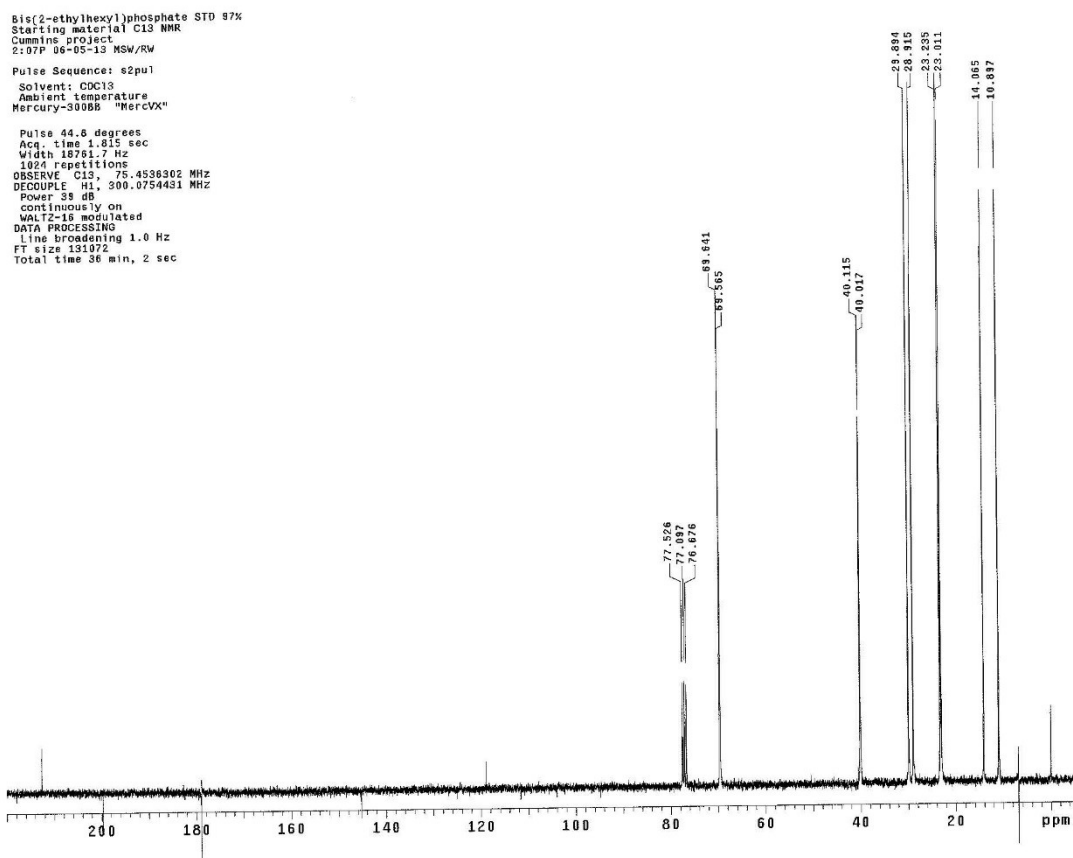


Figure F.7: ^{13}C NMR of Bis(2-ethylhexyl) phosphate in CDCl_3

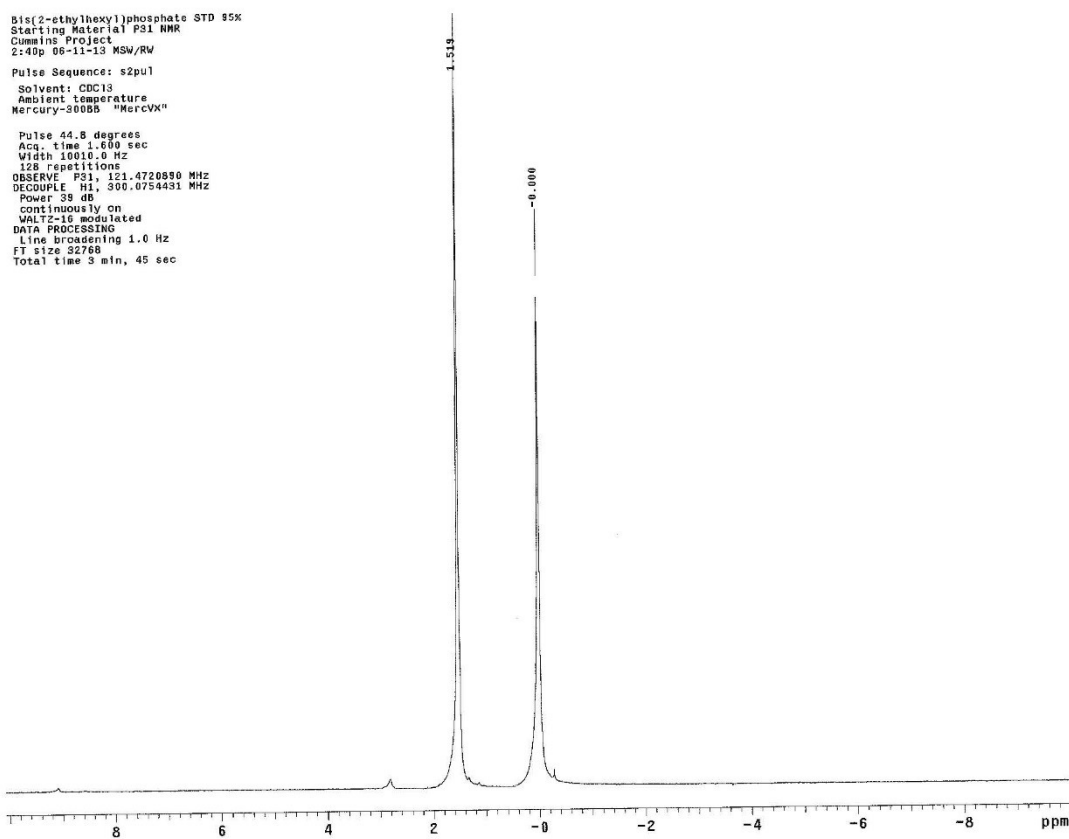


Figure F.8: ^{31}P NMR of Bis(2-ethylhexyl) phosphate in CDCl_3

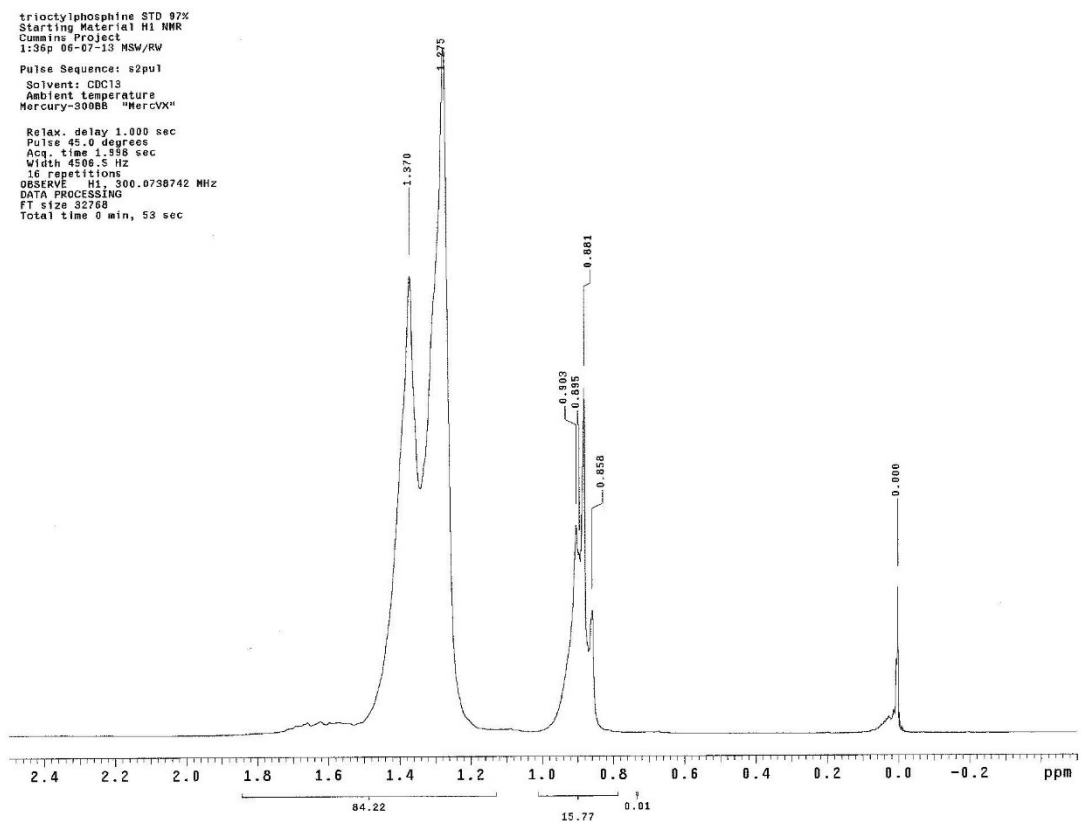


Figure F.9: ^1H NMR of trioctyl phosphine in CDCl_3

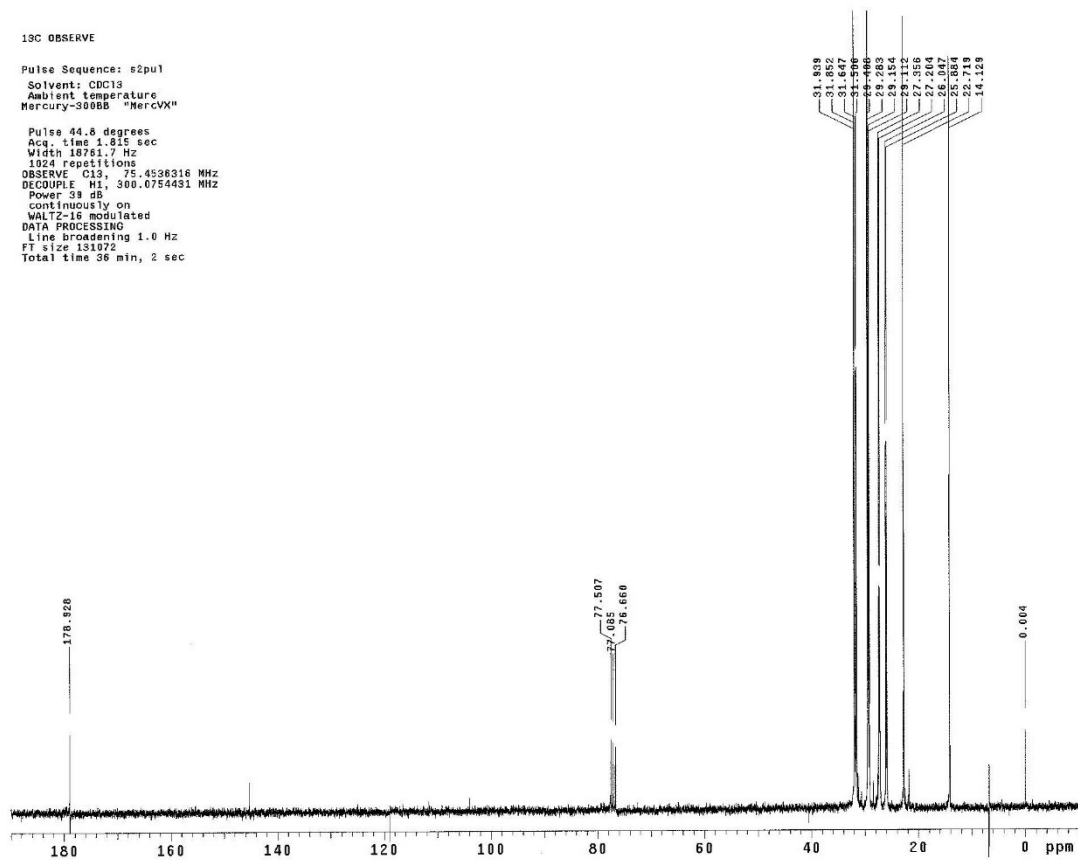


Figure F.10: ^{13}C NMR of trioctyl phosphine in CDCl_3

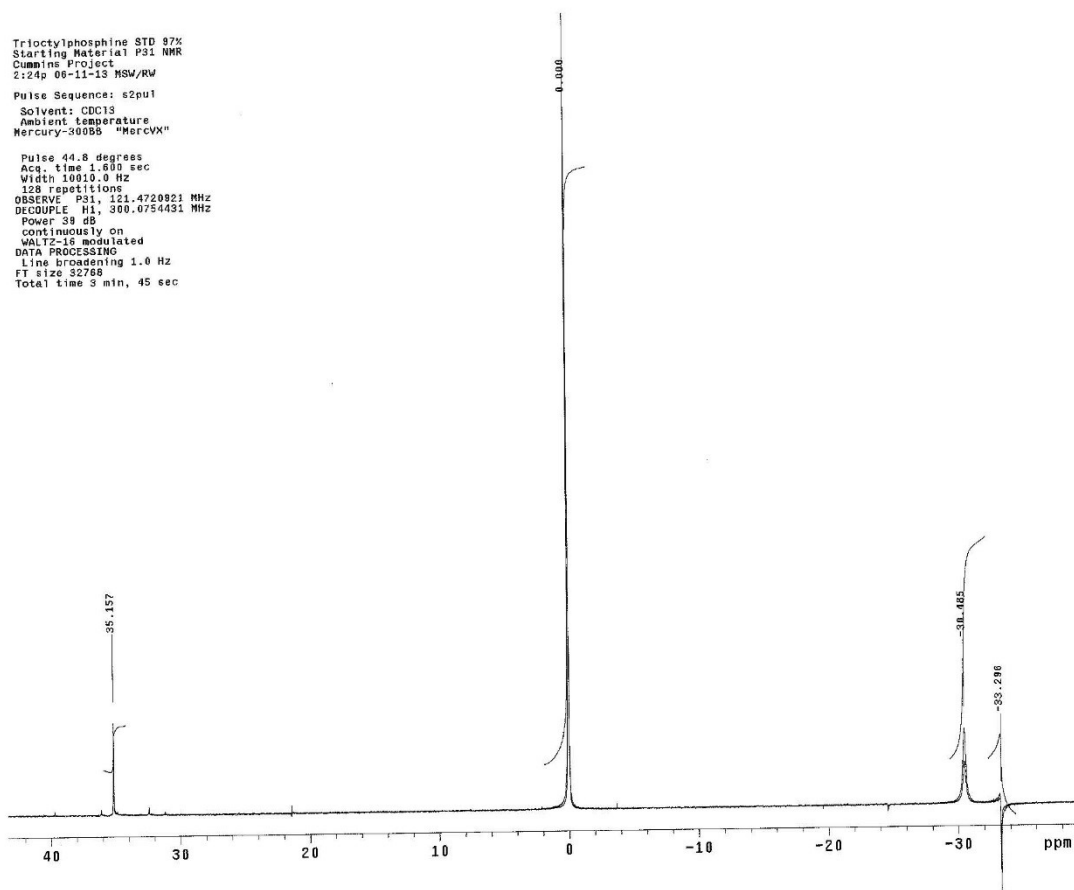


Figure F.11: ^{31}P NMR of trioctyl phosphine in CDCl_3

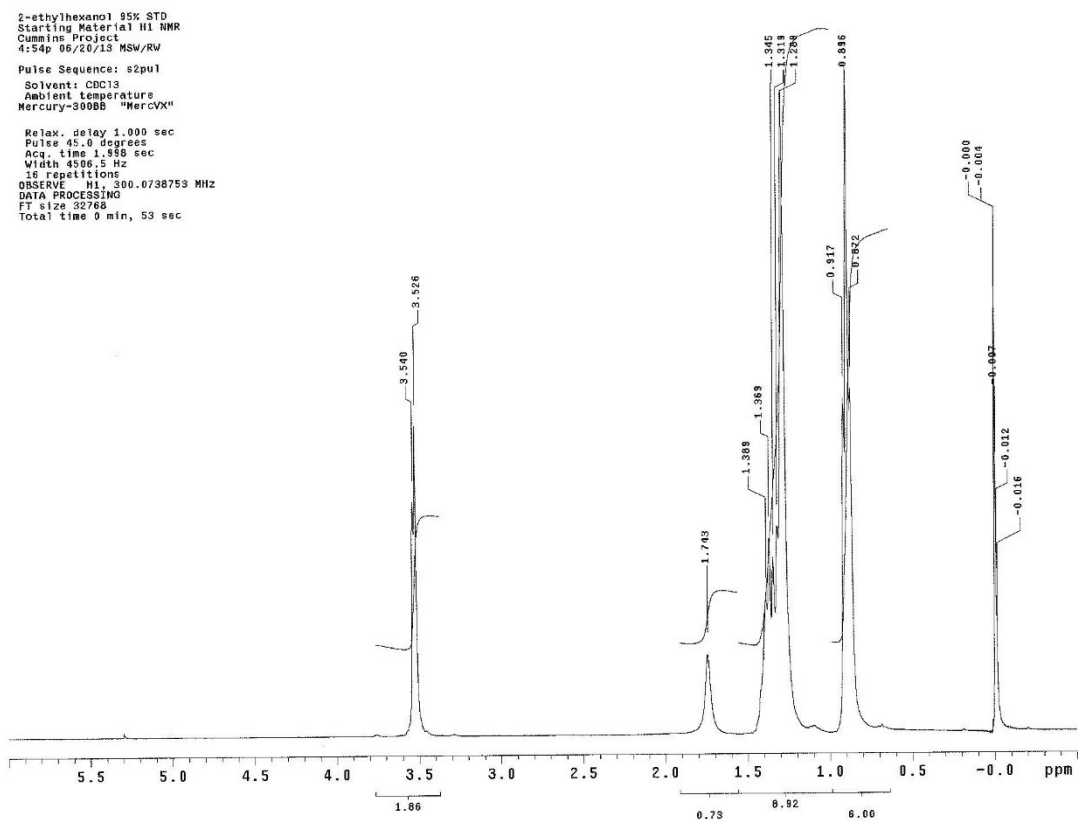


Figure F.12: ^1H NMR of 2-ethylhexanol in CDCl_3

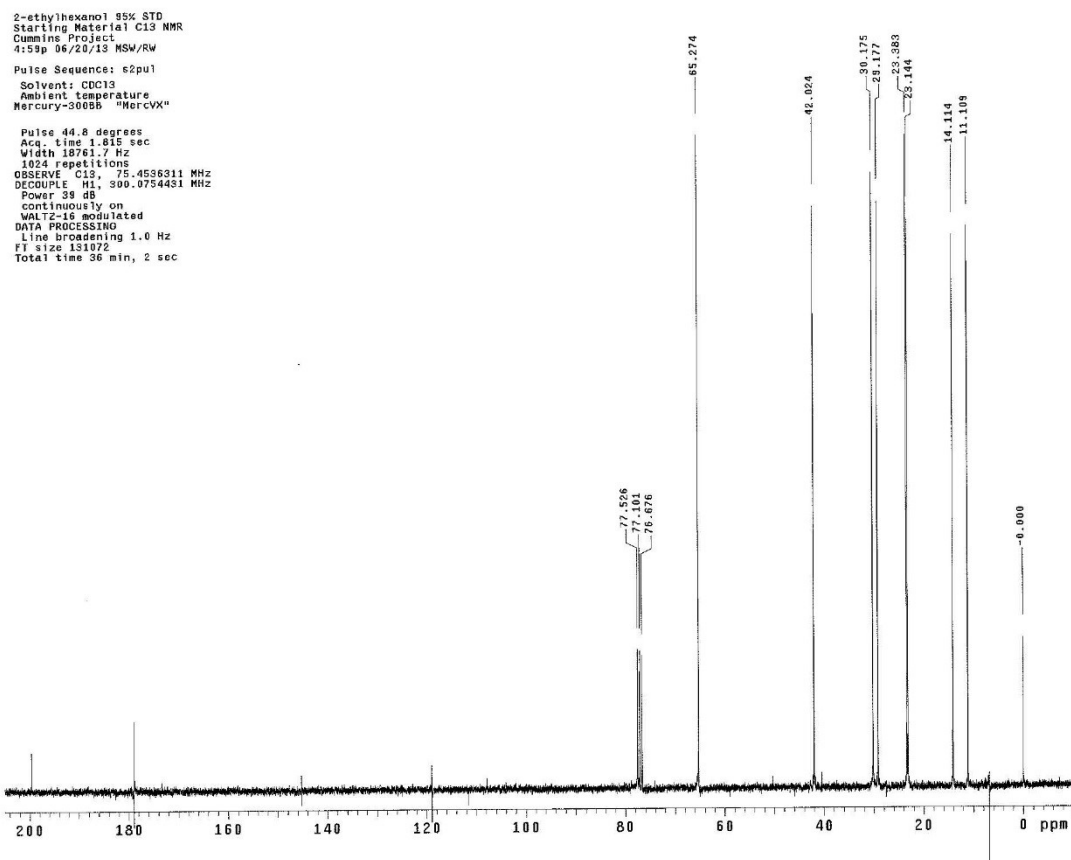


Figure F.13: ^{13}C NMR of 2-ethylhexanol in CDCl_3

Phosphoryl Chloride STD 85%
Starting Material PSI NMR
Cummins Project
1:48p 06/26/13 MSW/RW
Pulse Sequence: s2pu1
Solvent: CDCl3
Ambient temperature
Mercury-300SB "Mercury"
Pulse 44.8 degrees
Acq. time 1.600 sec
Width 10010.0 Hz
128 repetitions
OBSERVE P31, 121.4726827 MHz
DECOUPLE H1, 200.0754431 MHz
Power 39 dB
continuously on
WALTZ-16 modulated
DATA PROCESSING
Line broadening 1.0 Hz
FT size 32768
Total time 3 min, 45 sec

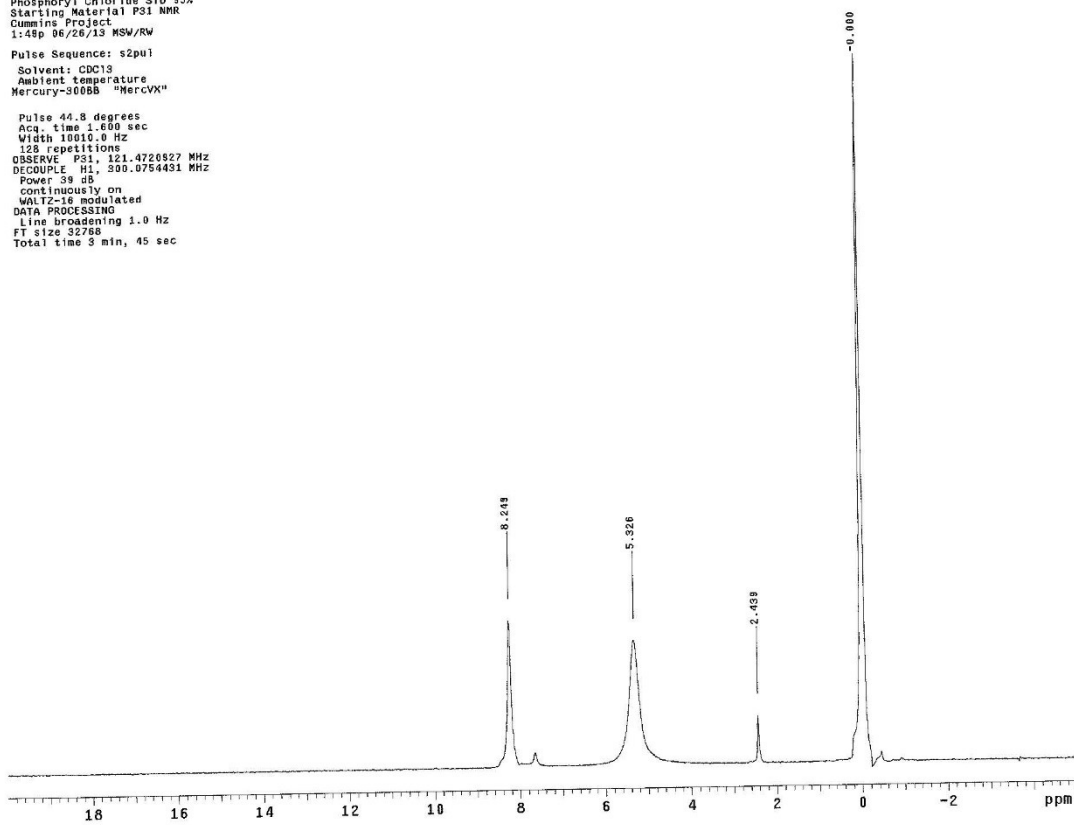


Figure F.14: ^{31}P NMR of phosphoryl chloride in CDCl_3

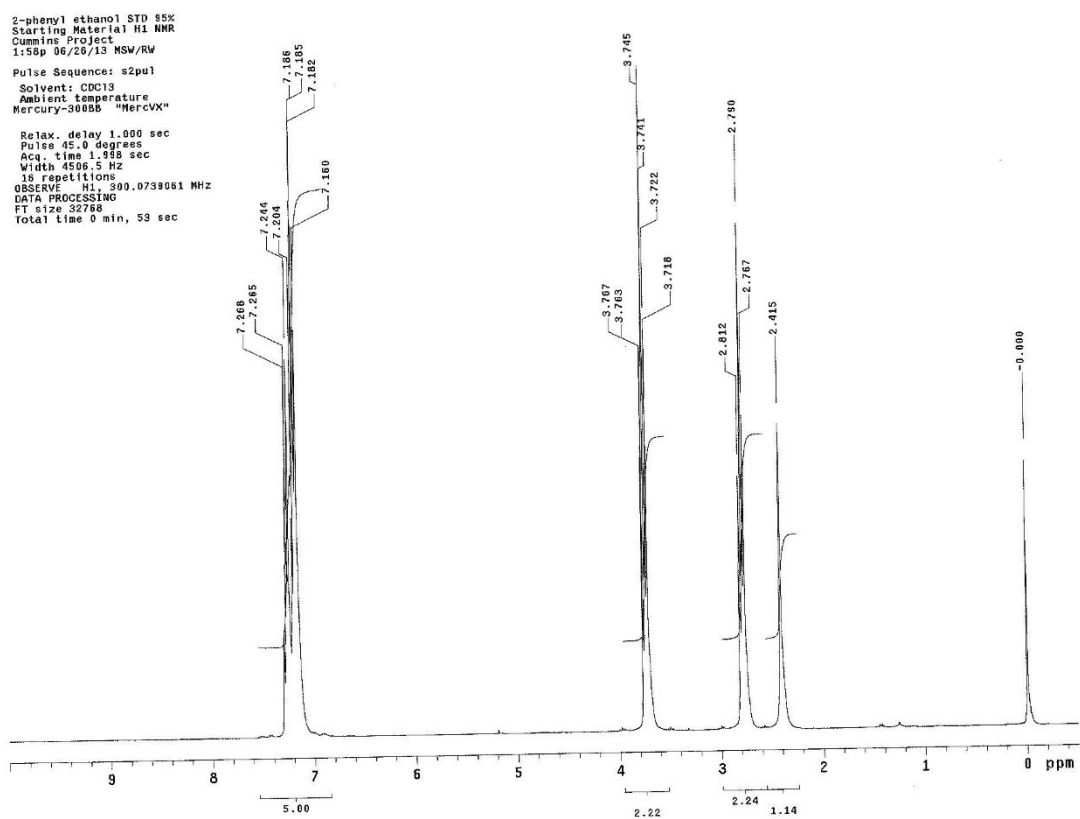


Figure F.15: ^1H NMR of 2-phenyl ethanol in CDCl_3

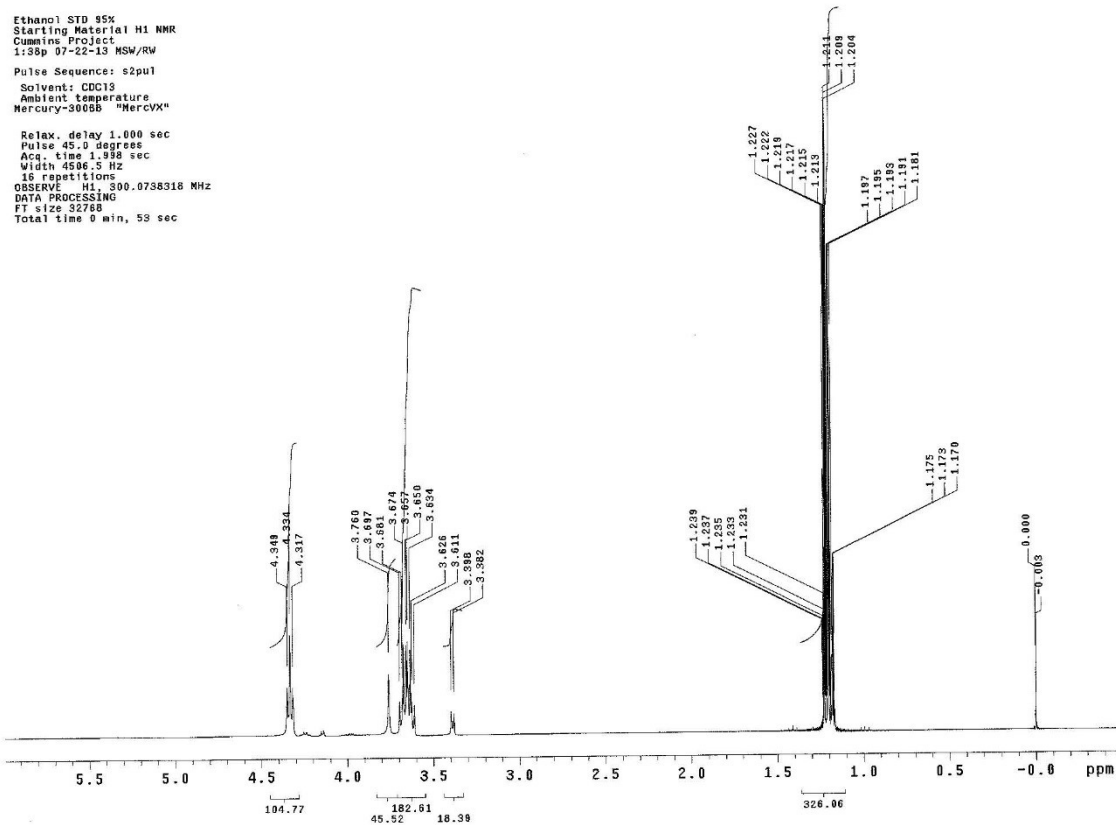


Figure F.16: ^1H NMR of ethanol in CDCl_3

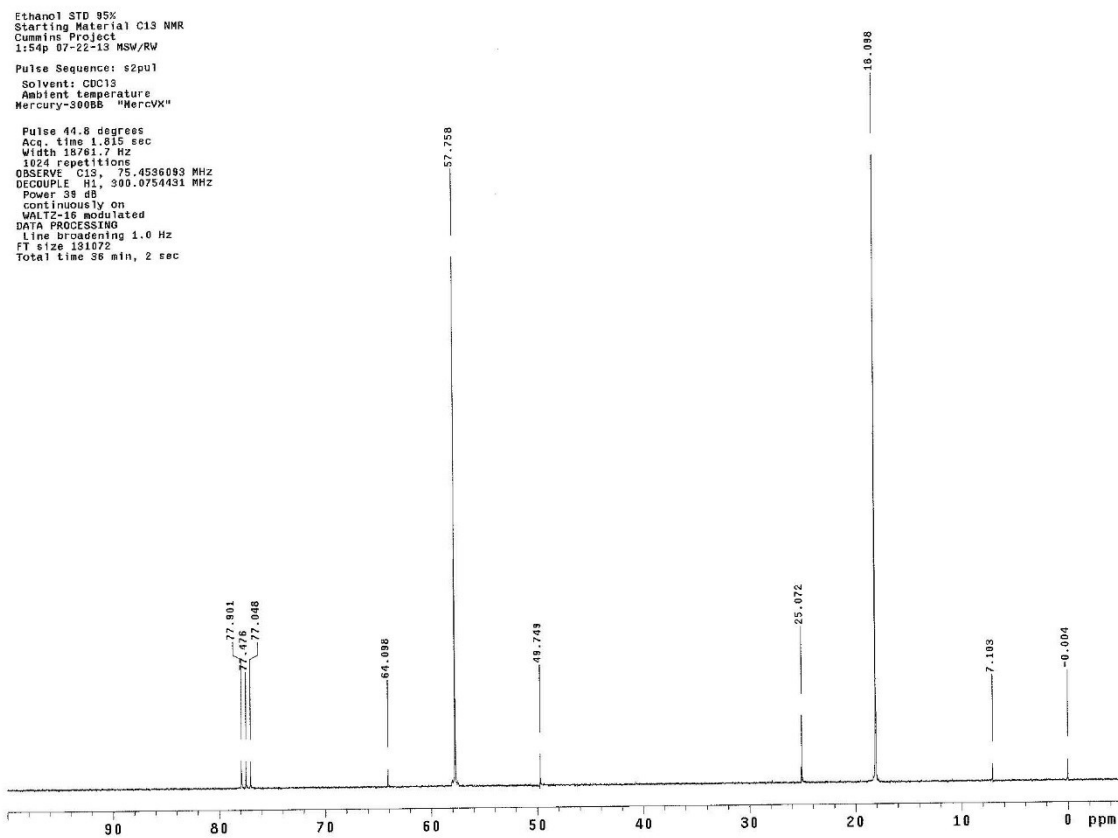


Figure F.17: ^{13}C NMR of ethanol in CDCl_3

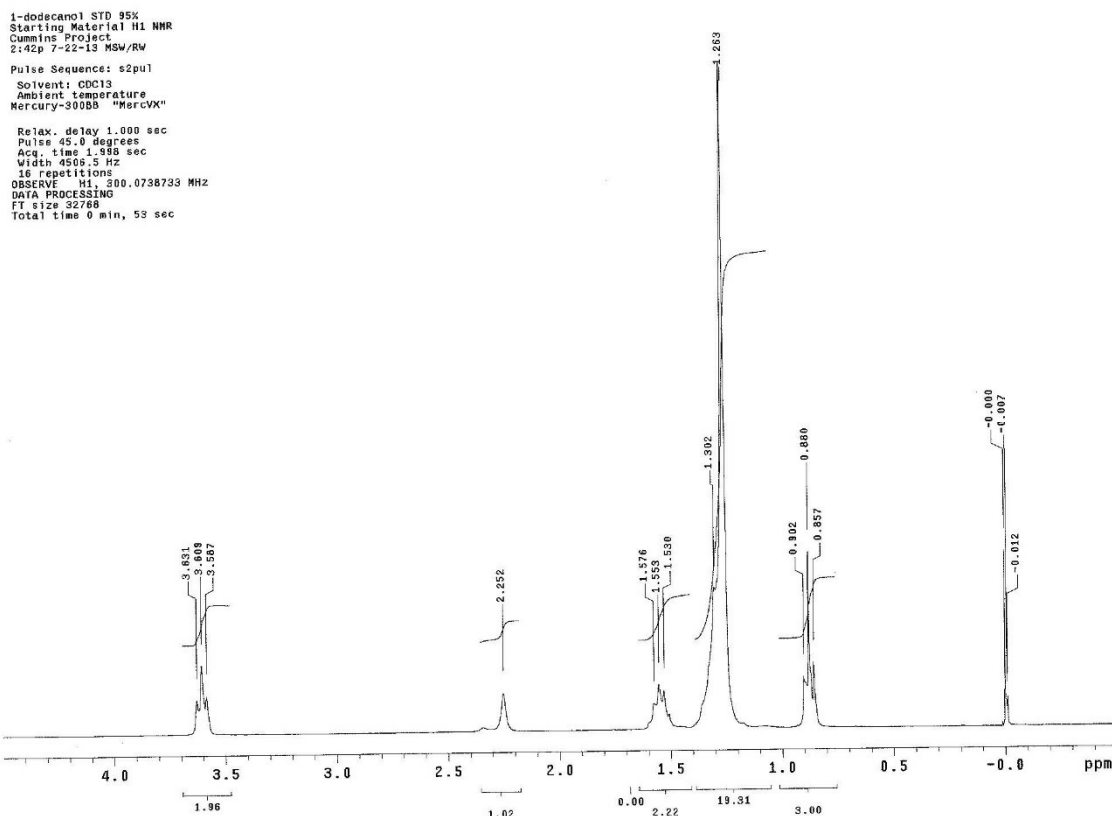


Figure F.18: ^1H NMR of 1-dodecanol in CDCl_3

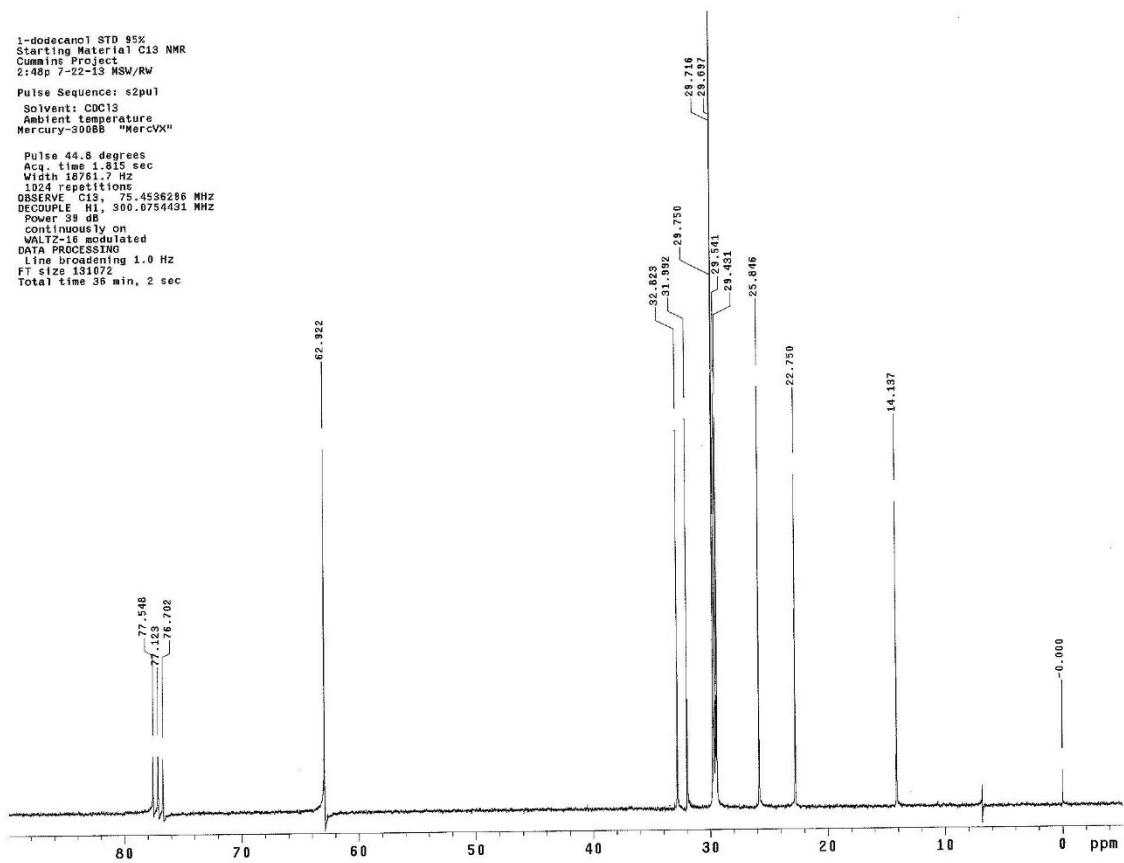


Figure F.19: ^{13}C NMR of 1-dodecanol in CDCl_3

Intermediate Cations and Anions

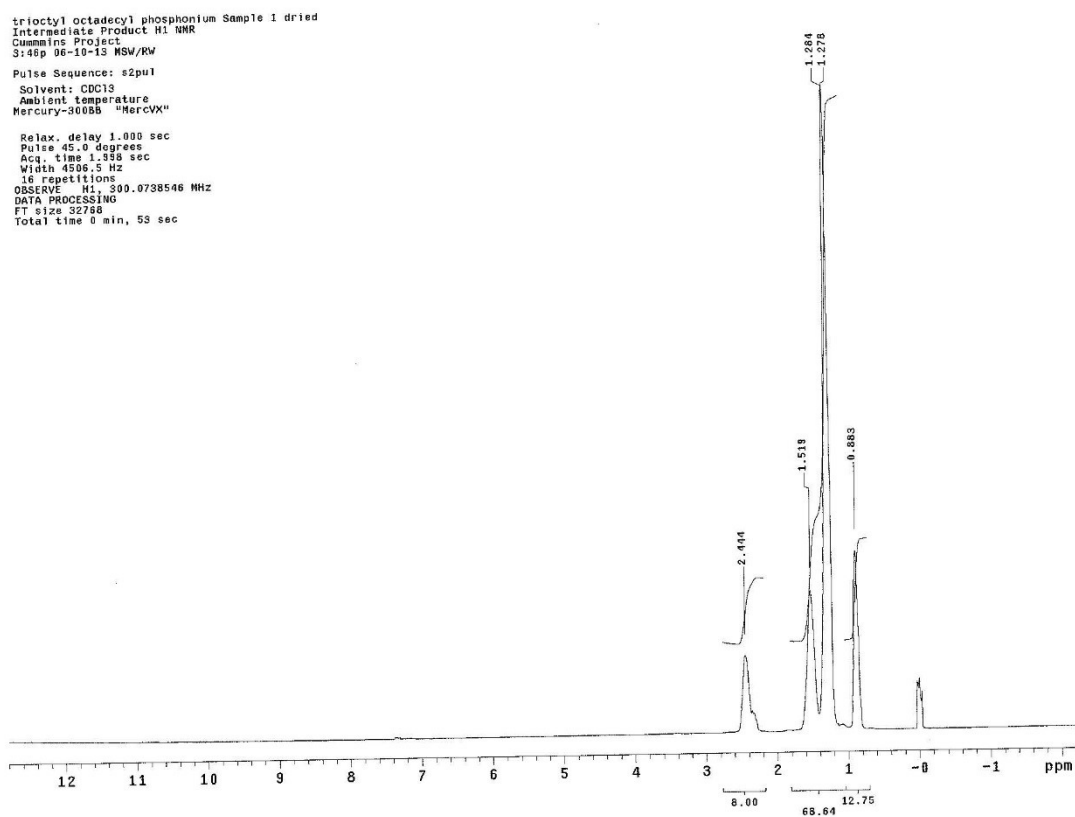


Figure F.20: ^1H NMR of trioctyl octadecyl phosphonium bromide in CDCl_3

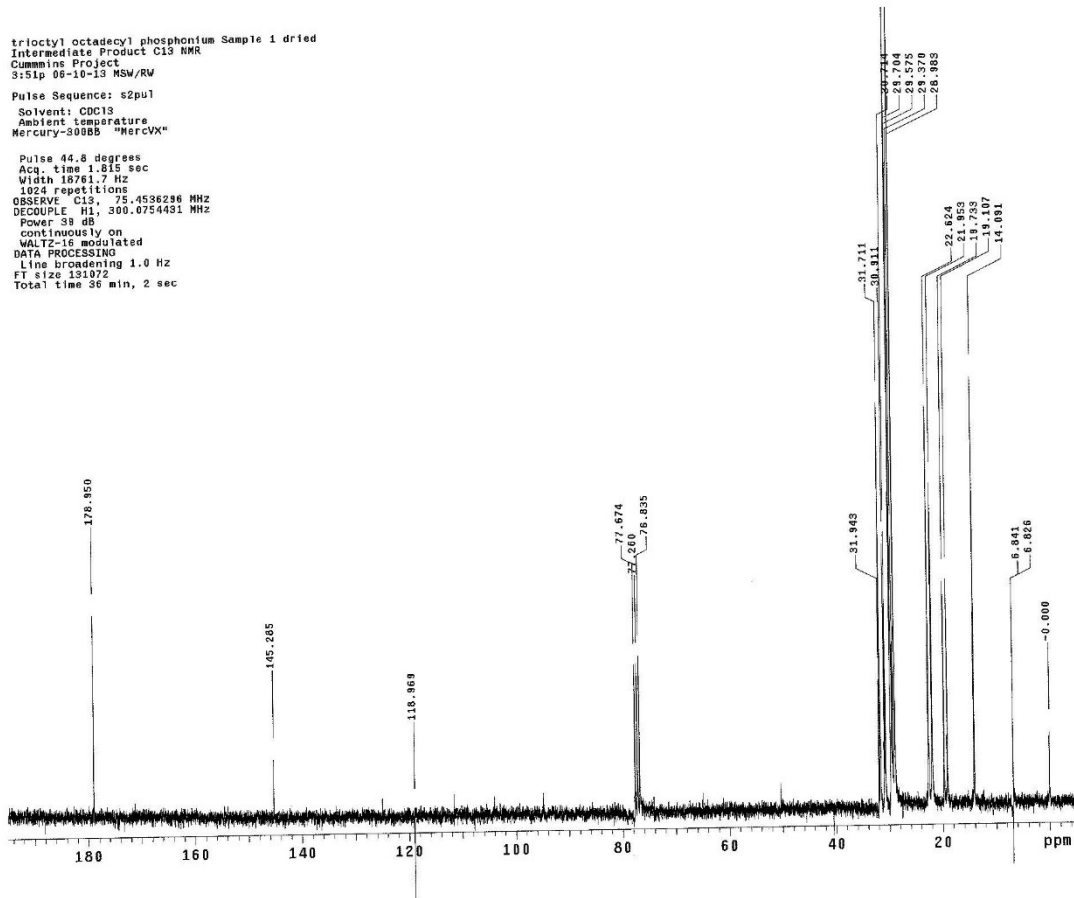


Figure F.21: ^{13}C NMR of trioctyl octadecyl phosphonium bromide in CDCl_3

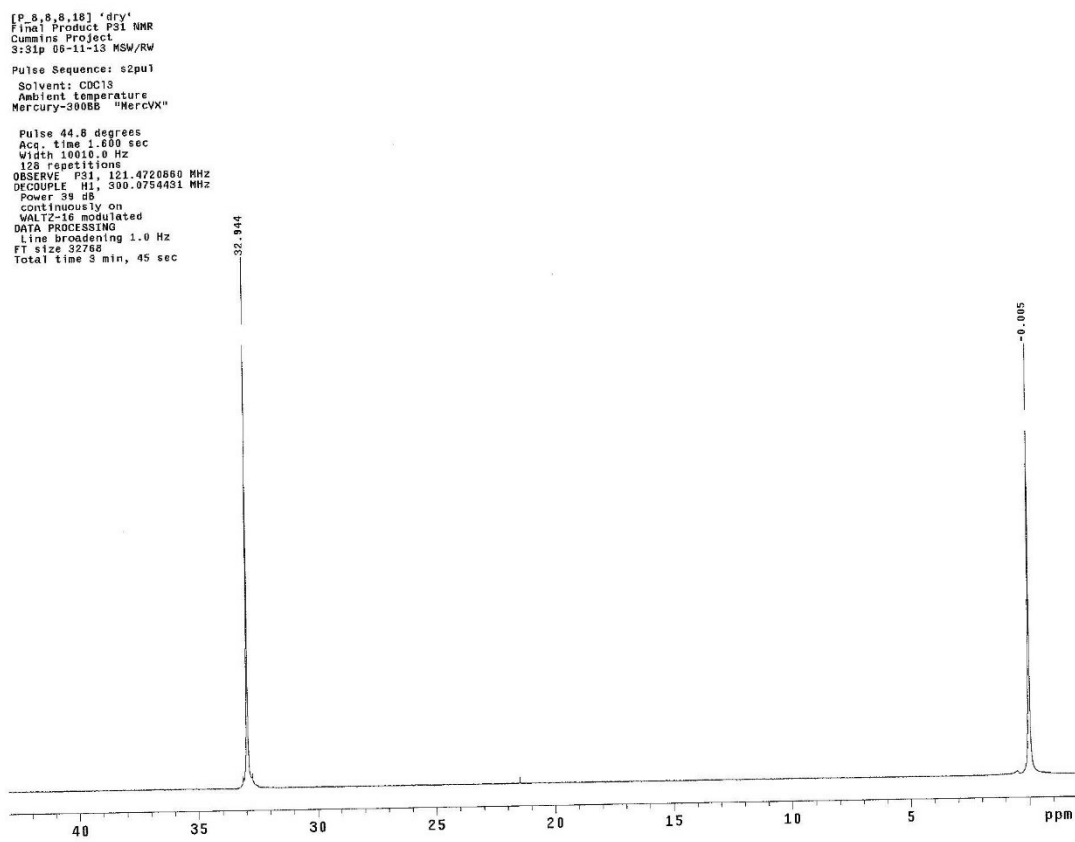


Figure F.22: ^{31}P NMR of trioctyl octadecyl phosphonium bromide in CDCl_3

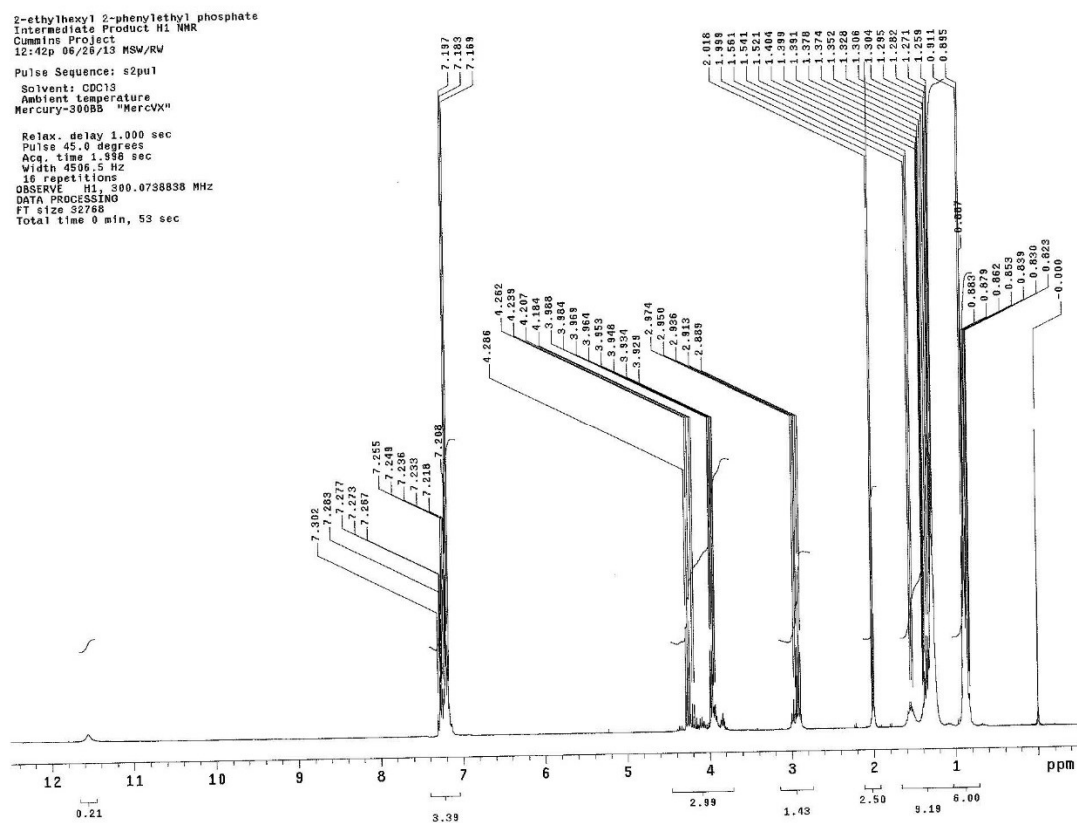


Figure F.23: ^1H NMR of 2-phenylethyl 2-ethylhexyl phosphate in CDCl_3

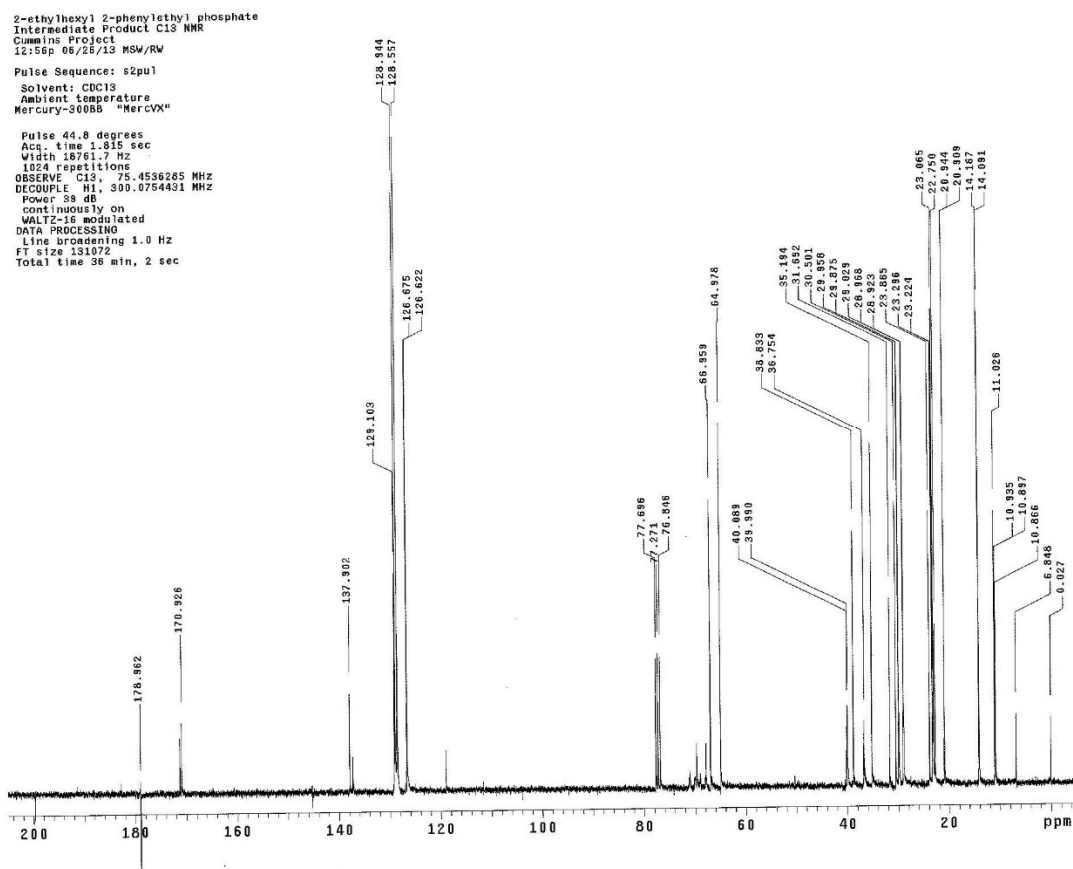


Figure F.24: ^{13}C NMR of 2-phenylethyl 2-ethylhexyl phosphate in CDCl_3

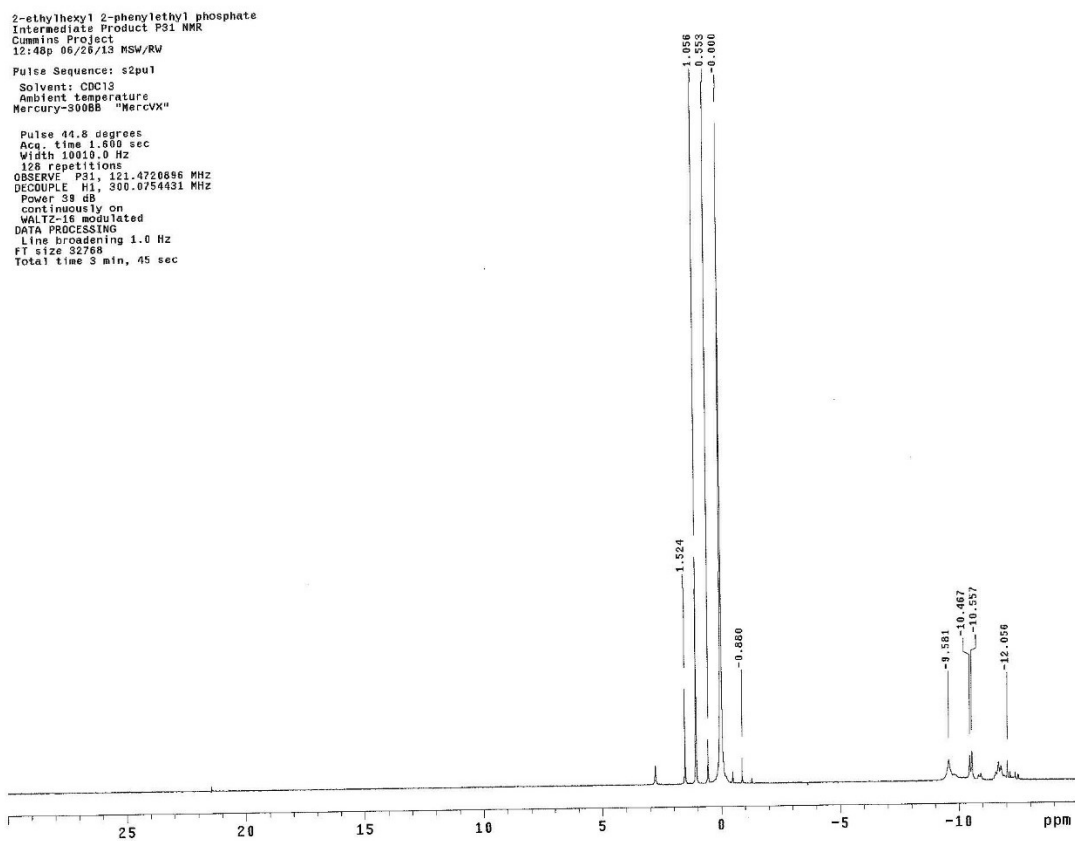


Figure F.25: ^{31}P NMR of 2-phenylethyl 2-ethylhexyl phosphate in CDCl_3

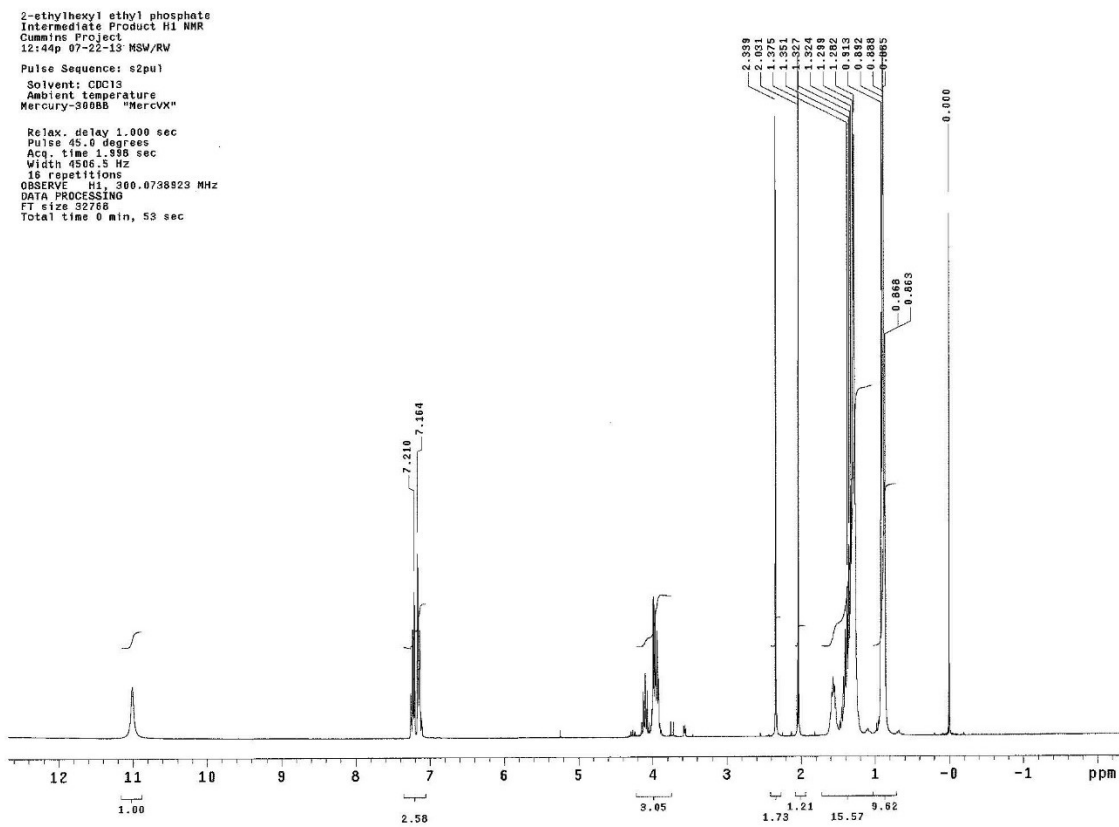


Figure F.26: ^1H NMR of ethyl 2-ethylhexyl phosphate in CDCl_3

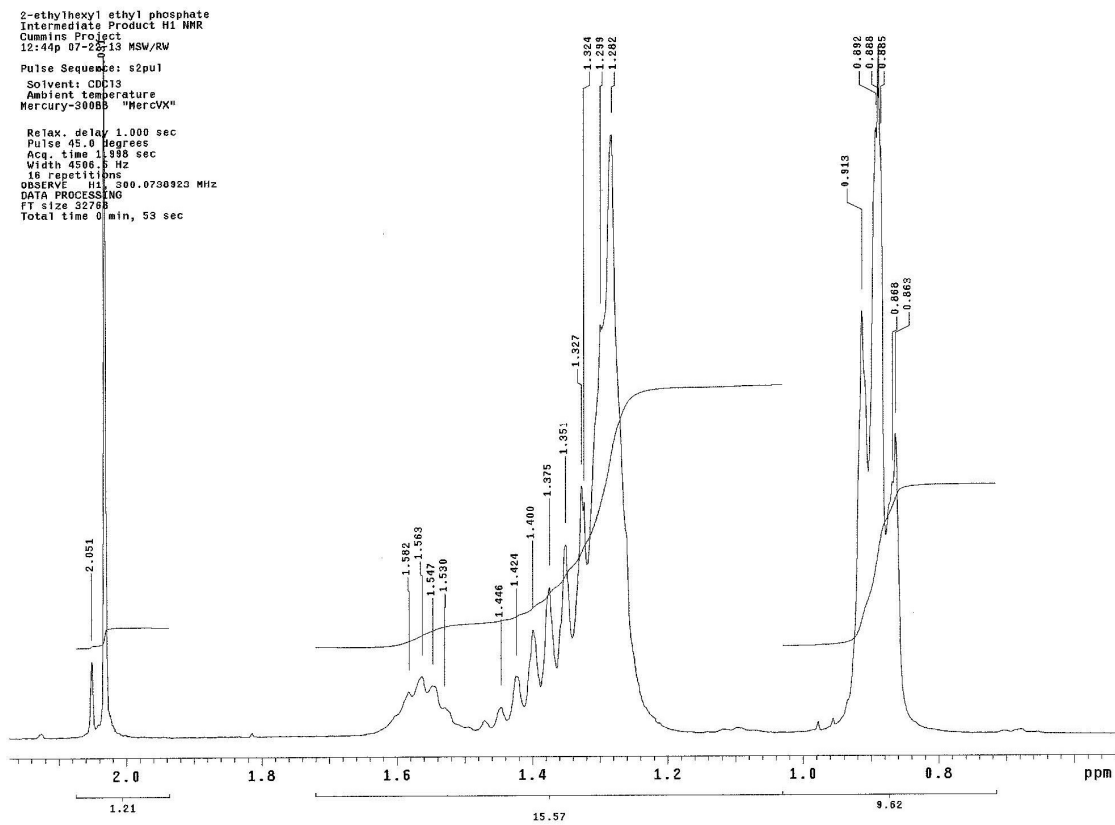


Figure F.27: ^1H NMR of ethyl 2-ethylhexyl phosphate in CDCl_3 between 0 and 2.5 ppm

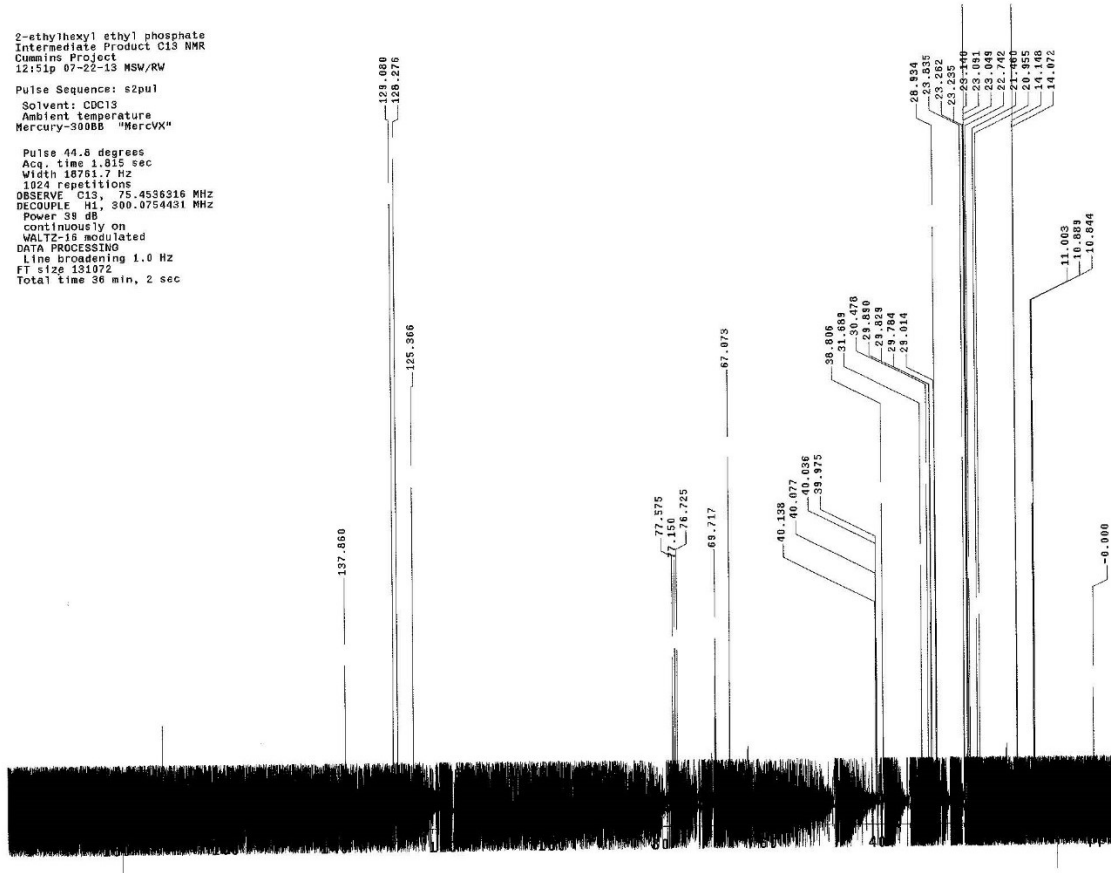


Figure F.28: ^{13}C NMR of ethyl 2-ethylhexyl phosphate in CDCl_3

2-ethylhexyl ethyl phosphate
Intermediate Product P31 NMR
Cummins Project
1:34p 07-22-13 MSW/RW
Pulse Sequence: s2pul
Solvent: CDCl3
Ambient temperature
Mercury-300BB "MerCVX"

Pulse 44.8 degrees
Acq. time 1.800 sec
Width 10010.0 Hz
128 repetitions
OBSERVE P31, 121.4721495 MHz
DECOUPLE H1, 300.0754431 MHz
Power 38 dB
continuously on
WALTZ-16 modulated
DATA PROCESSING
Line broadening 1.0 Hz
FT size 32768
Total time 3 min, 45 sec

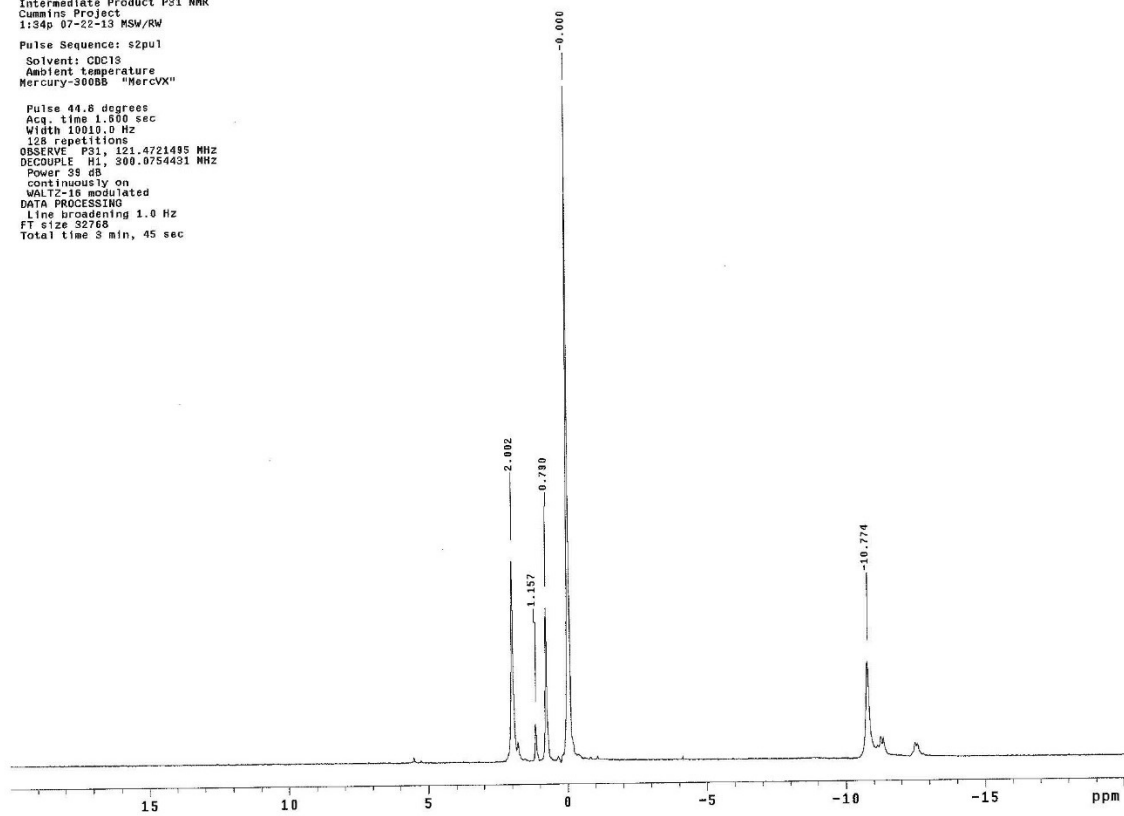


Figure F.29: ^{31}P NMR of ethyl 2-ethylhexyl phosphate in CDCl_3

ILs synthesized for Cummins, Inc. used as References

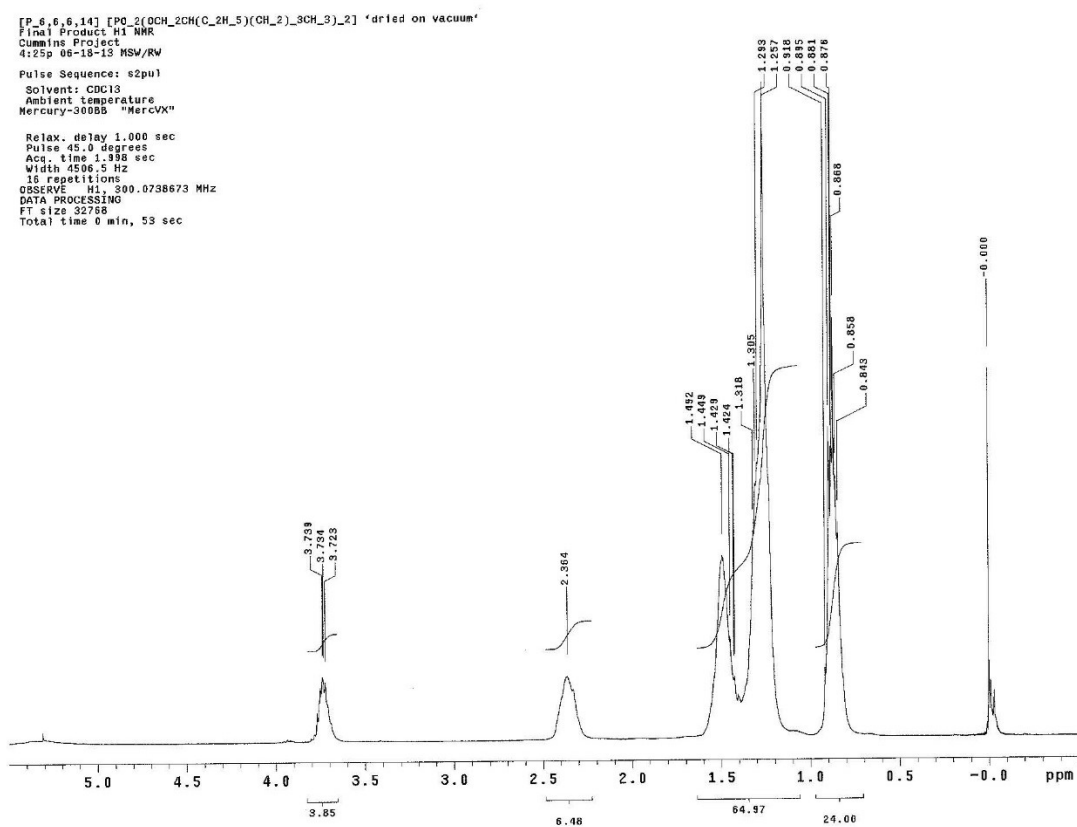


Figure F.30: ^1H NMR of trihexyl tetradecyl phosphonium bis(2-ethylhexyl) phosphate in CDCl_3

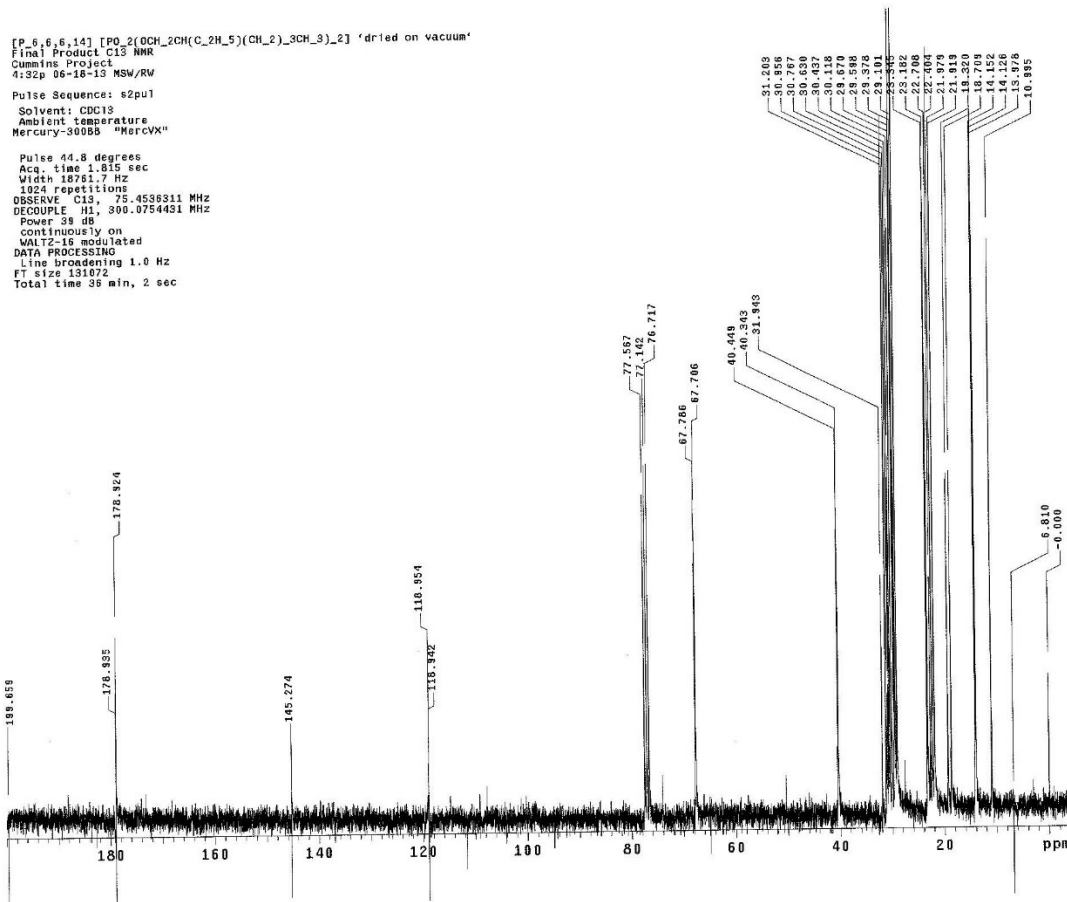


Figure F.31: ^{13}C NMR of trihexyl tetradecyl phosphonium bis(2-ethylhexyl) phosphate in CDCl_3

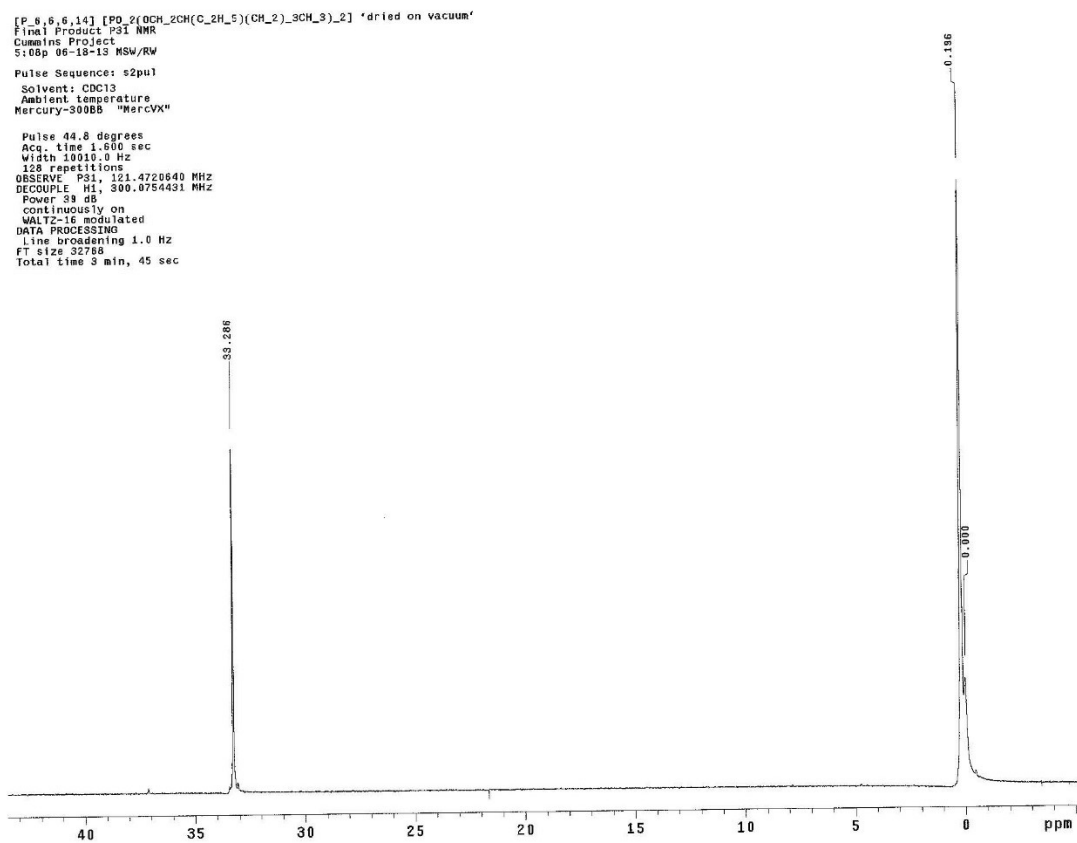


Figure F.32: ^{31}P NMR of trihexyl tetradecyl phosphonium bis(2-ethylhexyl) phosphate in CDCl_3

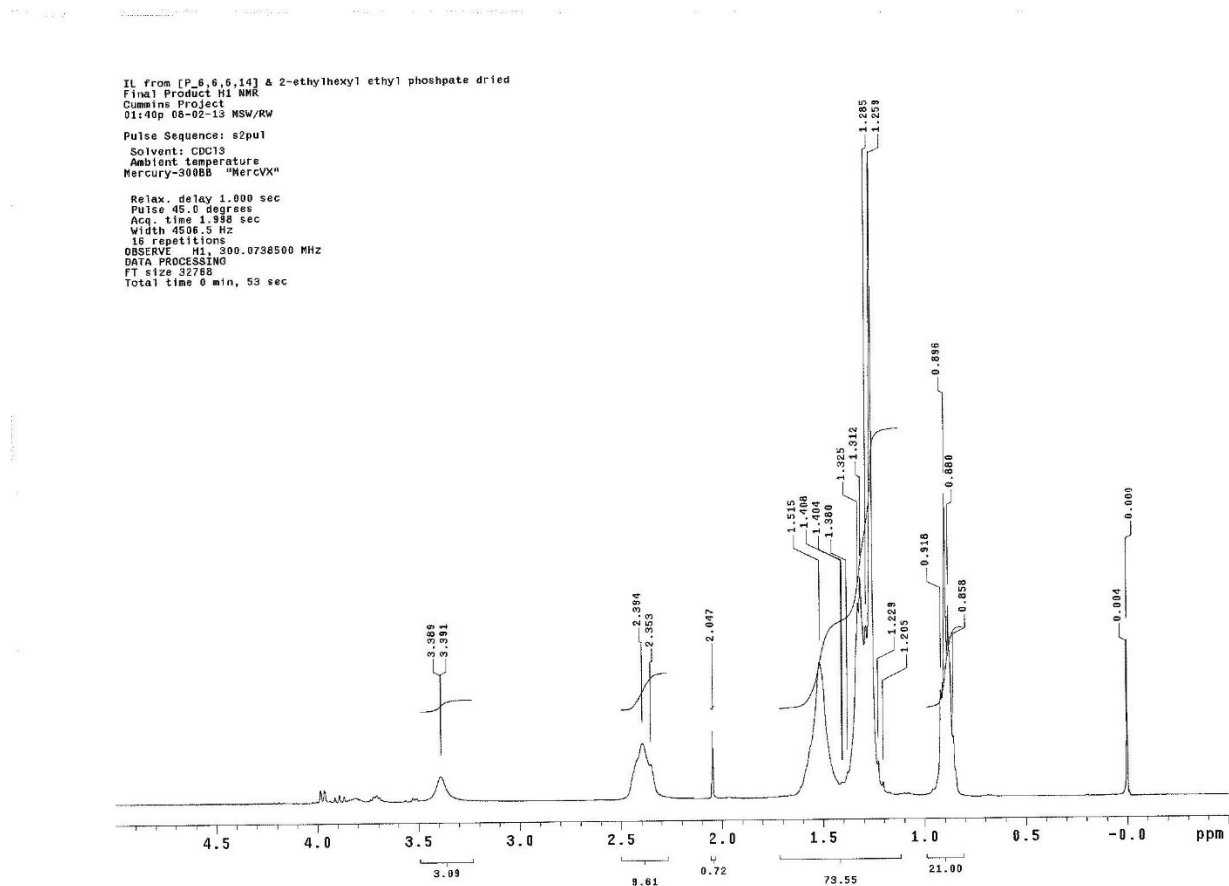


Figure F.33: ^1H NMR of trihexyl tetradecyl phosphonium ethyl 2-ethylhexyl phosphate in CDCl_3

IL from 2-ethylhexyl 2-phenylethyl phosphate & P_6,6,6,14
 Final Product C13 NMR
 Cummins Project
 1:47p 07-02-13 MSW/RW
 Pulse Sequence: s2pul
 Solvent: CDCl3
 Ambient temperature
 Mercury-300SB "Mercury"
 Pulse 44.8 degrees
 Acq. time 1.815 sec
 Width 18761.7 Hz
 1024 repetitions
 OBSERVE C13, 75.4536219 MHz
 DECOUPLE H1, 300.0754431 MHz
 Power 39 dB
 continuously on
 WALTZ-16 modulated
 DATA PROCESSING
 Line broadening 1.0 Hz
 FT size 131072
 Total time 36 min, 2 sec

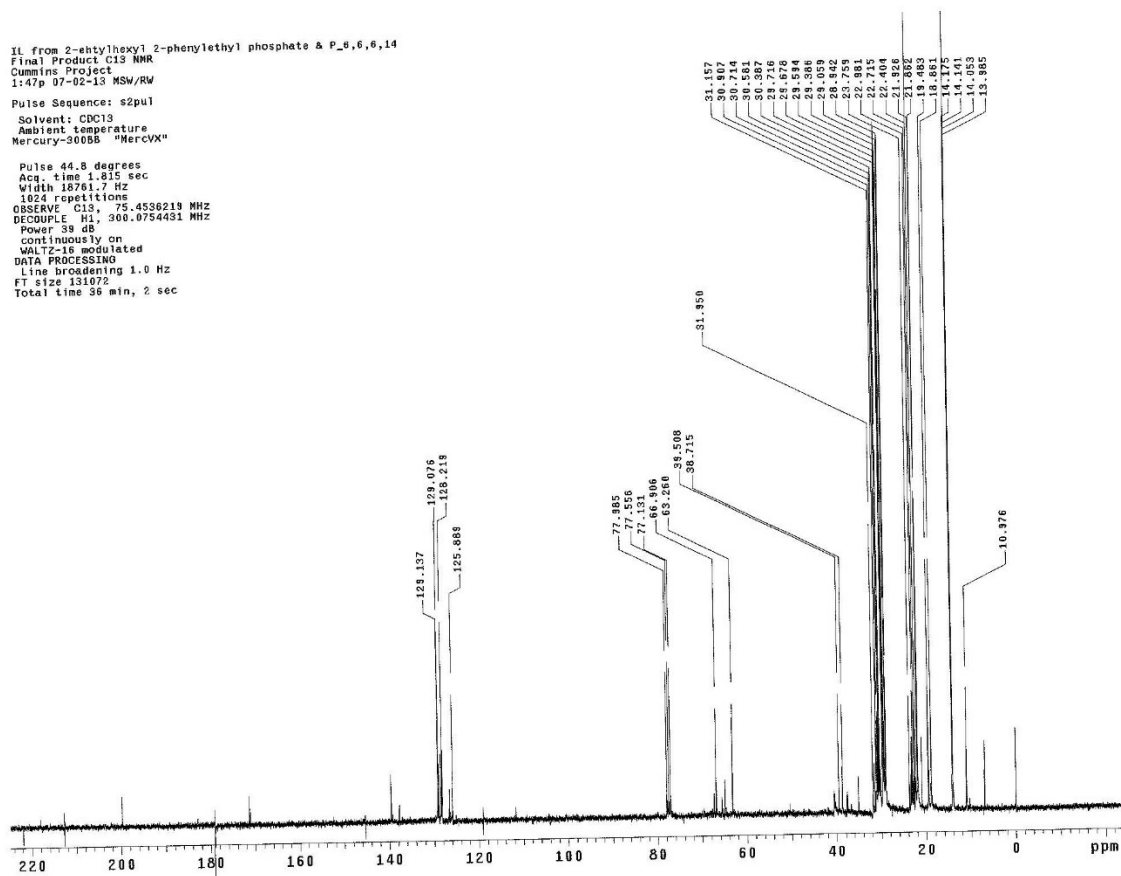


Figure F.34: ^{13}C NMR of trihexyl tetradecyl phosphonium ethyl 2-ethylhexyl phosphate in CDCl_3

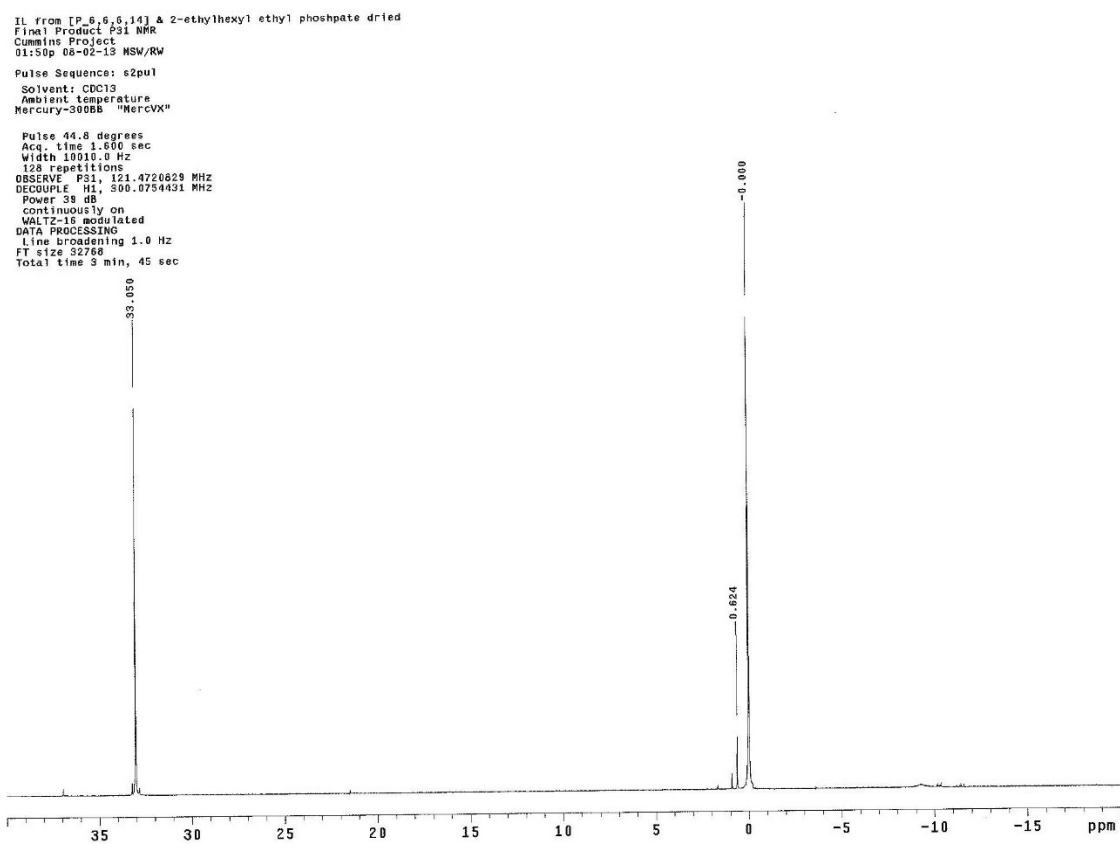


Figure F.35: ^{31}P NMR of trihexyl tetradecyl phosphonium ethyl 2-ethylhexyl phosphate in CDCl_3

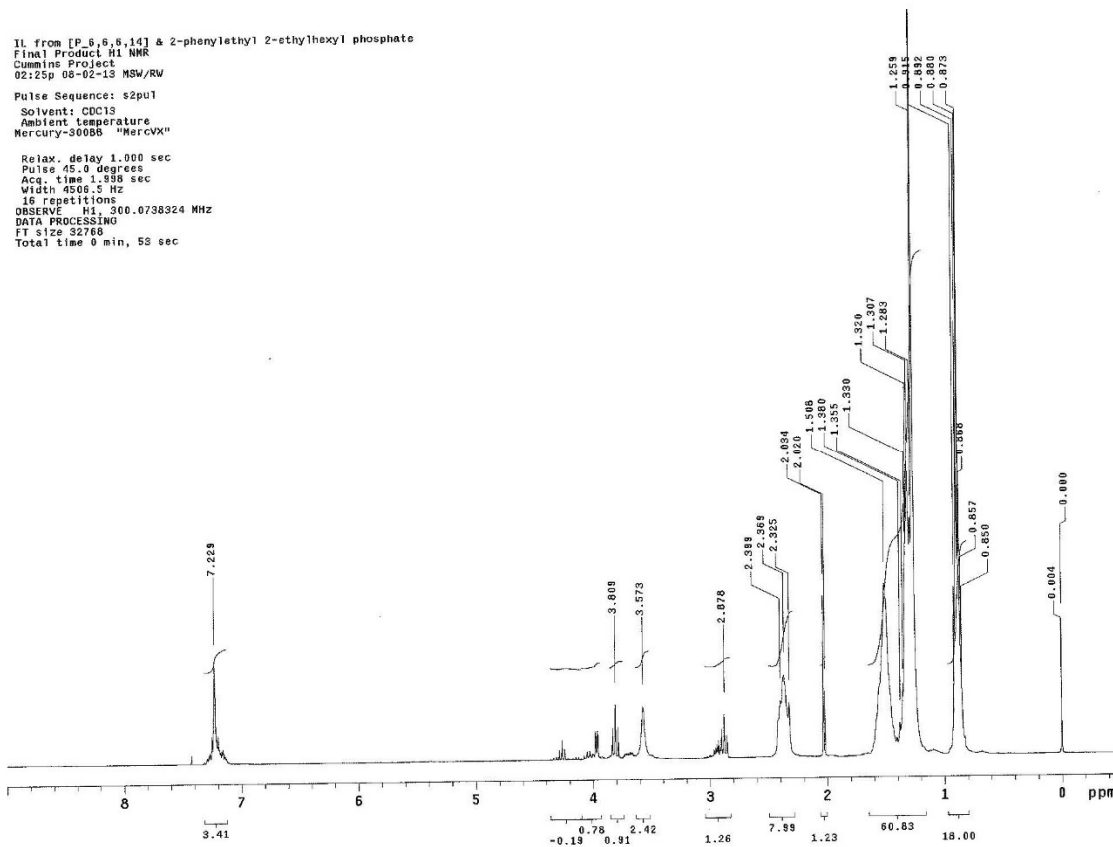


Figure F.36: ^1H NMR of trihexyl tetradecyl phosphonium 2-phenylethyl 2-ethylhexyl phosphate in CDCl_3

IL from [P_5,6,6,14] & 2-phenylethyl 2-ethylhexyl phosphate
Final Product P31 NMR
Cummins Project
02:35p 08-02-13 MSW/RW
Pulse Sequence: s2pu1
Solvent: CDCl3
Ambient Temperature
Mercury-80088 "MerCVX"
Pulse 44.8 degree
Acq. time 1.800 sec
Width 10010.0 Hz
128 repetitions
OBSERVE P31, 121.4720774 MHz
DECOUPLE H1, 300.0754431 MHz
Power 38 dB
continuously on
WALTZ-16 modulated
DATA PROCESSING
Line broadening 0.0 Hz
FT size 32768
Total time 3 min 45 sec

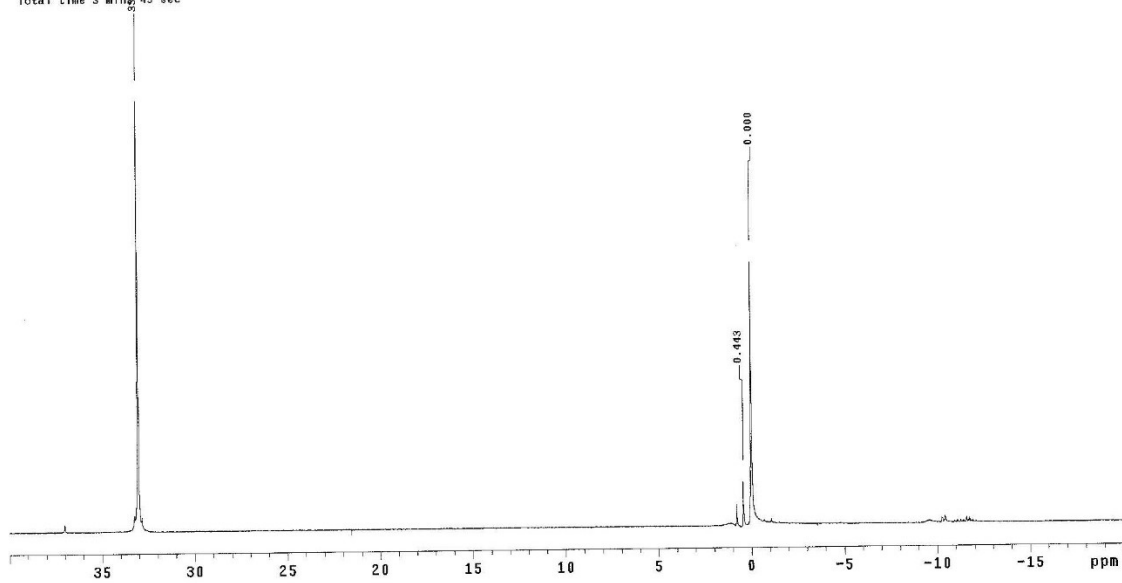


Figure F.37: ^{31}P NMR of trihexyl tetradecyl phosphonium 2-phenylethyl 2-ethylhexyl phosphate in CDCl_3

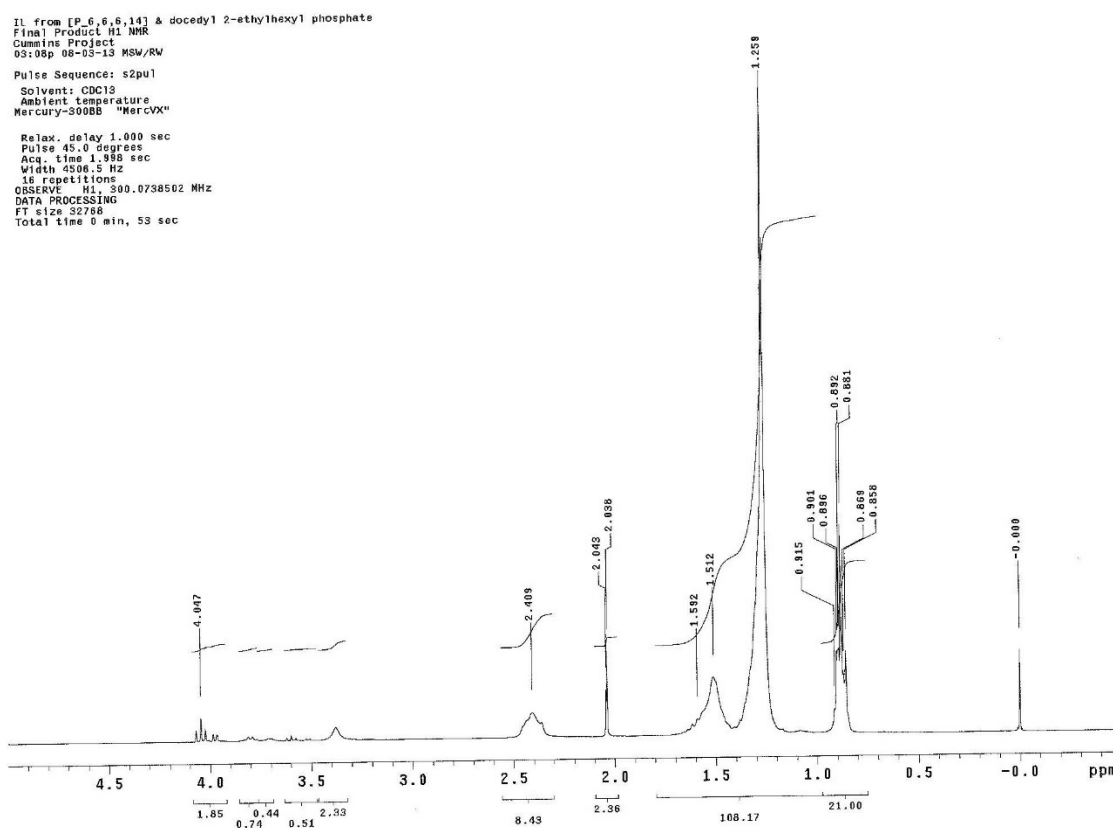


Figure F.38: ^1H NMR of trihexyl tetradecyl phosphonium dodecyl 2-ethylhexyl phosphate in CDCl_3

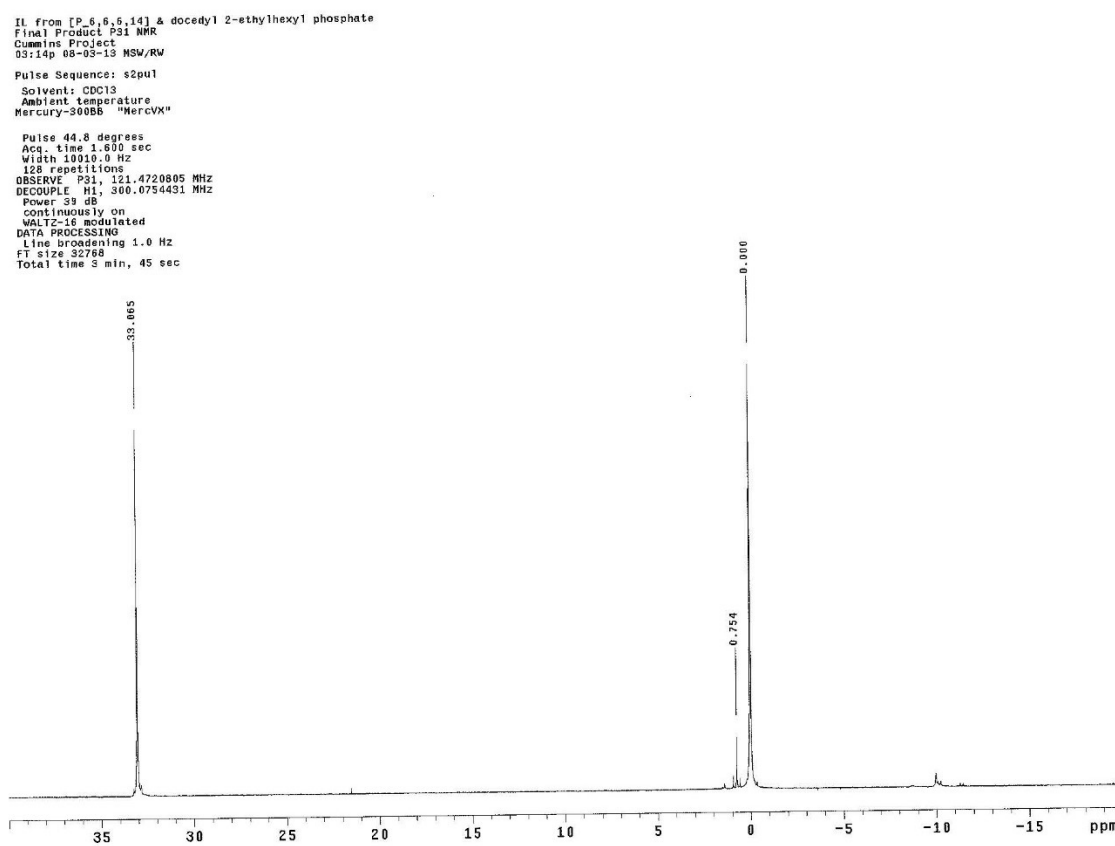


Figure F.39: ^{31}P NMR of trihexyl tetradecyl phosphonium dodecyl 2-ethylhexyl phosphate in CDCl_3

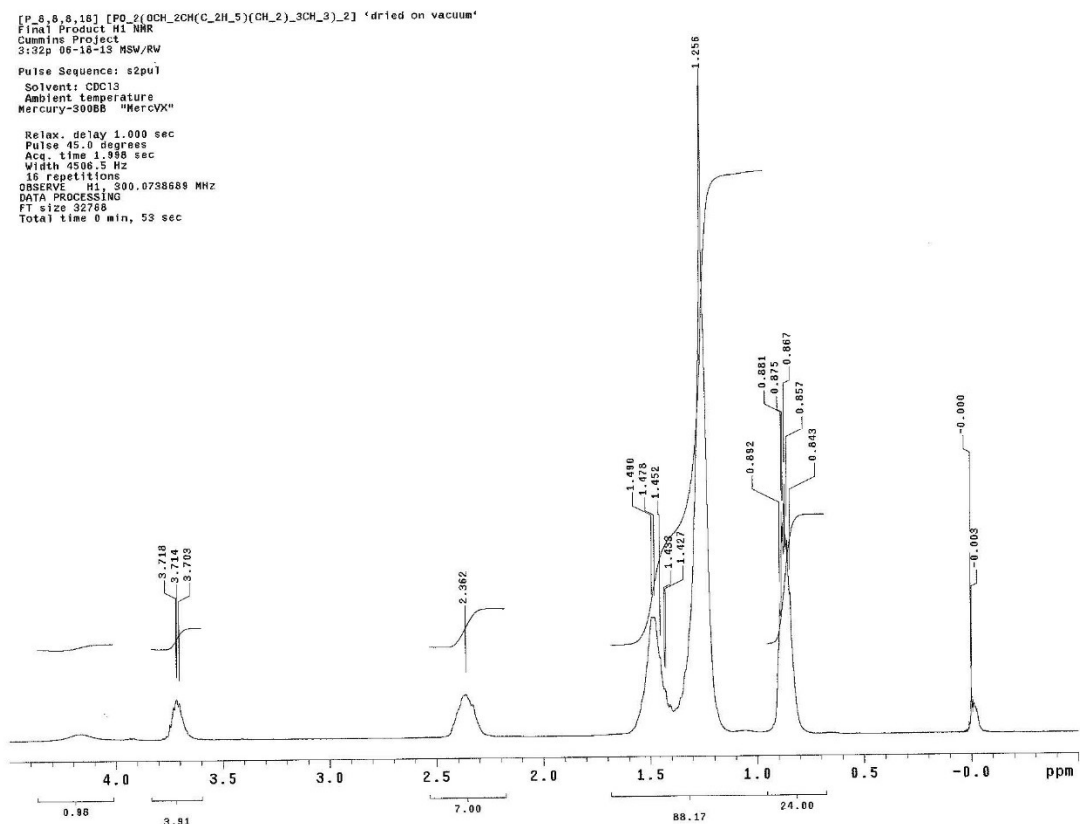


Figure F.40: ^1H NMR of trioctyl octadecyl phosphonium bis(2-ethylhexyl) phosphate in CDCl_3

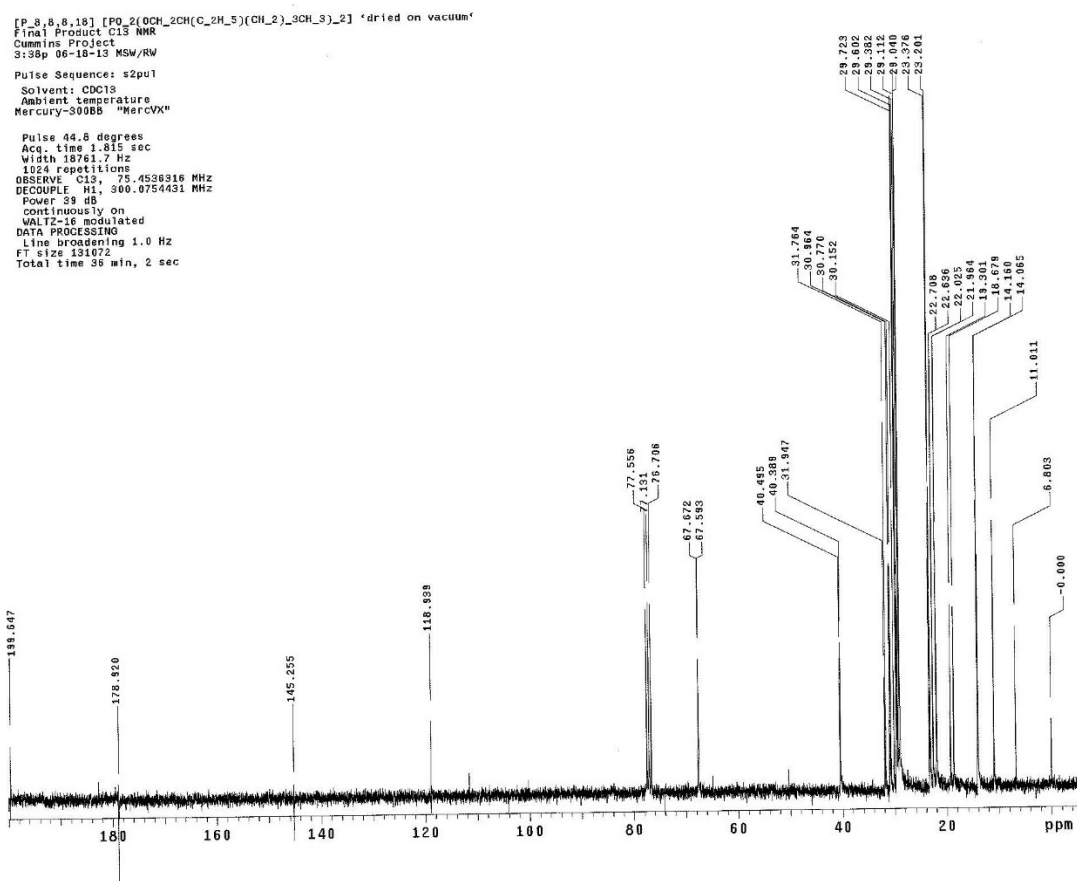


Figure F.41: ^{13}C NMR of trioctyl octadecyl phosphonium bis(2-ethylhexyl) phosphate in CDCl_3

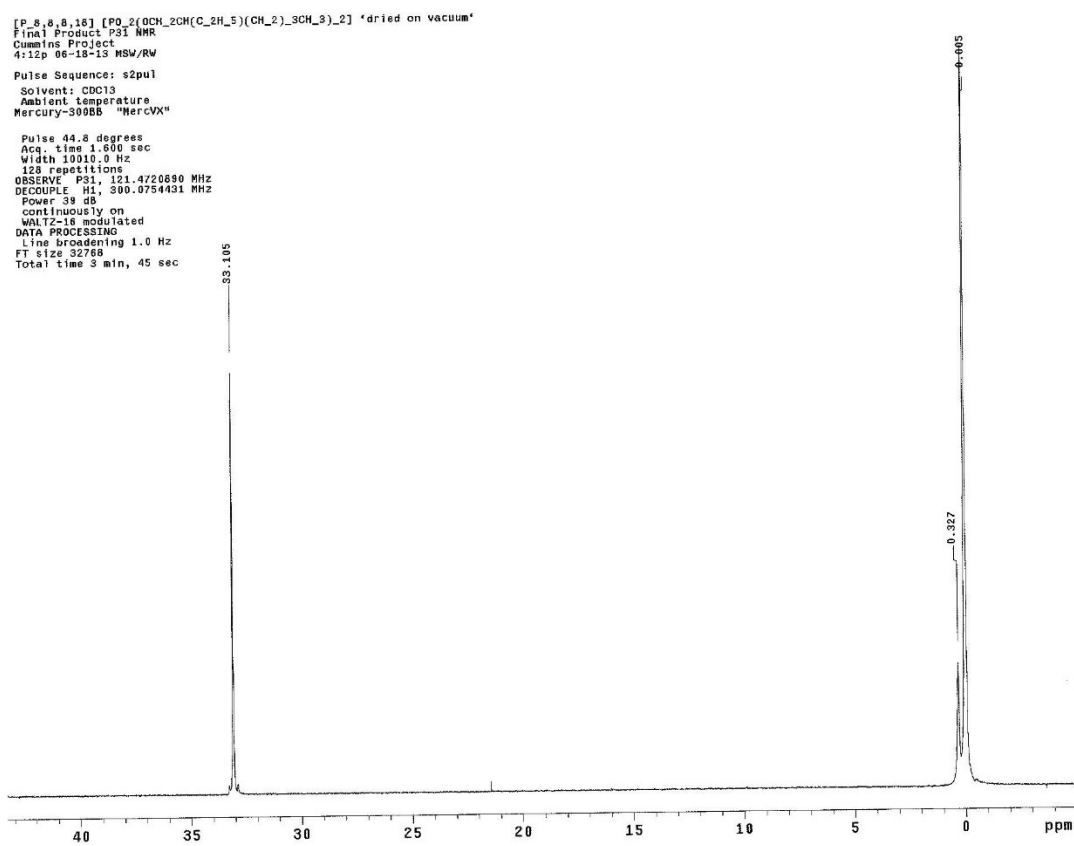


Figure F.42: ^{31}P NMR of trioctyl octadecyl phosphonium bis(2-ethylhexyl) phosphate in CDCl_3

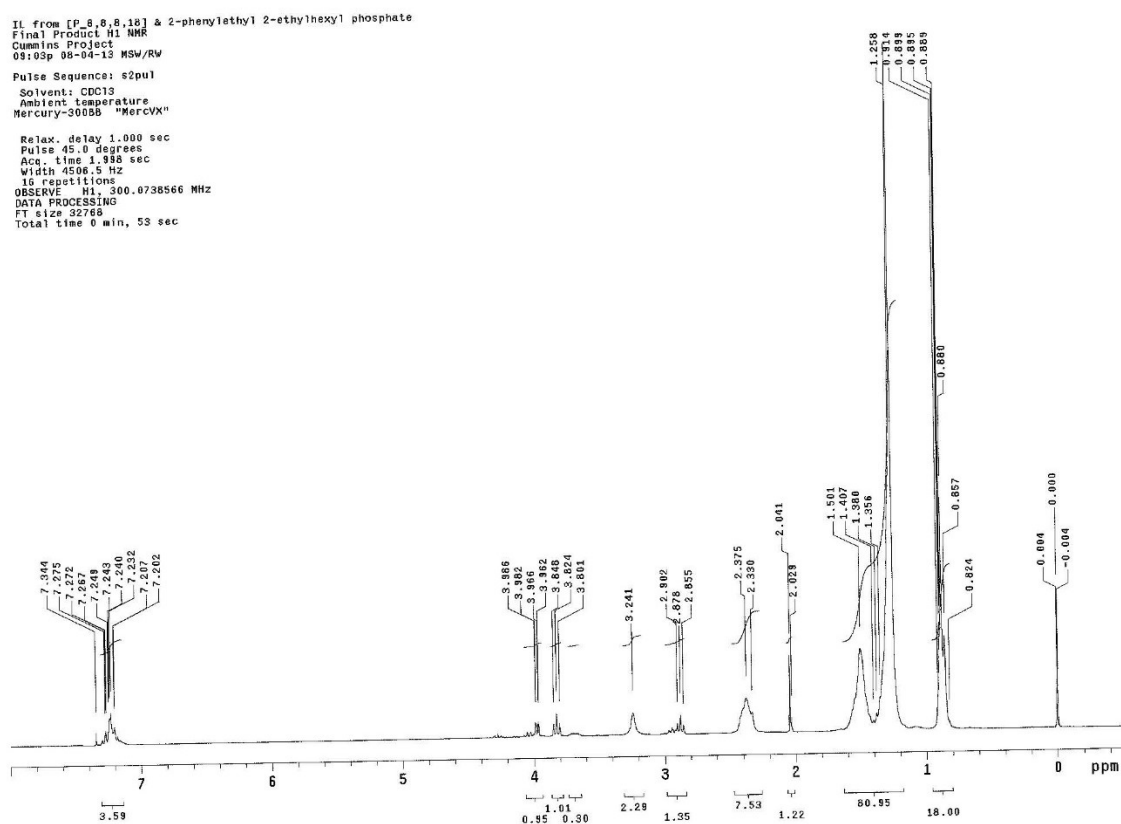


Figure F.43: ^1H NMR of trioctyl octadecyl phosphonium 2-phenylethyl 2-ethylhexyl phosphate in CDCl_3

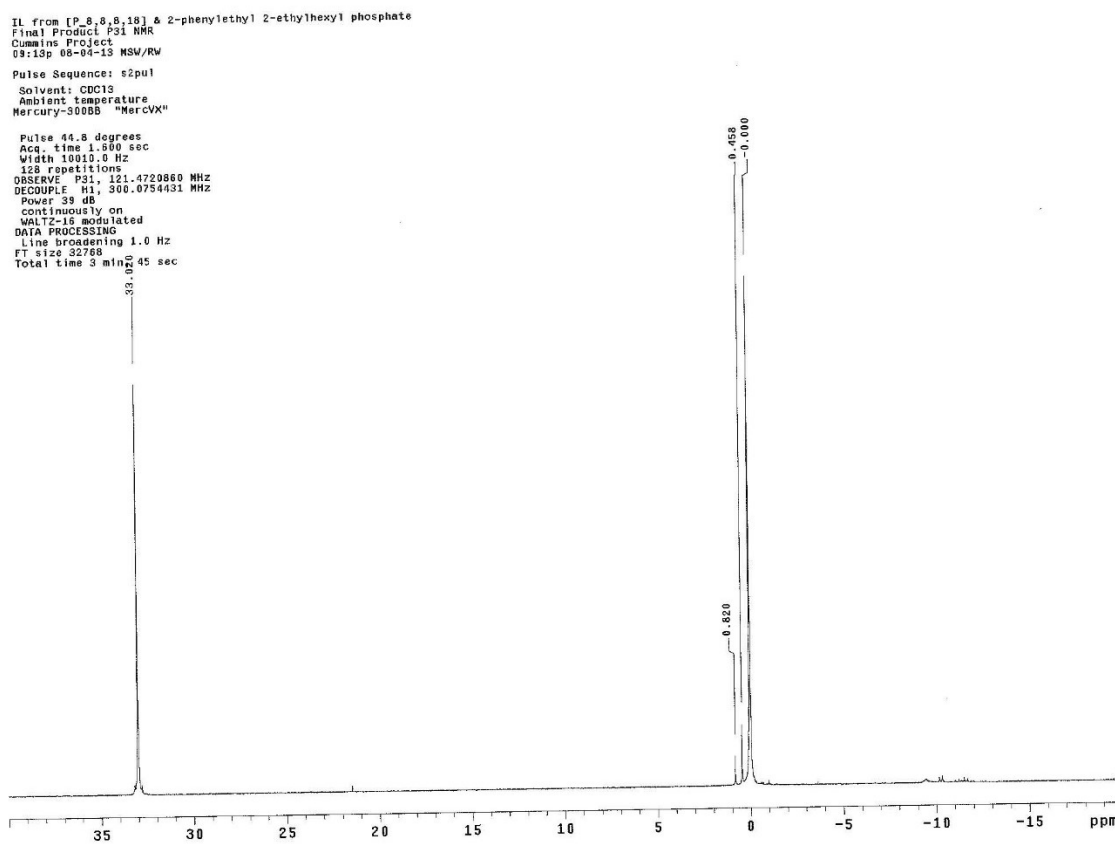


Figure F.44: ^{31}P NMR of trioctyl octadecyl phosphonium 2-phenylethyl 2-ethylhexyl phosphate in CDCl_3

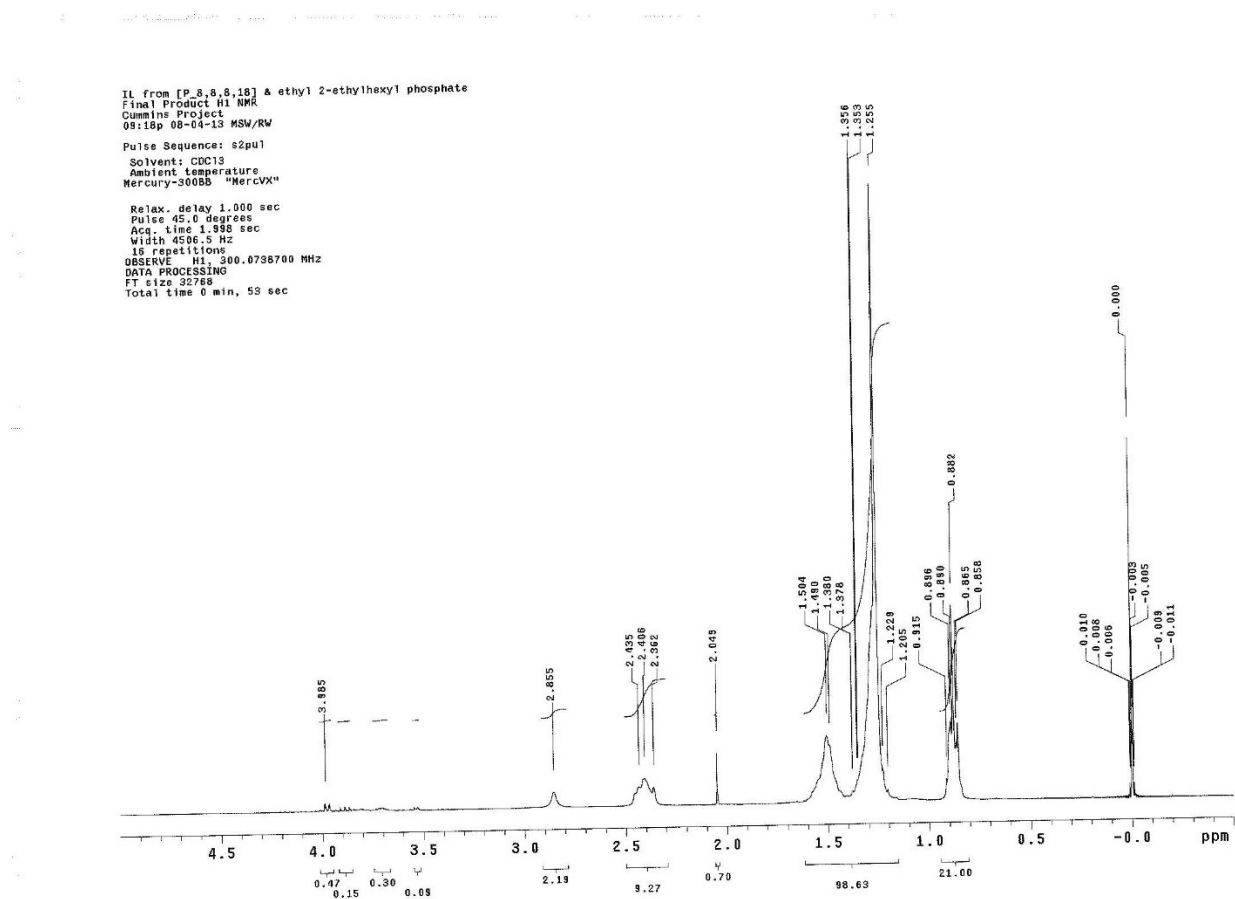


Figure F.45: ^1H NMR of trioctyl octadecyl phosphonium ethyl 2-ethylhexyl phosphate in CDCl_3

IL from [P,8,8,8,18] & ethyl 2-ethylhexyl phosphate
Final Product ^{31}P NMR
Cummins Project
08:25p 08-04-13 MSW/RW
Pulse Sequence: s2pu1
Solvent: CDCl_3
Ambient temperature
Mercury-300BB "Mercury"
Pulse 44.8 degrees
Acq. time 1.600 sec
Width 10010.0 Hz
128 repetitions
OBSERVE ^{31}P , 121.4720815 MHz
DECOUPLE ^1H , 300.0754431 MHz
Power 39 dB
continuously on
WALTZ-16 modulated
DATA PROCESSING
Line broadening 1.0 Hz
F1 size 32768
Total time 3 min, 45 sec

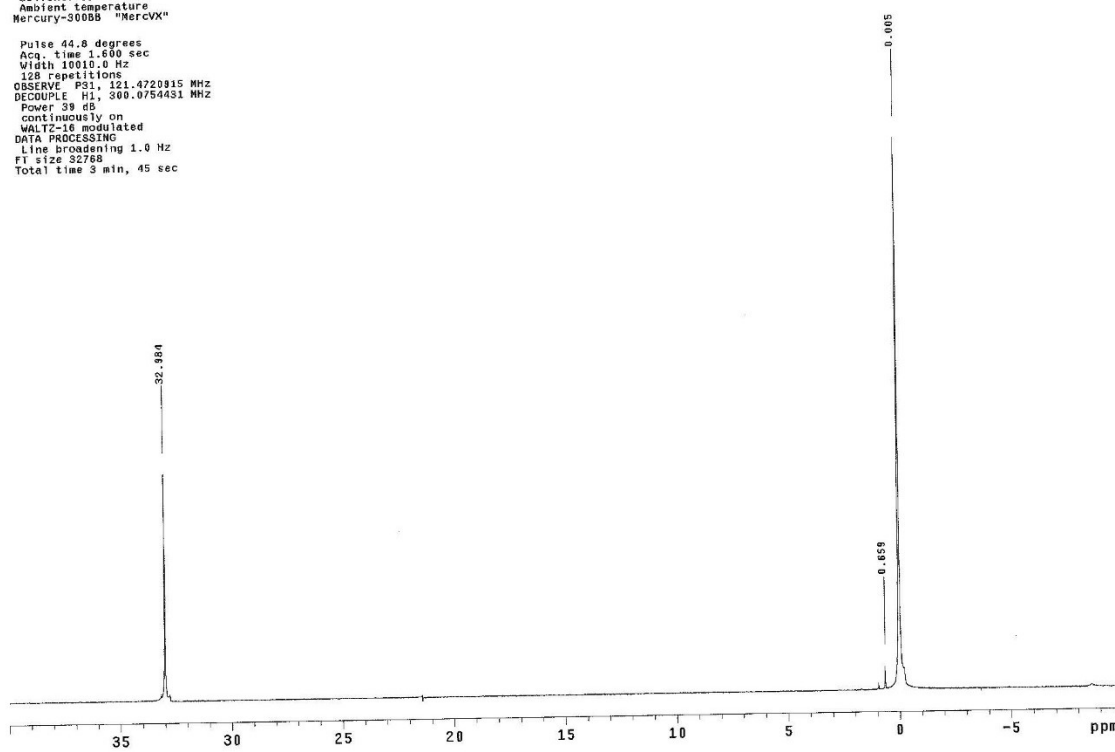


Figure F.46: ^{31}P NMR of trioctyl octadecyl phosphonium ethyl 2-ethylhexyl phosphate in CDCl_3

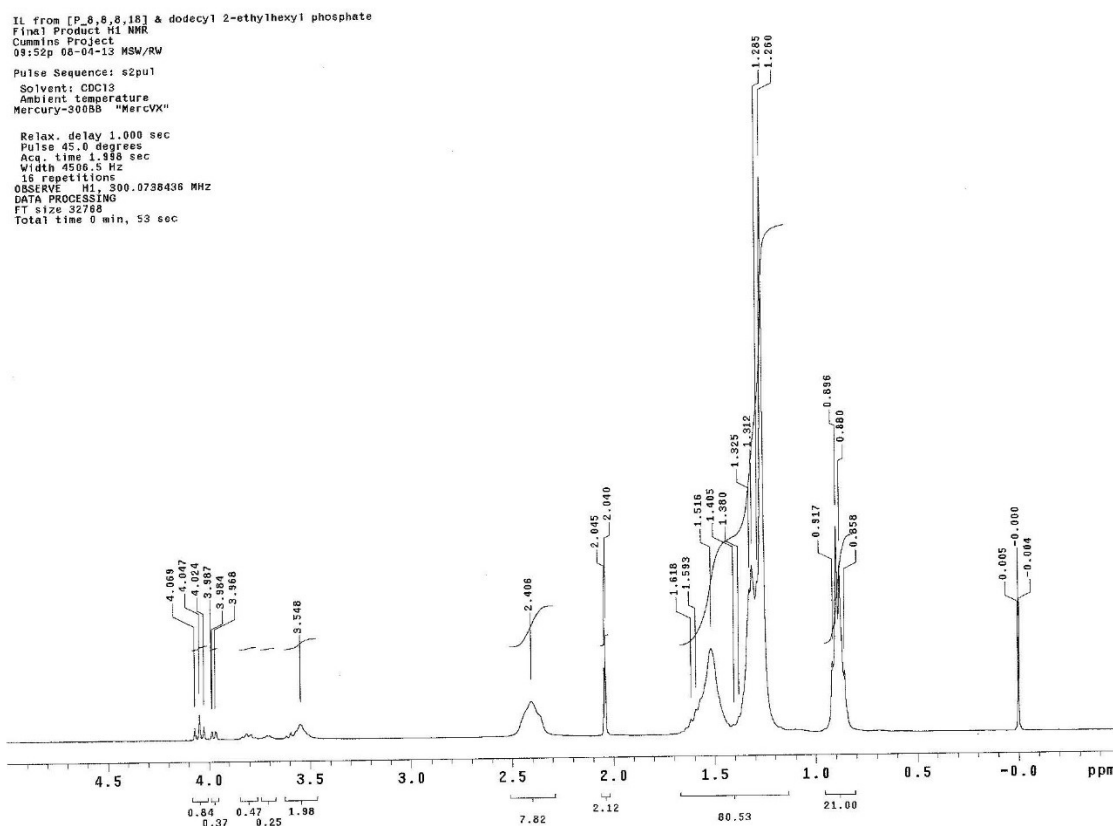


Figure F.47: ^1H NMR of trioctyl octadecyl phosphonium dodecyl 2-ethylhexyl phosphate in CDCl_3

IL from [P_8,8,8.18] & dodecyl 2-ethylhexyl phosphate
Final Product P31 NMR
Cummins Project
10:03p 08-04-13 MSW/RW
Pulse Sequence: s2pu1
Solvent: CDCl3
Ambient temperature
Mercury-300BB "MercVX"
Pulse 44.8 degrees
Acq. time 1.500 sec
Width 10010.0 Hz
128 repetitions
OBSERVE F31, 121.4720799 MHz
DECOUPLE H1, 300.0754431 MHz
Power 39 dB
continuously on
WALTZ-16 modulated
DATA PROCESSING
Line broadening 1.0 Hz
FT size 32768
Total time 3 min, 45 sec

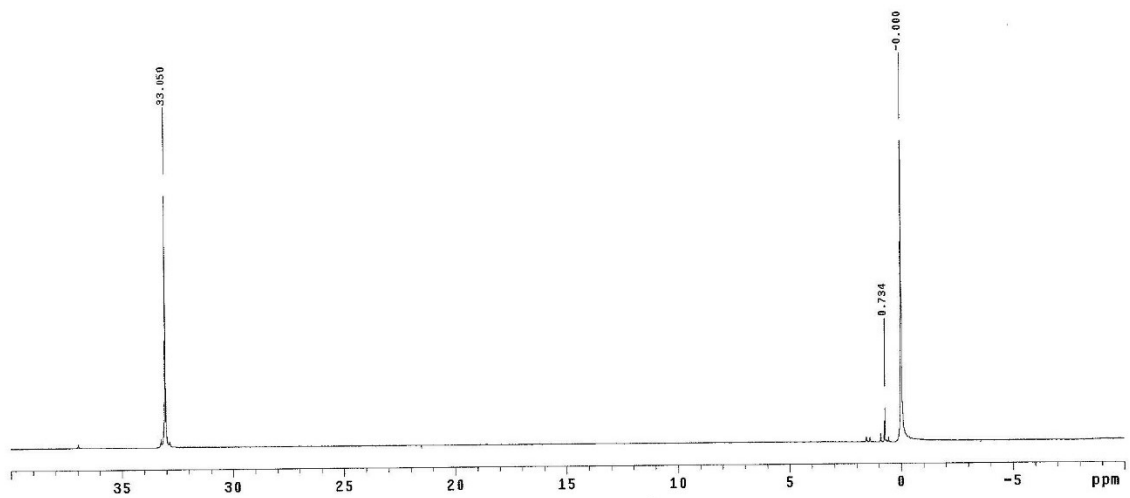


Figure F.48: ^{31}P NMR of trioctyl octadecyl phosphonium dodecyl 2-ethylhexyl phosphate in CDCl_3

Most Recently Synthesized Cation, Anions and ILs

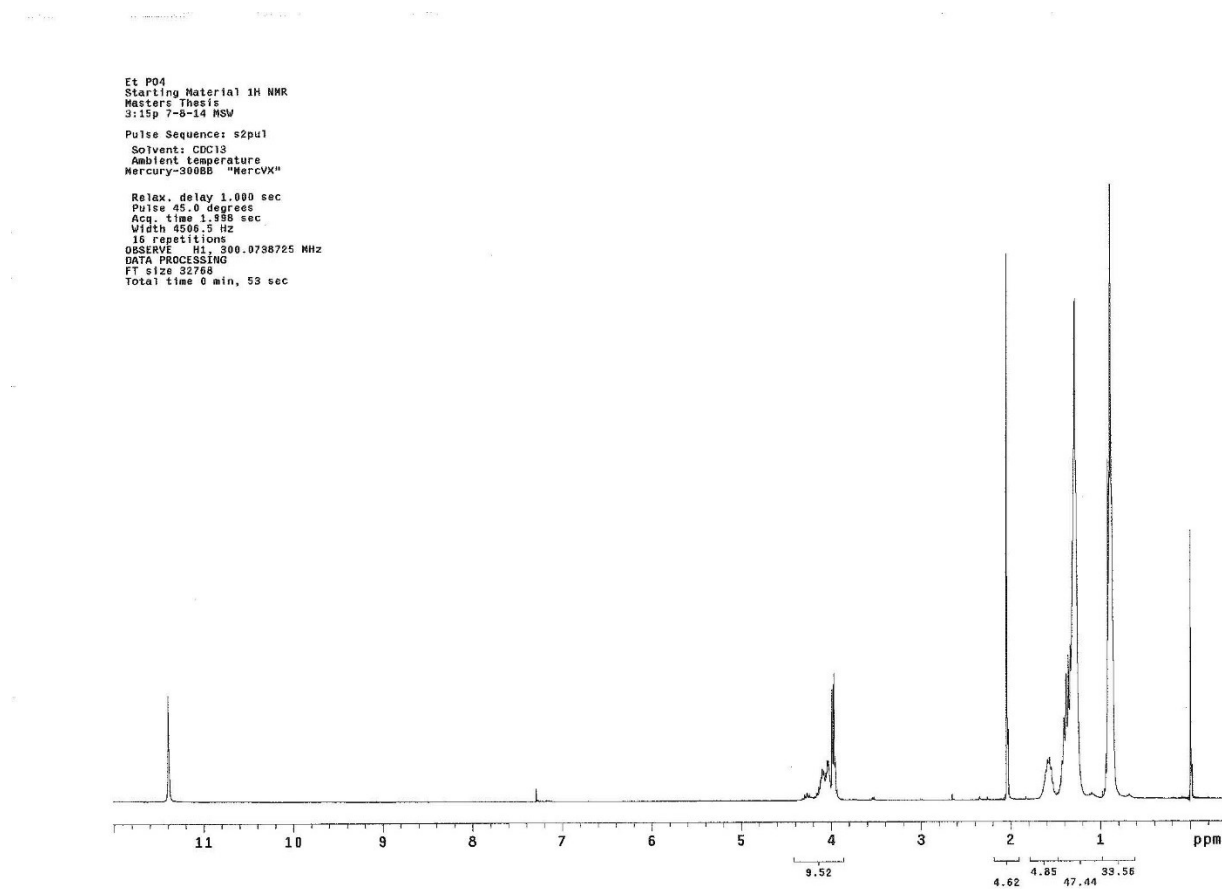


Figure F.49: ^1H NMR of ethyl 2-ethylhexyl phosphate in CDCl_3

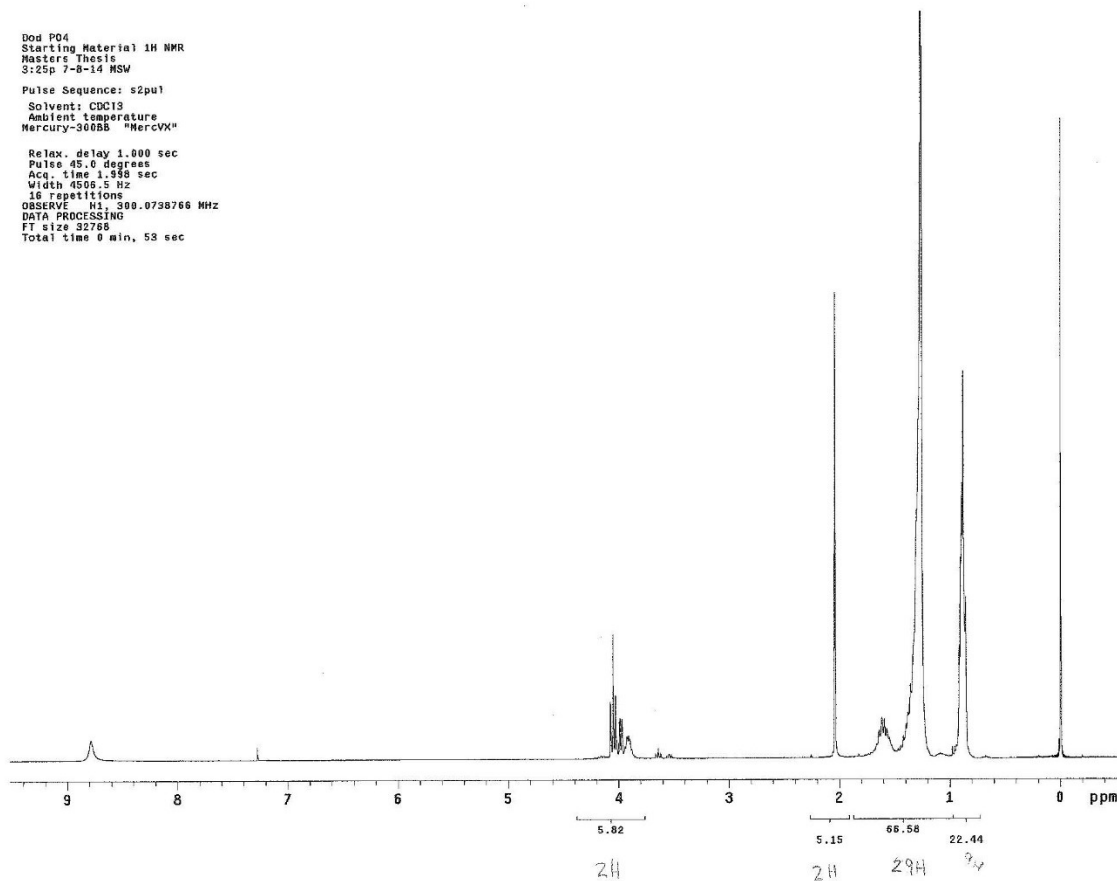


Figure F.50: ^1H NMR of dodecyl 2-ethylhexyl phosphate in CDCl_3

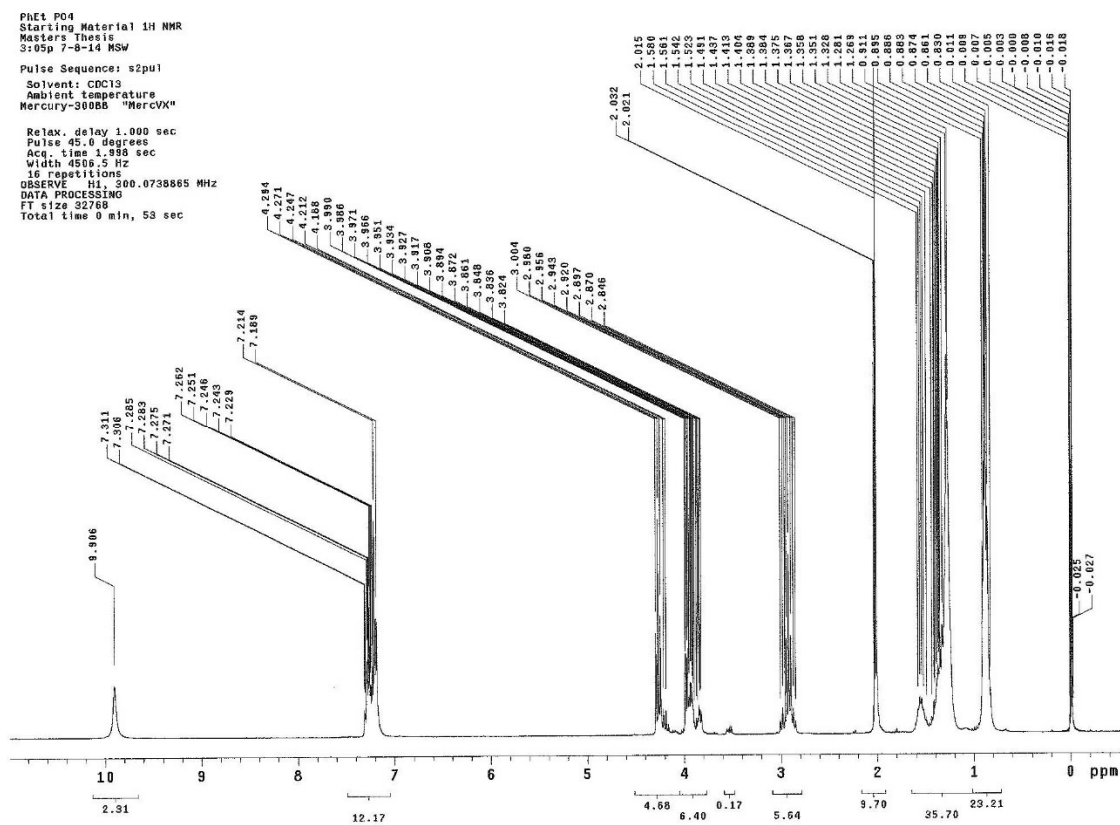


Figure F.51: ^1H NMR of 2-phenylethyl 2-ethylhexyl phosphate in CDCl_3

P8_8_8_18
Intermediate 1H NMR
Masters Thesis
9:30p 7-5-14 MSW

Pulse Sequence: s2pu1
Solvent: CDCl3
Ambient temperature
Mercury-300BB "MercVX"

Relax. delay 1.000 sec
Pulse 45.0 degrees
Acq. time 1.998 sec
Width 4506.5 Hz
16 repetitions
OBSERVE H1, 300.0738744 MHz
DATA PROCESSING
FT size 32768
Total time 0 min, 53 sec

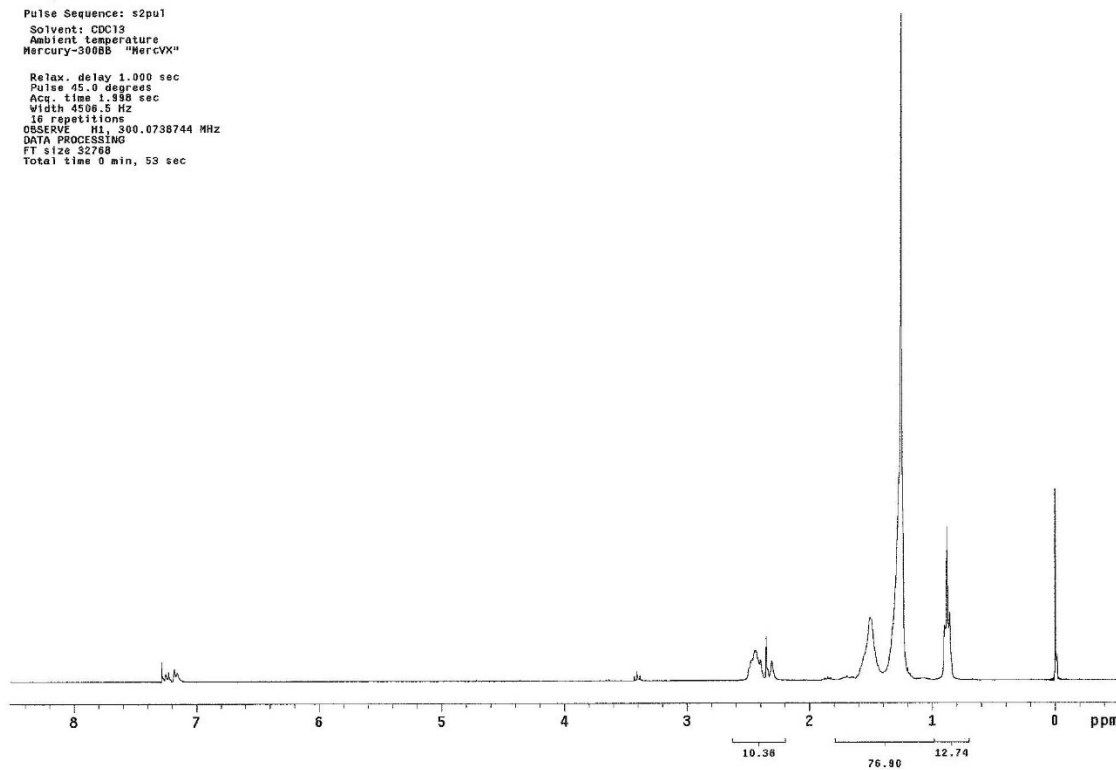


Figure F.52: ¹H NMR of trioctyl octadecyl phosphonium bromide in CDCl₃

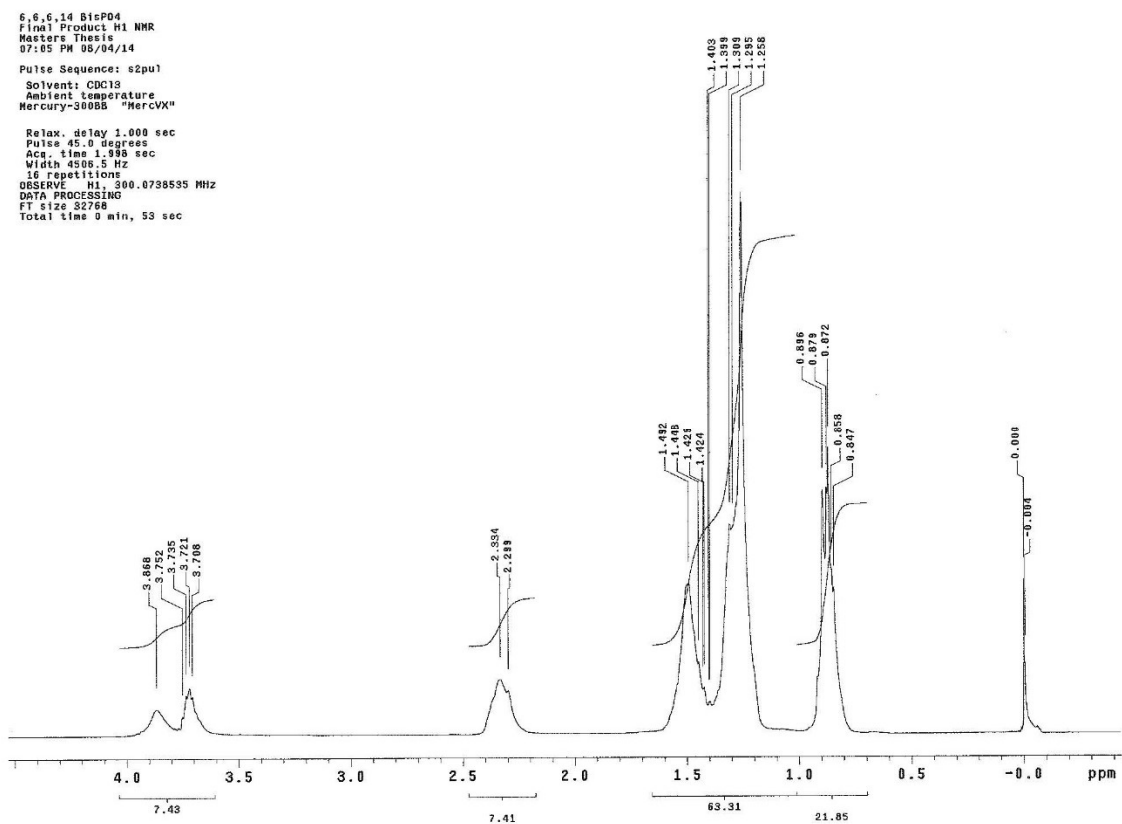


Figure F.53: ^1H NMR of trihexyl tetradecyl phosphonium bis(2-ethylhexyl) phosphate in CDCl_3

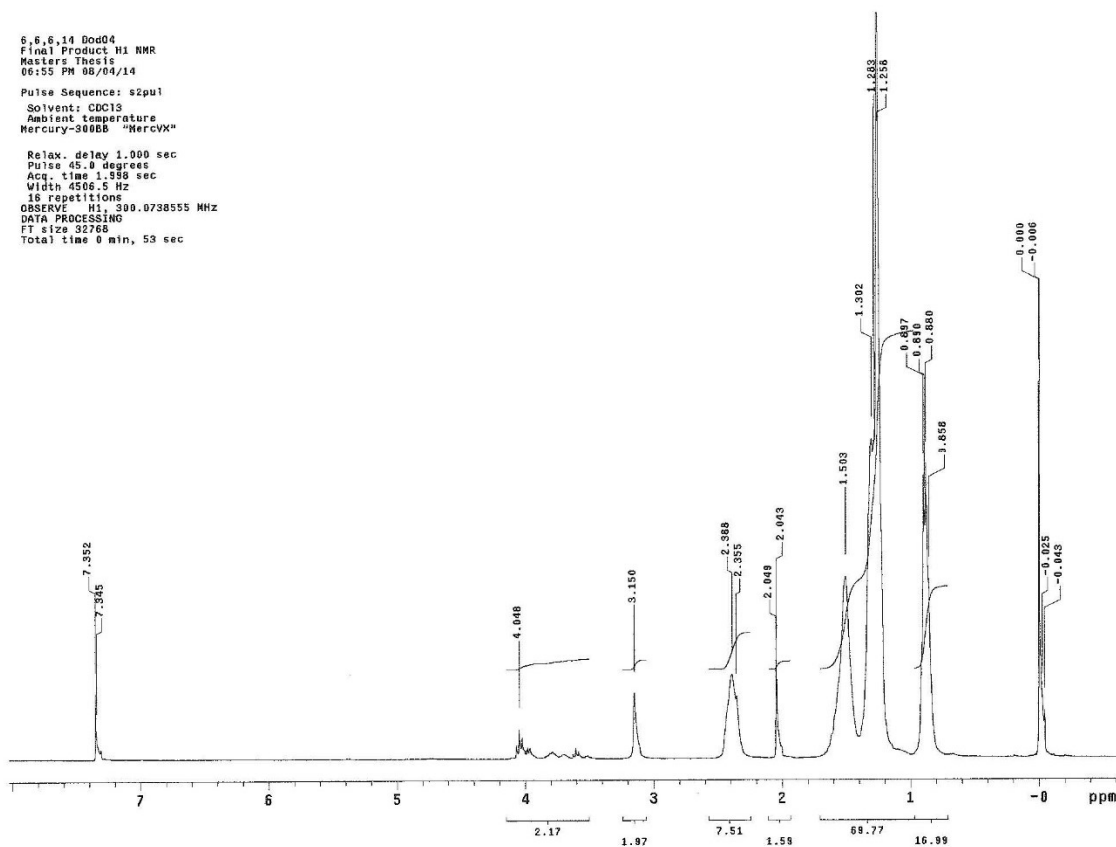


Figure F.54: ¹H NMR of trihexyl tetradecyl phosphonium dodecyl 2-ethylhexyl phosphate in CDCl₃

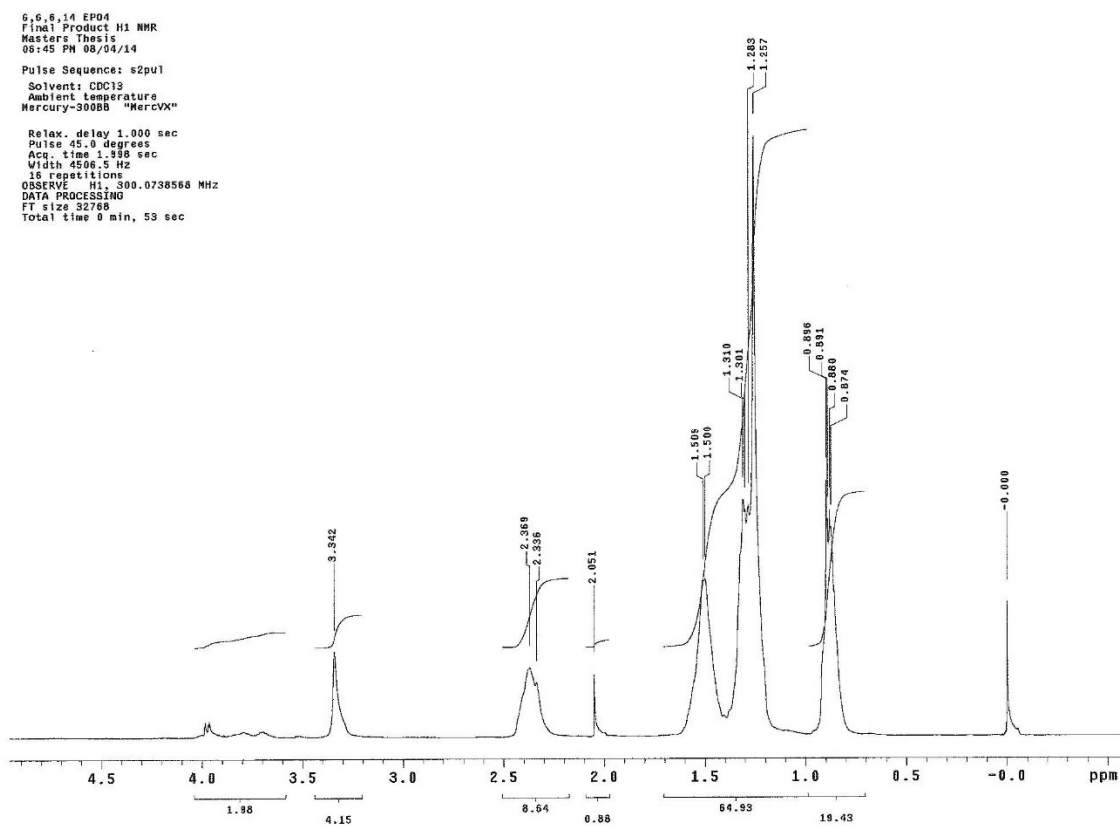


Figure F.55: ^1H NMR of trihexyl tetradecyl phosphonium ethyl 2-ethylhexyl phosphate in CDCl_3

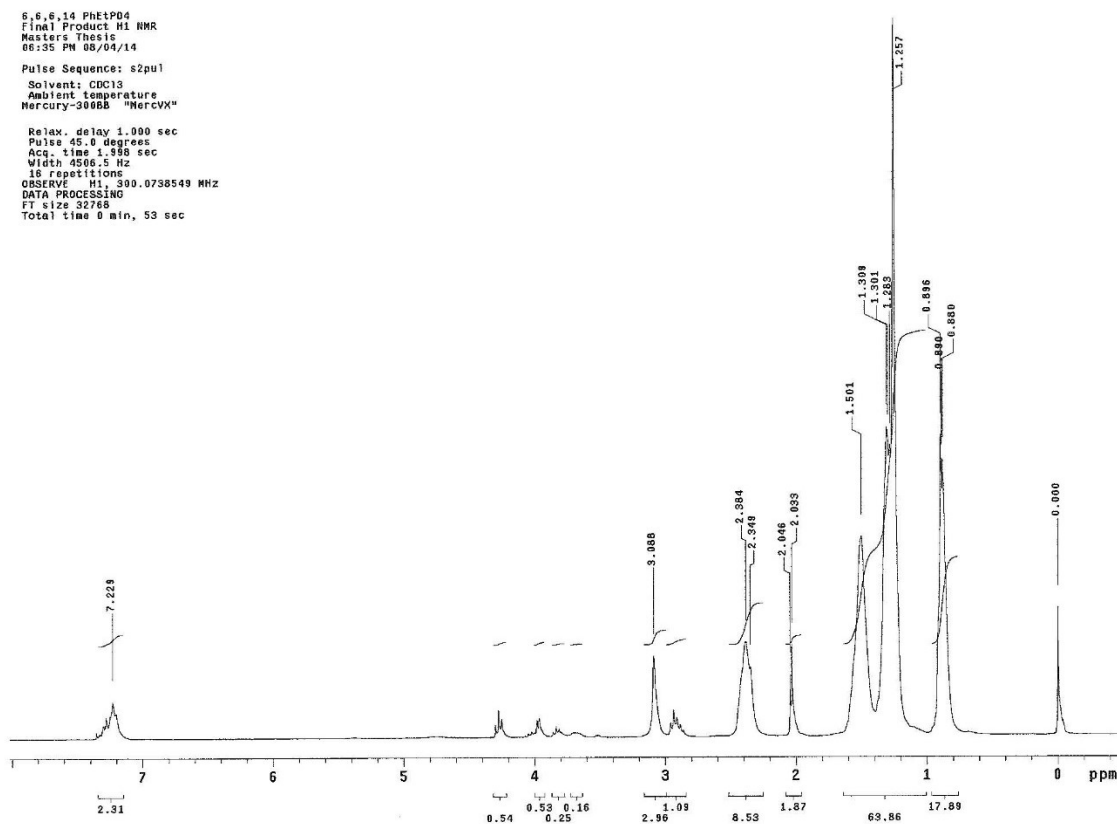


Figure F.56: ^1H NMR of trihexyl tetradecyl phosphonium 2-phenylethyl 2-ethylhexyl phosphate in CDCl_3

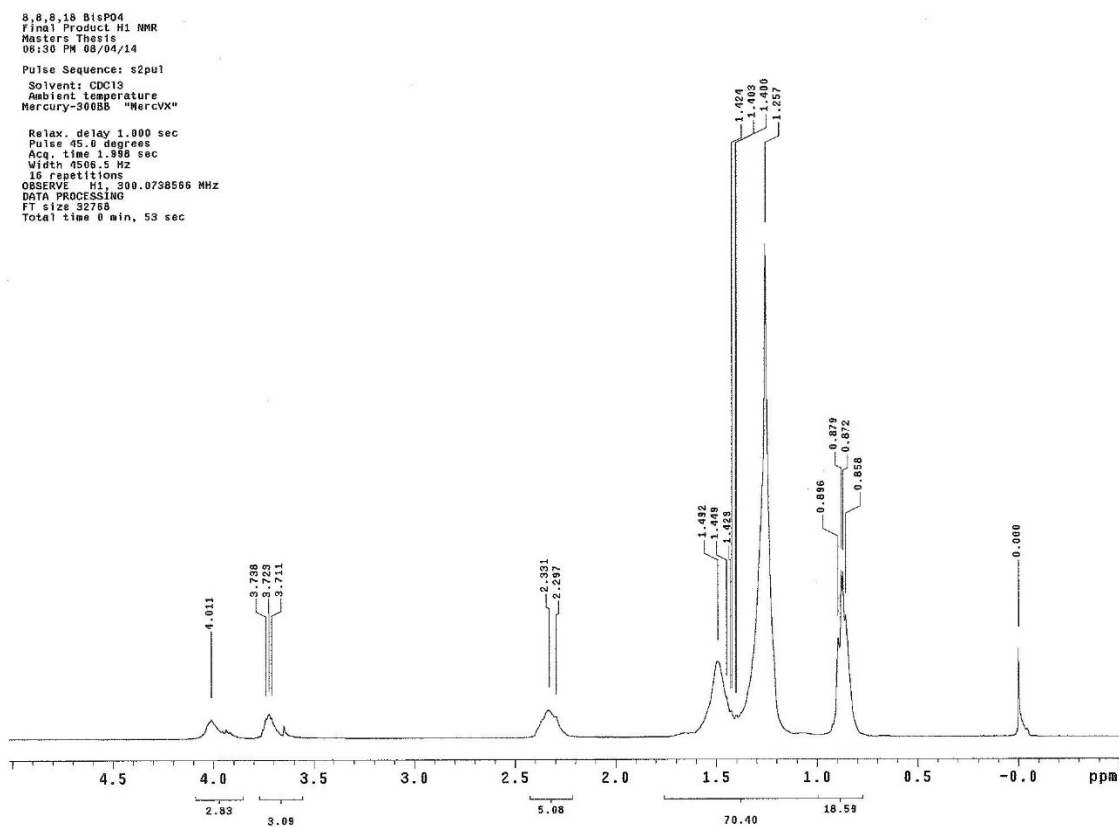


Figure F.57: ^1H NMR of trioctyl octadecyl phosphonium bis(2-ethylhexyl) phosphate in CDCl_3

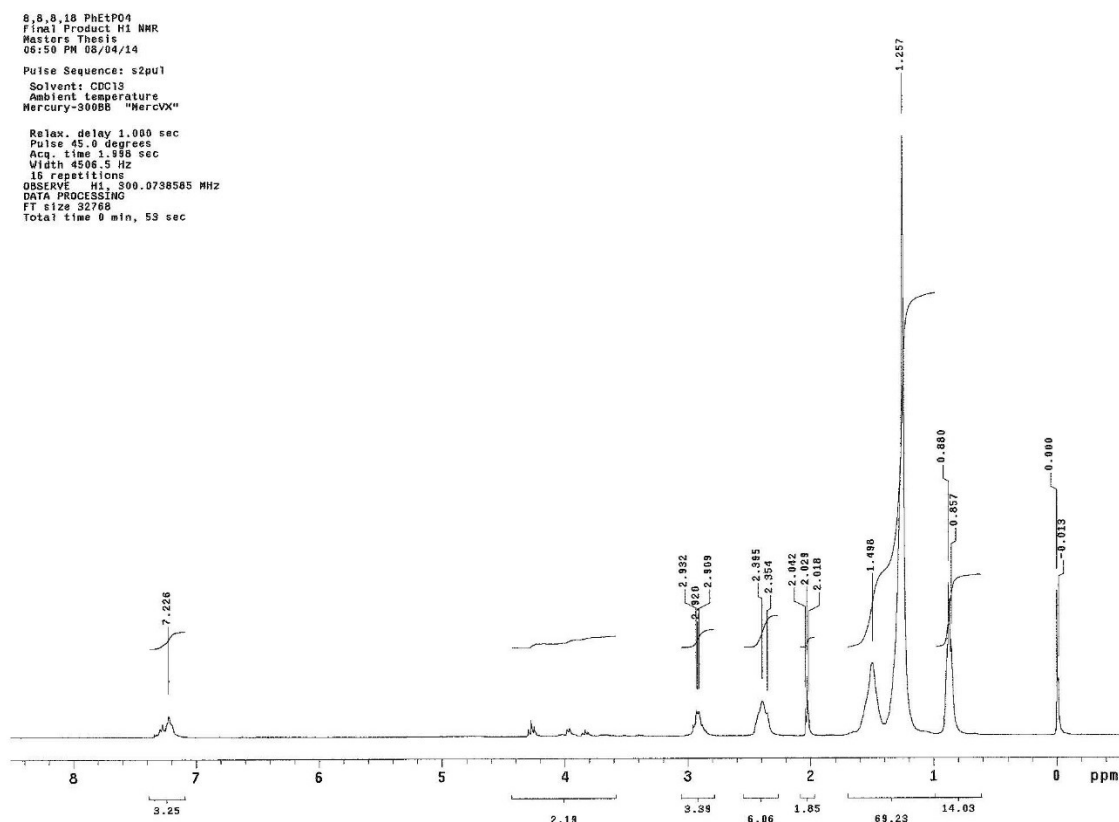


Figure F.58: ^1H NMR of trioctyl octadecyl phosphonium 2-phenylethyl 2-ethylhexyl phosphate in CDCl_3

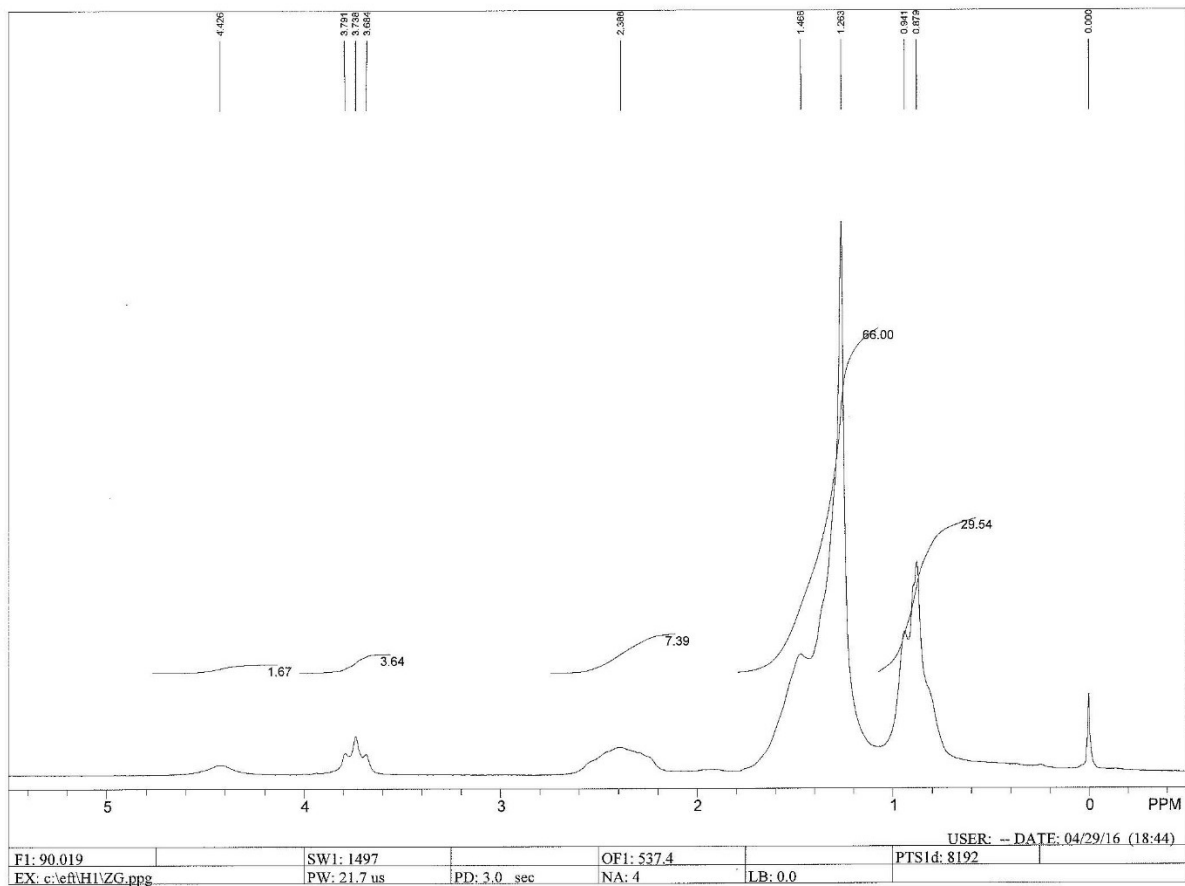
^1H NMR of ILs heated at 100°C for 1 hour

Figure F.59: ^1H NMR of heated trihexyl tetradecyl phosphonium bis(2-ethylhexyl) phosphate in CDCl_3

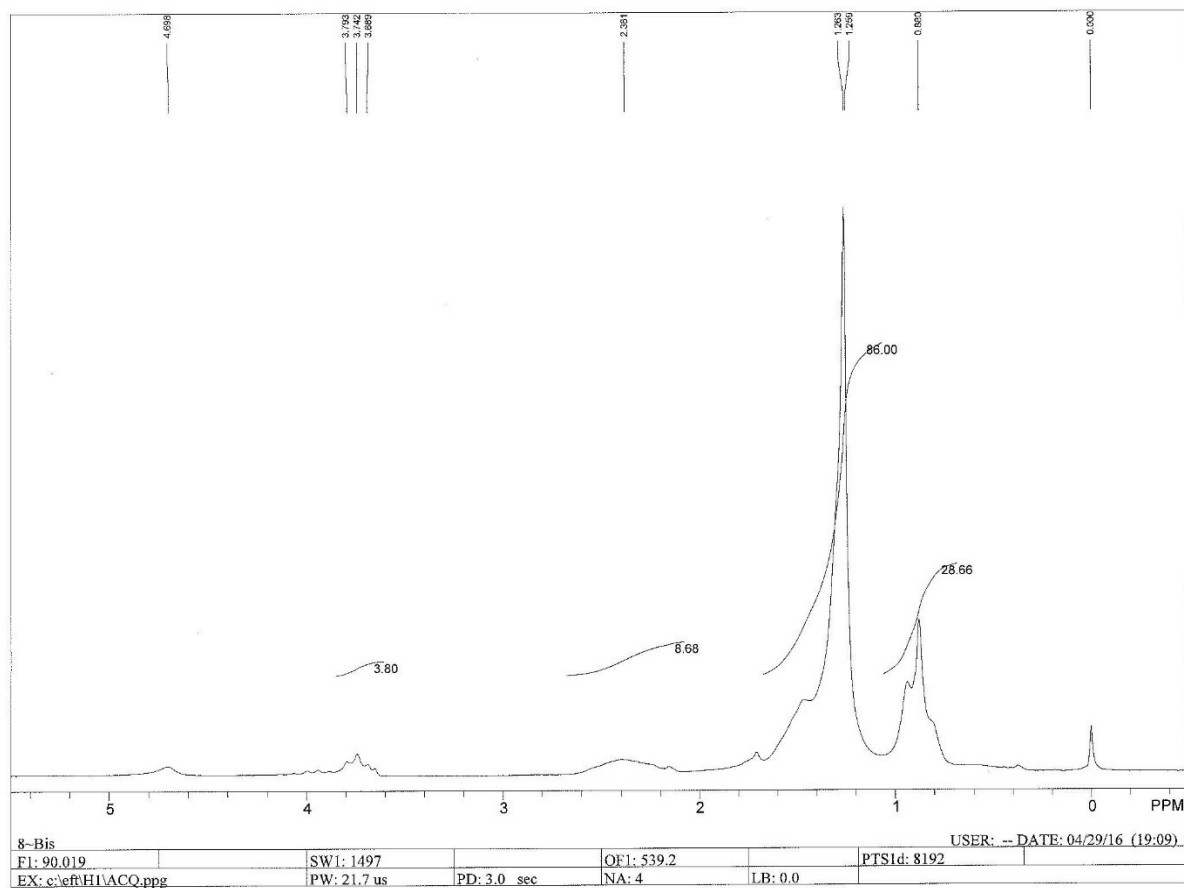


Figure F.60: ^1H NMR of heated trioctyl octadecyl phosphonium bis(2-ethylhexyl) phosphate in CDCl_3

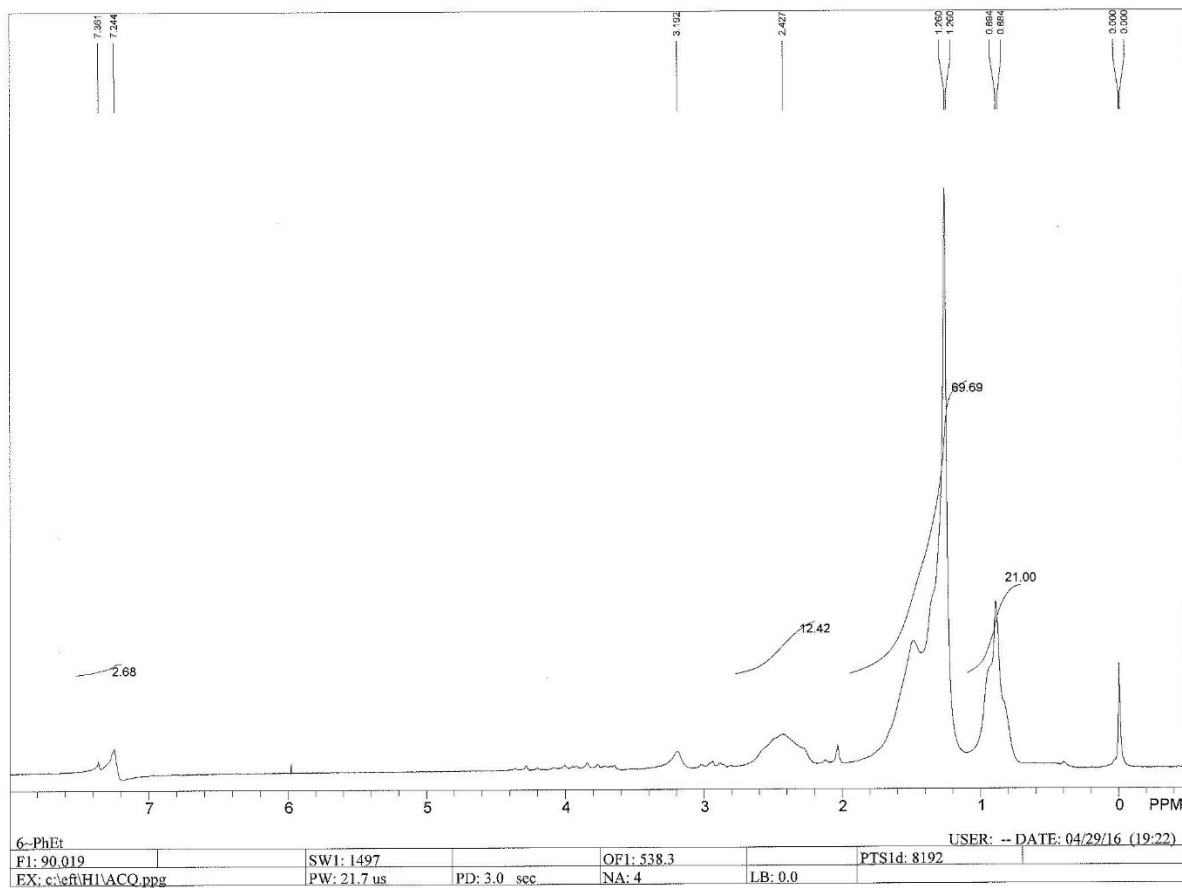


Figure F.61: ^1H NMR of heated trihexyl tetradecyl phosphonium 2-phenylethyl 2-ethylhexyl phosphate in CDCl_3

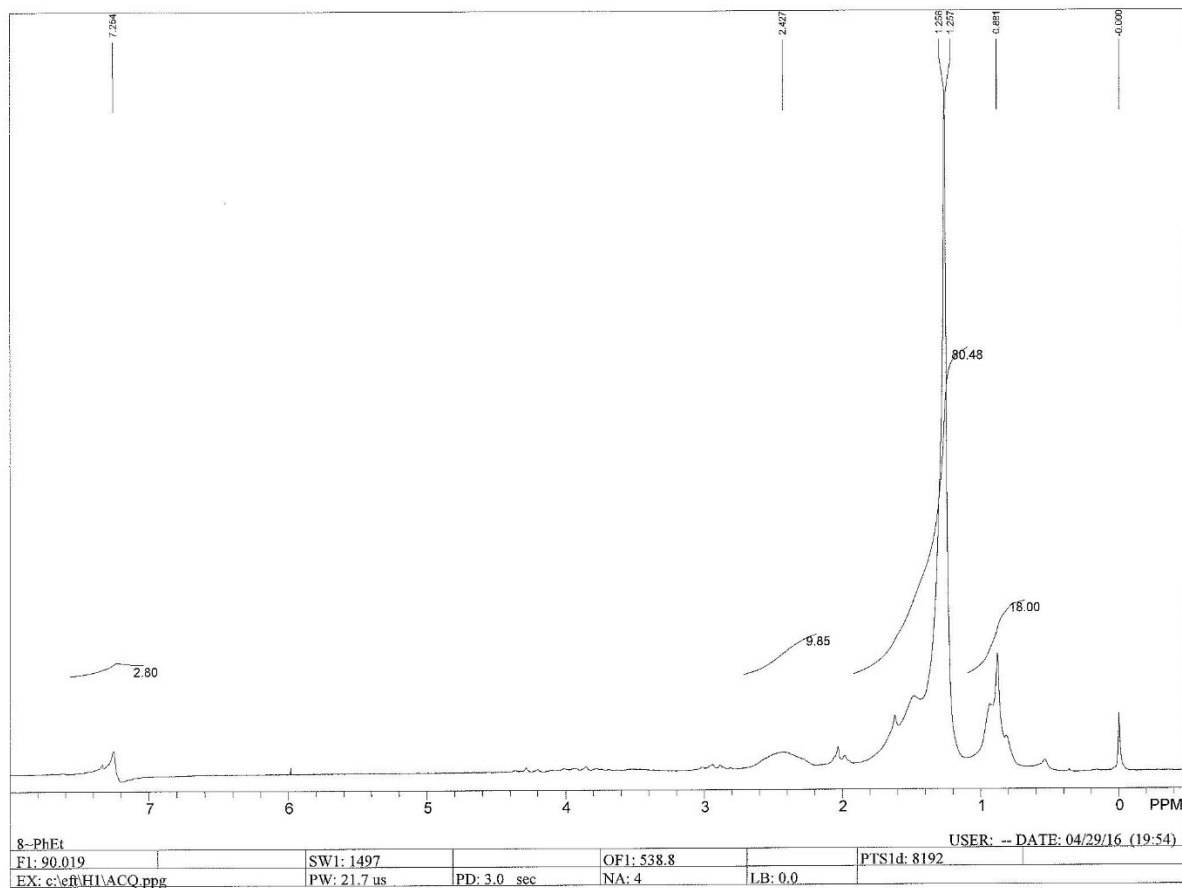


Figure F.62: ^1H NMR of heated trioctyl octadecyl phosphonium 2-phenylethyl 2-ethylhexyl phosphate in CDCl_3

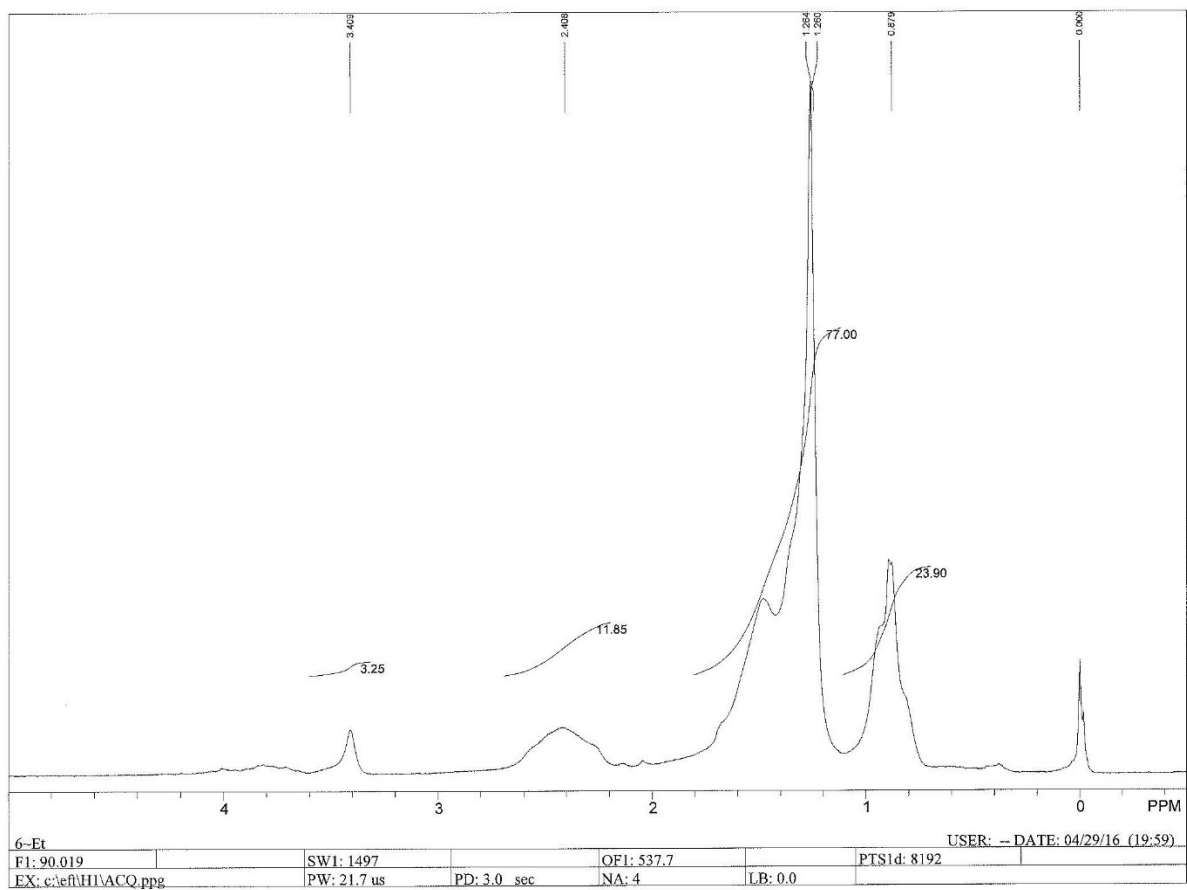


Figure F.63: ^1H NMR of heated trihexyl tetradecyl phosphonium ethyl 2-ethylhexyl phosphate in CDCl_3

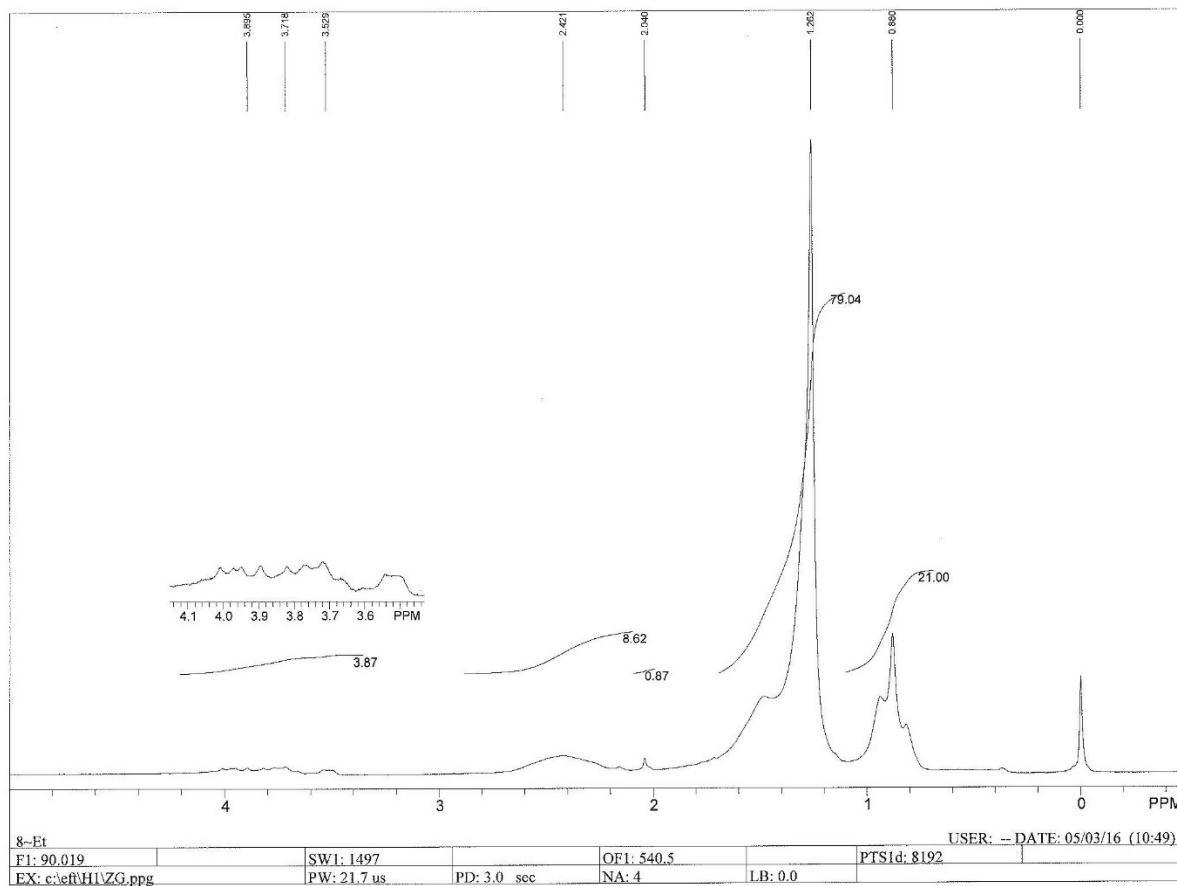


Figure F.64: ^1H NMR of heated trioctyl octadecyl phosphonium ethyl 2-ethylhexyl phosphate in CDCl_3

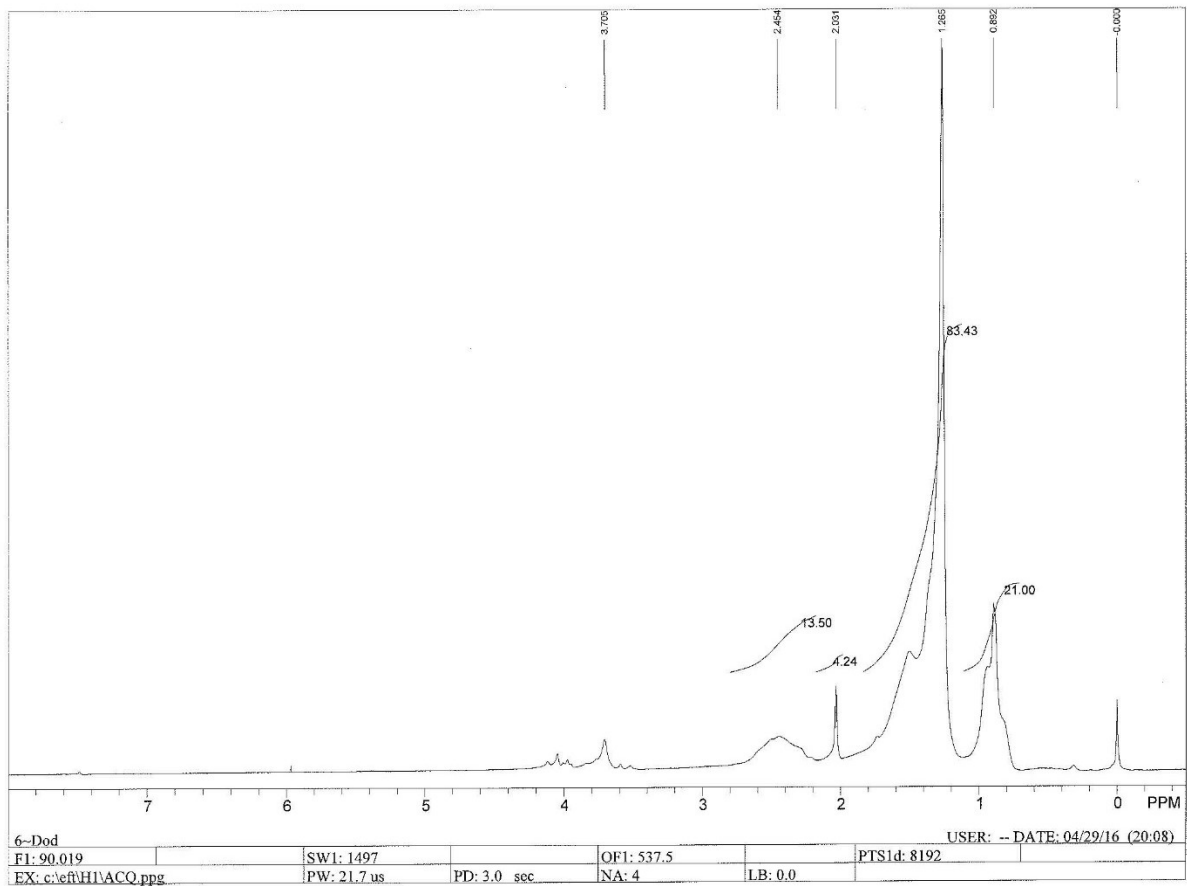


Figure F.65: ^1H NMR of heated trihexyl tetradecyl phosphonium dodecyl 2-ethylhexyl phosphate in CDCl_3

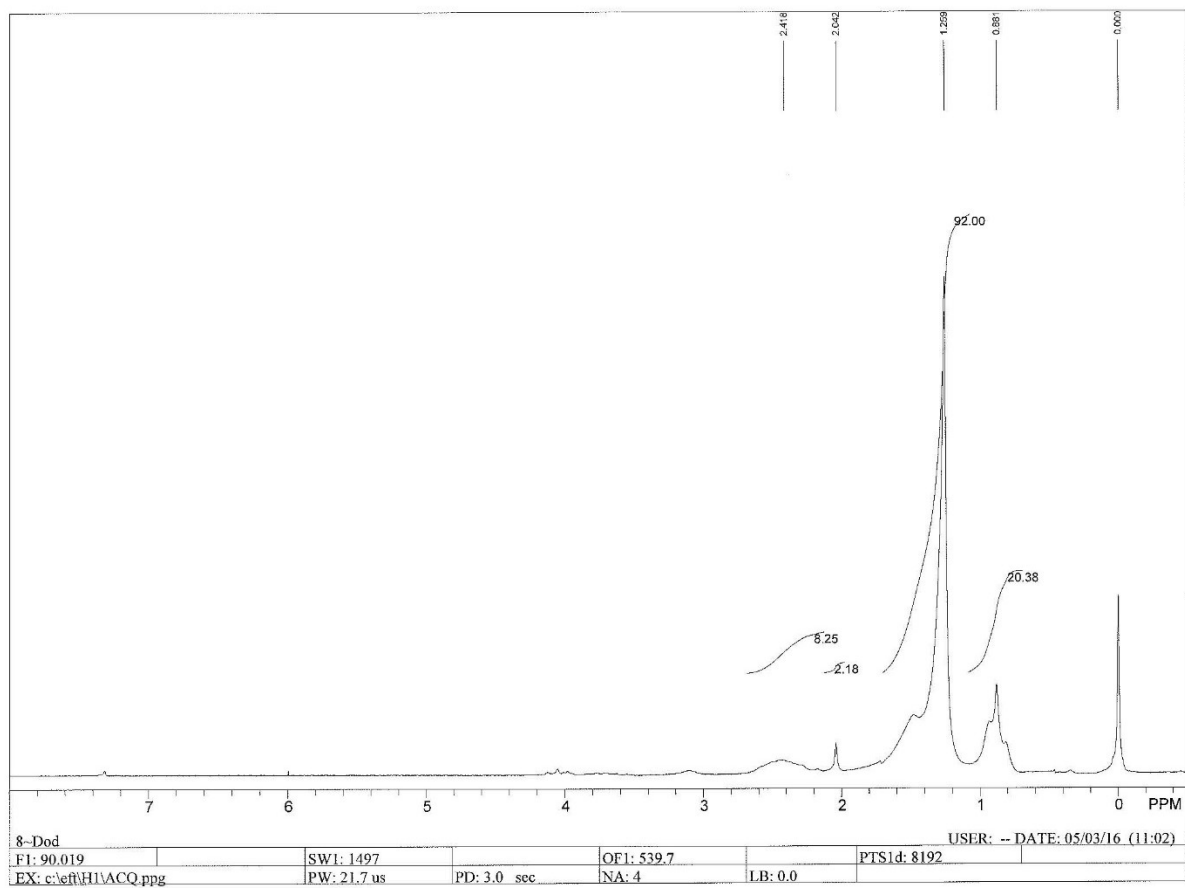


Figure F.66: ^1H NMR of heated trioctyl octadecyl phosphonium dodecyl 2-ethylhexyl phosphate in CDCl_3